Development of Organic Photoredox-Mediated Ring-Opening Metathesis Polymerization through Expanded Functionalities of Initiators and Monomers

Pengtao Lu

A dissertation

submitted in partial fulfillment of the

requirements for the degree of

Doctor of Philosophy

University of Washington

2019

Reading Committee:

Prof. Andrew J. Boydston, Chair

Prof. Gojko Lalic

Prof. Alshakim Nelson

Program Authorized to Offer Degree:

Department of Chemistry

University of Washington

Abstract

Development of Organic Photoredox-Mediated Ring-Opening Metathesis Polymerization through Expanded Functionalities of Initiators and Monomers

Pengtao Lu

Chair of the Supervisory Committee:
Professor Andrew J. Boydston
Department of Chemistry

Ring-opening metathesis polymerization (ROMP), which is derived from transition-metal-based olefin metathesis, has evolved into one of the most prevalent technologies for making functional polymeric materials. Due to the nature of this polymerization method, the metal alkylidene remains covalently bound to the polymer chain end until the introduction of various quenchers to terminate the polymerization. However, the removal of resultant metal by-products requires multiple purification steps. Recently, our group pioneered establishment of organic photoredox-mediated ROMP (*o*-ROMP), which is driven by the motivation of developing a metal-free alternative to traditional ROMP. This thesis aims to contribute to the study of *o*-ROMP by describing our investigations in the field, with a particular emphasis on expanding scopes of functional initiators and monomers. Chapter 1 is an introduction to *o*-ROMP, which start with explanation of community interests on developing organic photoredox-mediated controlled polymerization (OPCP). The general mechanisms of these novel polymerizations, including the properties of various organic photoredox catalysts, will be reviewed first. The flowing discussion will focus on different kinds of established OPCPs, which emphasizes on unique scopes for each specific methods. We will end up the

introduction part with our previous efforts on developing *o*-ROMP. Chapter 2 begins with our initial attempts on testing the feasibility of grafting *o*-ROMP from small-molecular multitopic initiators. The successful combination of this multidirectional growth mode with the design of macroinitiators facilitate preparation of polyether-based triblock copolymer and polystyrene-based graft copolymer, which are both acid cleavable. Chapter 3 describes our recent efforts on expanding the scope of macroinitiator towards polyesters and polycarbonates, which are derived from organocatalyzed ring-opening polymerization (*o*-ROP). Grafting from bifunctional initiators in one pot, stepwise *o*-ROP and *o*-ROMP succeed in making biocompatible block copolymers via a completely metal-free pathway. Finally, Chapter 4 discusses our ongoing efforts in the expansion of monomer scopes, aiming to make functional polymers solely through *o*-ROMP strategy. The successful adoption of those deprotection-free functional monomers not only make it possible to enable post-polymerization modification, but also provide opportunity to control chain architectures of resulted polymer.

TABLE OF CONTENTS

LIST OF FIGURES

LIST OF SCHEMES

LIST OF TABLES

ACKNOWLEDGEMENTS

Even it is meant to be hard to get a Ph.D degree, last five years are still much more difficult than I expected. I guess it is a terrible metaphor, but I sometimes do feel my life in the graduate school is like a single molecule (or atom) in classic Collision theory: Not all collisions (experiments) bring about chemical change (conference presentations or journal publications). So, there are many people to whom I want to express my sincere gratitude as they acted like "catalysts" in my last five years: the support and guidance, which they offered to me, dramatically lower the barrier of my pathway toward the final degree.

First, I want to express my greatest appreciation to my advisor, Prof. AJ Boydston, who is always very open on sharing his thoughts with us. To me, including other group members, AJ has always been a benchmark on how to achieve success in the lab. He's always patient about our unsuccessful experiments, and he will try his best to guide you through those breakdown. His influence is not just on chemistry, since I also learn a lot from him on how to manage a group with productive outcome. I want to thank all Boydston group members, especially those who I have the fortune to work with. Among those great chemists, I want to emphasize my appreciation to Dr. Mike Larsen and Dr. Kelli Ogawa, who are real trailblazers on laying down two distinct research areas for me to investigate.

Outside the Boydston lab, I want to thank all of my committee members: Prof. Alshakim Nelson, Prof. Goijko Lalic and Prof. Cole DeForrest. Their suggestions and comments, especially those from Prof. Nelson and Prof. Lalic as they also served as my second-year exam committee members, definitely had great impact on how I shaped my research projects. Besides instructions on chemistry, Prof. Nelson also shared his tips on making good decisions for my own career. I also want to appreciate Prof. Lalic's for his "intimidating" class on physical organic chemistry, since it enlightened what I should master in graduate school. The facility staff members at the Chemistry Department are all highly committed to what they are responsible for. I want to thank Dr. Rajan Paranji, Dr. Adrienne Roehrich and Dr. Martin Sadilek not only

for maintaining such wonderful NMR and Mass Spectroscopy facilities, but also being great sources for tackling my trouble on experiments.

Finally, I want to thank all of my friends, especially those who go through the graduate school with me at either Seattle or Akron. I'm 100% sure that what I learned from them is way more than what they took in from me. My family, including my parents and my wife, has always been my most reliable source of support. Without their love, I can't imagine what my life will become.

DEDICATION

To my wife Xiying and our daughter Ellie

Chapter 1. Introduction to Organic Photoredox-Mediated Ring-Opening Metathesis Polymerization (*o*-ROMP)

Section 1: General Concept of Organic Photoredox-Mediated Controlled Polymerization (OPCP)

1.1.a Historical Perspective

In the history of polymer science, one of the greatest accomplishments from polymer chemists is undoubtedly the discovery and development of various controlled polymerizations (CPs). The implementation of these CPs enables access to polymer with exceptional control over its architecture, molecular weight, dispersity ($Đ$) and chain-end functionality.[1]

In the meantime, light has been demonstrated as an inexpensive external stimulus to trigger polymerizations. The development of photopolymerization has enabled various techniques, ranging from conventional coatings and adhesives to high-tech photolithography and additive manufacturing (AM). While light offers the opportunity to both temporally and spatially control the polymer chain growth, it can also be used to reversibly switch the polymerization between "on" and "off" states. So, the successful adoption of light to mediate the process of CPs will provide an unprecedented control over macromolecular synthesis.[2]

Alongside with the renaissance of photoredox chemistry in organic synthesis,[3] polymer chemistry community start to apply transition metal-based photocatalysts as photoredox catalysts to mediate the controlled polymerizations.[4] The relatively straightforward preparation of these metal catalysts facilitates their applications. The installation of various ligands onto those metal centres also enable the fine-tuning of their catalytic performance. Although these organometallic photoredox catalysts demonstrate excellent control over the polymerization, the use of metallic compounds can be intrinsically expensive. Besides the cost of precious metal, the extra purification steps to remove metallic contamination from final materials would also prohibit the industrial applications of those metal-mediated photoredox controlled polymerizations (MPCPs).

To overcome the limitation of MPCPs, organic photoredox-mediated controlled polymerizations (OPCPs) have been proposed and realized through the adoption of cheap OPCs and accessible light sources, which at least demonstrated certain advantages over traditional CPs. For example, OPCPs have proven to be efficient techniques for modifying substrate surfaces. The employment of photocontrolled polymerization enables spatiotemporal control over the modification. Compared to traditional controlled radical polymerization, the procedures of corresponding OPCPs are largely user-friendly with no need for gloveboxes or rigorously inert conditions, which can be attributed to the oxygen tolerance. The purification will also be simplified since standard centrifugation techniques allows for simple separation of residual OPCs. Importantly, the employment of non-metal catalyst has made these OPCPs suitable for functionalizing surface of bio-related substrate.

1.1.b. General Rules of OPCPs

Scheme 1.1. (a) General reaction schemes for OPCPs. (b) Plots of molecular weight (square) and dispersity (triangle) as a function of monomer conversion. (c) On/Off light cycling experiment illustrating photocontrolled feature.

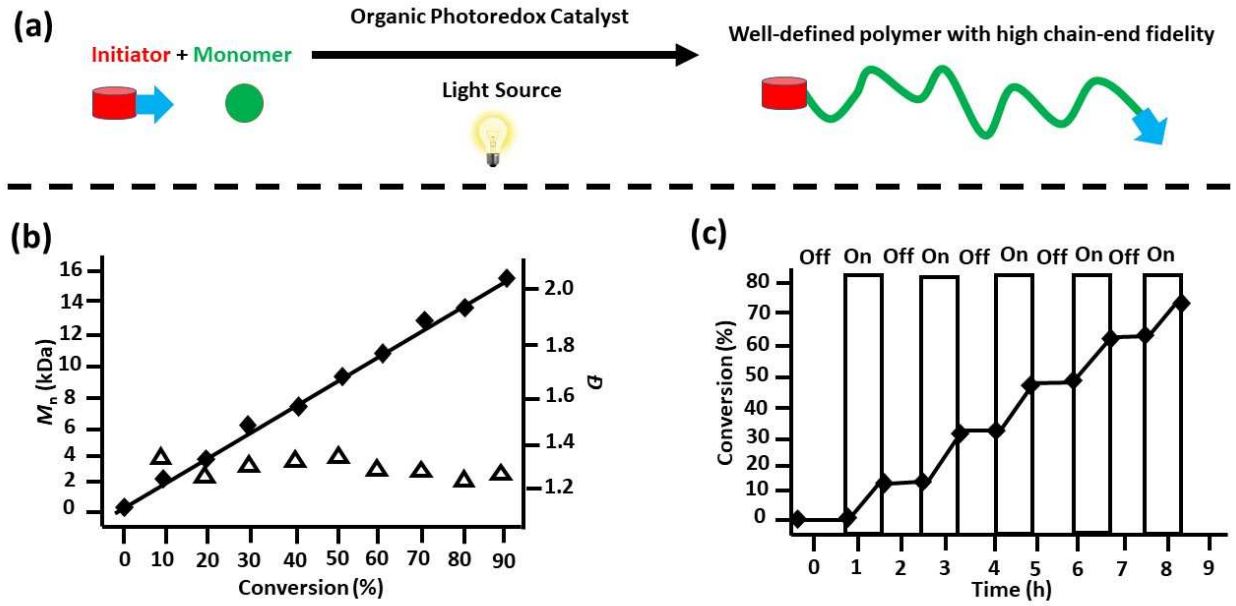

It is useful to emphasize general criteria for this type of new polymerization (Scheme 1.1). First, the elementary reaction of OPCPs should involve the redox reaction, an electron-transfer process, between excited OPCs and monomer substrates [Sub]. Second, these photopolymerizations should keep the same characteristics as previously established CPs, such as 1) linear increase of molecular weight or monomer conversion versus time, 2) relatively low molecular weight dispersity ($Đ$ < 1.4), and 3) high fidelity of polymer chain ends as is necessary for synthesis of block copolymers. Finally, OPCPs should be photocontrolled, not photoinitiated, which means chain propagation can be toggled on and off with light as external stimulus.

Scheme 1.2. General mechanism of OPCPs. (a) Reductive Photoredox cycle of OPC. (b) Oxidative Photoredox cycle of OPC. [Sub]: substrate that undergo redox reaction between excited OPCs. M: select monomer.

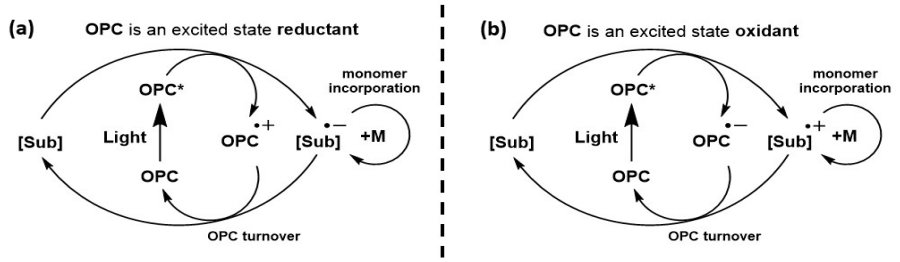

Compared to conventional photoinitiated polymerization, the unparalleled performance of OPCPs on light cycling experiments can be attributed to their unique mechanisms.[5] Although the specific mechanism for each OPCP will be discussed in their own section, a general polymerization mechanism is outlined in Scheme 1.2. For all OPCPs discussed in this review, the first step is photo-excitation of the OPC. The excited state catalyst then undergoes single electron transfer with a substrate [Sub], such as initiators or dormant polymer chain ends, to generate open-shell intermediates as propagation species for each polymerization.

The general mechanism can be categorized by the primary direction of the electron transfer with respect to the excited state catalyst, OPC*. In a reductive photoredox cycle, the excited state OPC* is quenched by donating an electron to [Sub], while in the oxidative photoredox cycle, OPC* is quenched by accepting an electron from [Sub]. The key step of OPCPs is the redox reaction

between open-shell OPC intermediates and active polymer chain ends, since then ground-state catalysts will be regenerated, and polymer chain fidelity can also be retained. As rationalized in the general mechanism of OPCPs, it is important to consider both photophysical and electrochemical properties of each OPC for distinct polymerization. Although a detailed discussion on those properties is out of the scope of this review, a general overview of select OPC families is provided, including their chemical structures and related photophysical and electrochemical properties (Figure 1.1 and Table 1.1).

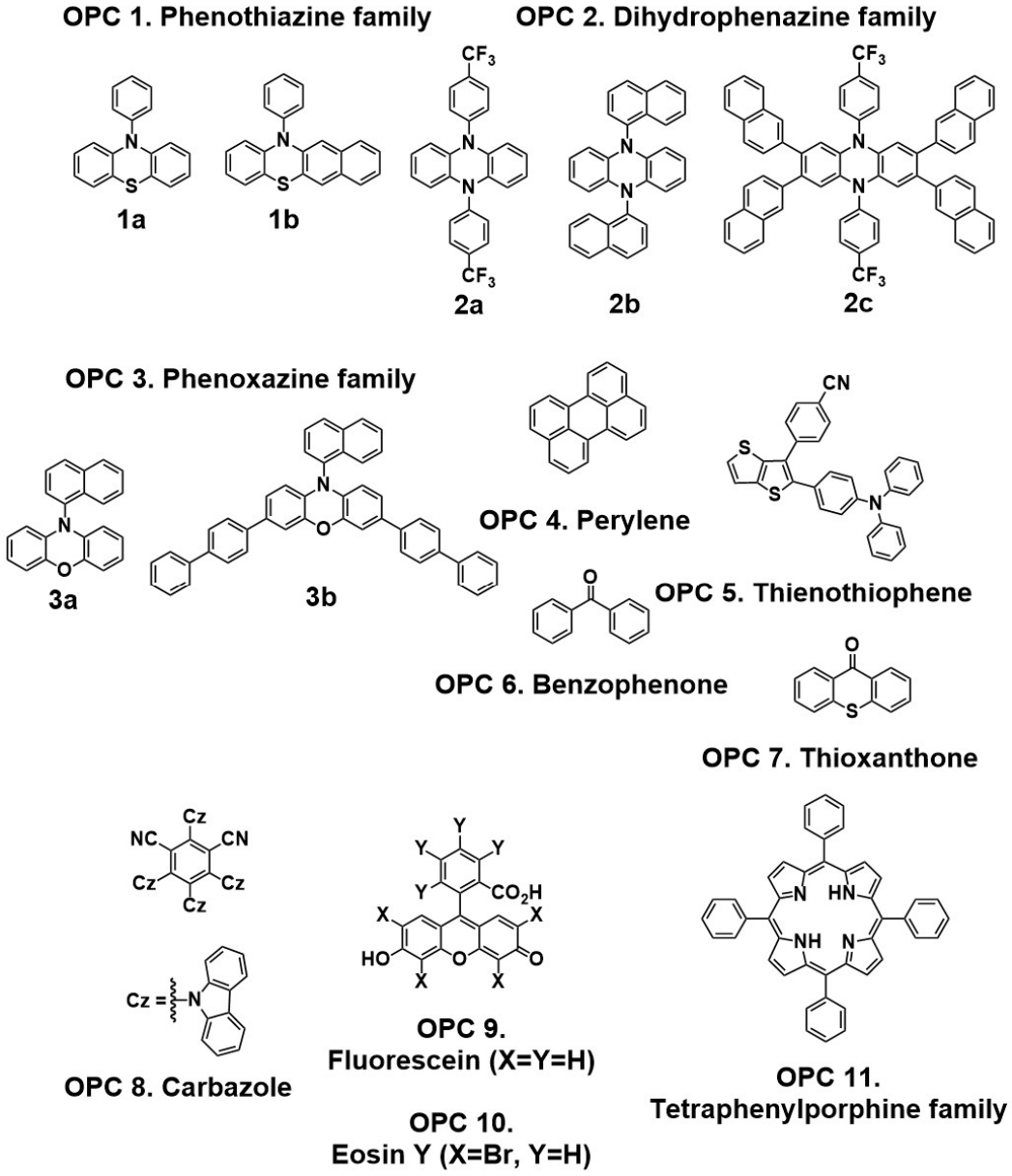

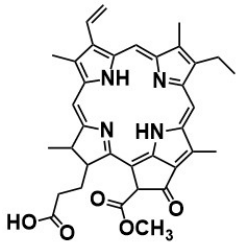

OPC 12.
Phenophorbide a

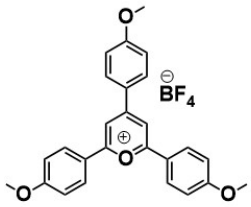

OPC 13.
***p*-methoxy pyrylium**

Figure 1.1. Chemical structures of common OPCs applied for OPCPs.

Table 1.1. Photophysical and Electrochemical Properties of OPCs

OPC	λ_{max} (nm)	E* (V vs SCE)	Photoredox Cycle
1a	320	-2.1 ($OPC^{+\bullet}/OPC^*$)	Reductive
1b	369	N/A	Reductive
2a	367	-1.80 ($OPC^{+\bullet}/OPC^*$)	Reductive
2b	366	-1.64 ($OPC^{+\bullet}/OPC^*$)	Reductive
2c	388	-1.84 ($OPC^{+\bullet}/OPC^*$)	Reductive
3a	323	-1.67 ($OPC^{+\bullet}/OPC^*$)	Reductive
3b	388	-1.80 ($OPC^{+\bullet}/OPC^*$)	Reductive
4	436	-1.87 ($OPC^{+\bullet}/OPC^*$)	Reductive
5	365	-1.27 ($OPC^{+\bullet}/OPC^*$)	Reductive
6	335	+1.50 ($OPC^*/OPC^{\bullet-}$)	Oxidative
7	360	+1.52 ($OPC^*/OPC^{\bullet-}$)	Oxidative
8	375	-1.06 ($OPC^{+\bullet}/OPC^*$)	Oxidative
9	437	+1.25 ($OPC^*/OPC^{\bullet-}$) -1.55 ($OPC^{+\bullet}/OPC^*$)	Oxidative Reductive
10	520	+1.23 ($OPC^*/OPC^{\bullet-}$) -1.58 ($OPC^{+\bullet}/OPC^*$)	Oxidative Reductive
11	418	-1.30 ($OPC^{+\bullet}/OPC^*$)	Reductive
12	409, 667	N/A	Reductive
13	430, 470	+1.89 ($OPC^*/OPC^{\bullet-}$)	Oxidative

Section 2: General Discussion on The Scope of Established OPCPs

1.2.a Organic Photoredox-Mediated Atom Transfer Radical Polymerization (o-ATRP)

Since the pioneering report by Matyjaszewski and Sawamoto,[6] traditional metal-mediated ATRP has evolved into one of the most common techniques for making well-defined polymers.[7] The controlled feature of ATRP relies on the reversible deactivation of propagating sites of the growing polymer chain. That dynamic equilibrium between dormant alkyl halide and active radical species, which is mediated by a redox reaction involving a metal catalyst, is illustrated in Scheme 1.3.a. Since the activation the alkyl halide initiator is realized via a reducing organometallic compound, it is reasonable to hypothesize that chain end activation in ATRP may also be triggered by a strongly reducing excited state OPC. In 2014, the Hawker and Miyake groups each independently published seminal papers on organic photoredox-mediated ATRP (*o*-ATRP) featuring two different catalysts, OPC **1a** (Hawker) and OPC **4** (Miyake).[8]

Scheme 1.3. (a) General mechanism for traditional metal-mediated ATRP. (b) Reductive photoredox cycle in *o*-ATRP (c) Oxidative photoredox cycle in *o*-ATRP

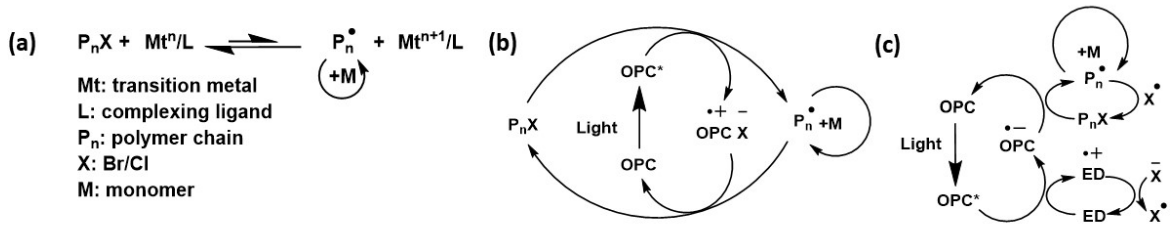

Notably, perylene (OPC **4**) can be excited with visible light, which is attractive for photo-chemoselectivity and operational simplicity. However, the initial perylene system displayed low initiation efficiencies (< 50 %) and relatively high $Đ$ (> 1.50), which led subsequent studies to the optimization of phenothiazine frameworks.[8b] Compared with the initial phenothiazine OPC **1a**, the corresponding derivative OPC **1b**, designed by the Matyjaszewski group, showed better performance in the polymerization of methacrylates

and facilitated controlled polymerization under visible light.[9] The mechanism of *o*-ATRP catalysed by OPC **1a** was also elucidated by Matyjaszewski and coworkers through a combination of computational and experimental works.[10] The results suggested that the activation process undergoes a dissociative electron-transfer mechanism, while the exact reverse pathway is favoured in the deactivation process. Another interesting report on OPC **1a** came from the Bergbreiter group, in which they successfully prepared a recyclable catalyst by attaching the OPC onto polyisobutylene (PIB).[11] This PIB-bound OPC can be easily separated from polymer products and reused via a facile biphasic separation process. Successful reuse was demonstrated for 3 cycles.

Miyake and coworkers, on the other hand, turned toward development of phenoxazine and dihydrophenazine families, which could also be excited with visible light after structural optimization that came from the help of DFT calculations.[12] The modular synthesis of OPCs with different substituents greatly expanded the number and performance of applicable catalysts for *o*-ATRP. For example, compared to OPC **2a** under similar conditions, OPC **2b** exhibited a much higher initiator efficiency (99.3% with **2b** vs 52.0% with **2a**) and an impressively low $Đ$ (1.08 when M_w = 12.3 kDa). Moreover, for *o*-ATRP mediated by **2b**, the plot of M_n versus monomer conversion exhibits a *y* intercept of 850 Da, illustrating the accomplishment of control over polymerization after the addition of only ~ 6 methyl methacrylate units. A recent paper introduced a new member of the dihydrophenazine family, OPC **2c**. In comparison with **2a** and **2b**, OPC **2c** produced polymer with excellent molecular weight control and low dispersity at low catalyst loadings of 5 – 50 ppm, while achieving near quantitative initiator efficiency.[13] For the phenoxazine family, in comparison with **3a**, OPC **3b** not only absorbed in visible light region, but also

exhibited a better control over the polymerization, as demonstrated by the synthesis of polymer with much lower polydispersity ($Đ < 1.20$). OPC **3b** retained its great performance even when the reaction mixture was exposed to air. These results greatly simplify the operational procedure of *o*-ATRP.[14]

In addition to OPCs from phenothiazine, dihydrophenazine, and phenoxazine families, other catalysts such as OPC **5** and **8** also operate through reductive photoredox cycle (Scheme 1.3.b).[15] Although OPC **8** mediated the polymerization under blue light irradiation with exceptionally low ppm-level catalyst loading, they typically gave polymers with broader molecular weight distribution ($Đ > 1.50$) compared to those made through OPC **5** ($Đ \sim 1.30$). Upon irradiation, both catalysts lead to a photomediated process resulting in the formation of polymers with control over molecular weight, low dispersity and chain-end functionality, as confirmed by chain extension experiments. On the other hand, the Yagci and Zhu groups each independently demonstrated that *o*-ATRP can also be achieved through a oxidative photoredox cycle (Scheme 1.3.c).[16] Those catalytic systems are based upon integration of electron-deficient organic dyes (OPC **6**, **7**, **9** and **10**) and sacrificial electron donors (usually tertiary amines). Besides commercial availability of OPCs, the reductive quenching system also facilitated the first successful *o*-ATRP of styrene and the first demonstration of *o*-ATRP of acrylic monomers in aqueous media.[17] One caveat that potentially tempers these exciting breakthroughs, however, is the fact that tertiary amines can lead to undesired side reactions, such as hydrogen atom abstraction.[18]

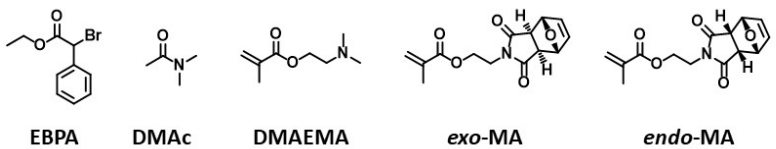

Figure 1.2. Select initiator, solvent and monomer for *o*-ATRP

Compared with assorted photocatalysts that have been intensely studied, investigation of other components of *o*-ATRP systems, such as initiators, monomers, and solvent, is still underdeveloped (Figure 1.2). For example, chloride-based initiating systems are currently incompatible with *o*-ATRP, which can be attributed to higher bond dissociation energies of alkyl chlorides compared to alkyl bromides. Miyake and coworkers investigated the effect of solvent polarity on phenazine-based OPCs.[19] The results indicated that careful design of catalysts' substituents may extend *o*-ATRP to nonpolar media. At present, ethyl *a*-bromophenylacetate (EBPA) and N, N-dimethylacetamide (DMAc) represent the best candidates for *o*-ATRP initiator and solvent species, respectively. That said, it is encouraging to see that the functionality within the monomer scope for *o*-ATRP, though limited to methacrylates, has expanded dramatically. Notable examples include biomass- and ionic liquid-derived methacrylates.[20] Moreover, *o*-ATRP has been shown to incorporate several methacrylates that were difficult for controlled polymerization via traditional metal-mediated ATRP (Figure 1.2). For example, controlled polymerization of dimethylaminoethyl methacrylate (DMAEMA) and acrylonitrile (AN) are traditionally challenging since pendant functional groups may interact with transition metal catalysts. The adoption of *o*-ATRP successfully offered controlled polymerization of these two demanding monomers and the metal-free merits may render these polymers suitable for electronic and biomedical applications.[21] Furthermore, traditional thermally initiated ATRP is not able to offer controlled polymerization of monomers with heat-sensitive functional groups, such as methacrylates bearing pendant maleimides that are protected via cycloaddition with furan. The corresponding *endo* adduct, *endo*-MA, display deprotection temperatures around 60 °C. Read de Alaniz, Hawker, and coworkers employed OPC **2a** for successful controlled polymerization of *endo*-MA at room temperature. Through the copolymerization of *endo*-MA and *exo*-MA, a

multifunctional polymer with pedant backbone groups was synthesized and it was demonstrated that this polymer could be used as versatile platform for sequential post-polymerization modification due to selective deprotection between *endo* and *exo* isomers.[22]

1.2.b Organic Photoredox-Mediated Reversible Addition Fragmentation Transfer Polymerization (o-PET-RAFT)

Unlike traditional ATRP, established RAFT mechanisms rely upon a degenerative chain transfer mechanism to afford control over polymerization (Scheme 1.4.a).[23] In this case, the active chain ends are rapidly exchanged between each chain transfer agent (CTA). In 2014, Boyer and coworkers disclosed the first report on photoinduced electron transfer RAFT (PET-RAFT) polymerization, which is mediated by strongly reducing Ir-based photocatalysts.[4b] Since PET-RAFT is free of external initiators, this technique excludes the potential by-products that would be present in thermally initiated RAFT process. Like the mechanism of *o*-ATRP, the employed catalysts can also manipulate *o*-PET-RAFT through either oxidative or reductive photoredox cycle (Scheme 1.4.b and 1.4.c). For example, OPC **10** can function as both mild oxidant and reductant after photoexcitation, and both excited species are operative through distinct mechanism.[24]

Scheme 1.4. (a) General mechanism for RAFT process. (b) Reductive photoredox cycle in *o*-PET-RAFT. (c) Oxidative photoredox cycle in *o*-PET-RAFT.

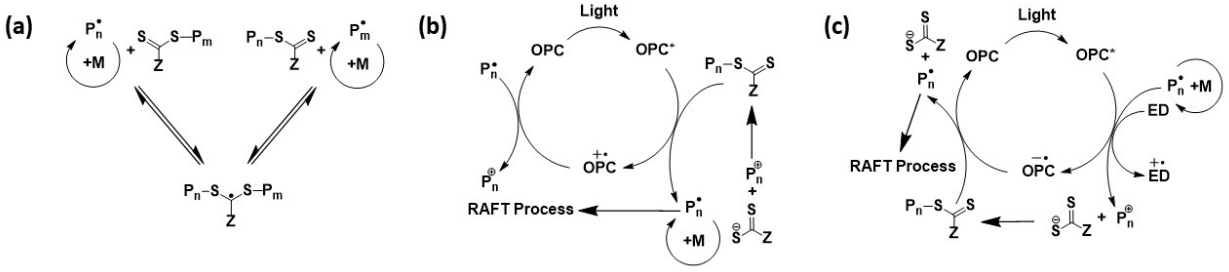

One of the exciting features of *o*-PET-RAFT is its high oxygen tolerance, which is attributed to the formation of singlet oxygen by intermolecular triplet-triplet annihilation between excited state OPC* and molecular oxygen (Figure 1.3.a). The resulted singlet oxygen will then react with either solvent (like DMSO) or electron donors (like tertiary amines) to greatly minimize the induction period.[25] It was also demonstrated that cooperation between ascorbic acid and OPCs can deliver an interesting energy storage system that could generate radicals after a short period of light irradiation.[26] The excellent oxygen tolerance makes *o*-PET-RAFT a great candidate for polymerization with ultralow volume reaction mixtures, where deoxygenation is hard to perform.[27] Computational simulation also assisted the screening and design of new catalysts for *o*-PET-RAFT. For example, the collaborative report from the Boyer and Miyake groups thoroughly correlated structures of halogenated xanthene dyes with their ability to mediate *o*-PET-RAFT, with the aid of DFT calculations.[28] This deeper understanding of structure-property-performance relationships facilitated the preparation of a new xanthene, OPC **14** (Figure 1.3.b)), which enabled a more efficient oxygen-tolerant technique. A recent work from Boyer and coworkers reported a fully-computer aided strategy in discovering an efficient pH-switchable OPC, and they demonstrated that the polymerization can be reversibly ceased by a slight change of pH or in the absence of light.[29]

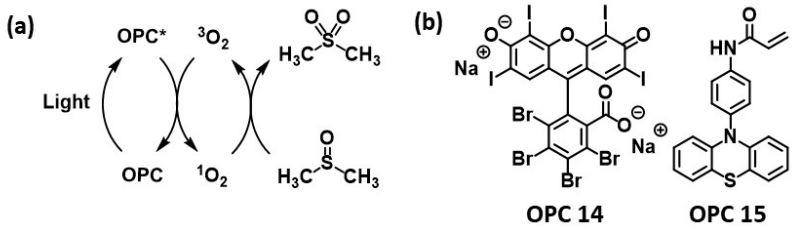

Figure 1.3. (a) General mechanism for oxygen tolerance in *o*-PET-RAFT. (b) Chemical structure of OPC **14** and **15**.

Another inspiring hallmark of *o*-PET-RAFT is the engagement of OPC **11** and **12**, which enable controlled polymerization with red light. These long wavelength systems potentiate utility

of *o*-PET-RAFT in biological applications. An electron donor-acceptor (EDA) system based on OPC **11** was designed to increase the collision frequency between acceptor (RAFT agent) and donor (metal-free porphyrin).[30] These EDA catalysts, compared to free porphyrin, were demonstrated to remarkably increase the polymerization rates. Additionally, Johnson and coworkers introduced OPC **1a** into *o*-PET-RAFT systems by using trithiocarbonate as an iniferter.[31] They also prepared an acrylate functionalized phenothiazine derivative OPC **15** (Figure 1.3.b), which was later chemically crosslinked with acrylamide to afford OPC-incorporated gels.[32] Compared to the previously mentioned PIB system, this type of solid supported OPC could be triggered by two distinct external stimuli (heat or light) to mediate controlled radical polymerization with broad monomer scopes. This also facilitated the recycling of catalysts since the same OPC gel was demonstrated to mediate 6 batches of polymerization without the loss of catalytic and controlled feature. Other solid-supported catalysts for mediating *o*-PET-RAFT, which are based on derivatives of OPC **10** and **11**, have also been developed and studied.[33]

Scheme 1.5. The selectivity of OPC **12** on (a) different CTAs; (b) different monomers.

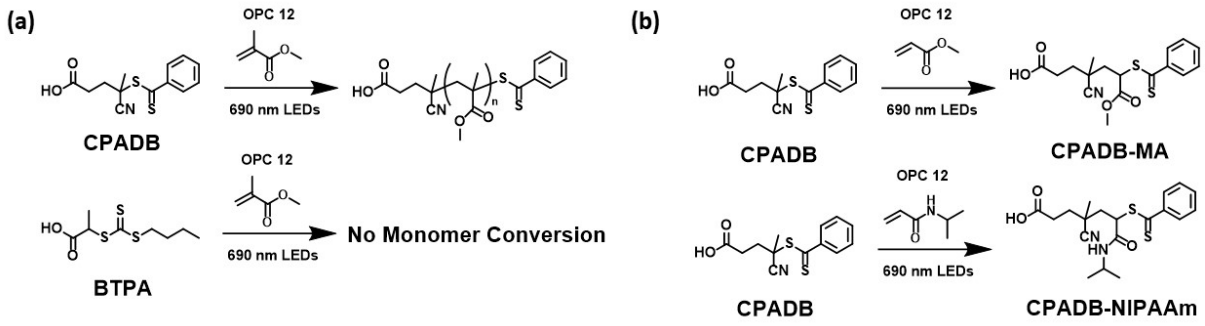

The monomer scope of *o*-PET-RAFT, compared to *o*-ATRP, includes methacrylates as well as other vinyl monomers, such as acrylates, acrylamide, and styrene.[34] Additionally, *o*-PET-RAFT shows a high selectivity on the photoactivation of different CTAs with respective catalysts (Scheme 1.5.a).[35] For example, after OPC **12** was excited, it selectively activated 4-cyanopentanoic acid dithiobenzoate (CPADB) over 2-(n-butyltrithiocarbonate)-propionic acid (BTPA). When

methyl methacrylate was polymerized in the presence of both CTAs, the results suggested that BTPA did not participate in the polymerization. This exceptional selectivity has never been reported in traditional thermal RAFT polymerization, which is attributed to the distinct mechanism of *o*-PET-RAFT.

Boyer and coworkers also realized that the photoactivation by OPC **12** displayed monomer selectivity during polymerization (Scheme 1.5.b).[36] In contrast to methacrylate monomers, the polymerization of other vinyl monomers, such as acrylates and acrylamide, was stopped after insertion of the very first monomer unit. The ceased polymerization was unraveled to be a result of considerable increase in the carbon-sulfur bond dissociation energy, since the insertion of monomer changed the α-carbon from tertiary to secondary. This precise single unit monomer insertion (SUMI) can afford pure mono-adducts in high isolated yields with low OPC concentrations. The application of this special form of *o*-PET-RAFT has been disclosed in the case of efficient preparation of discrete oligomers, which illustrates a powerful synthetic pathway to polymers with precise sequence.[37]

1.2.c Organic Photoredox-Mediated Controlled Cationic Polymerization (o-PET-CCP)

Traditional CCP of vinyl ethers typically involves alkyl halide initiators with strong Lewis acid co-initiators.[38] In an exciting departure from this platform, the Kamigaito group and Sugihara group each independently discovered a new cationic RAFT system initiated by organic acids, which also proceeds through a degenerative chain transfer mechanism (Scheme 1.6.a).[39] This cationic chain transfer mechanism is enabled by the high affinity between carbocationic species and sulfur atoms.

Scheme 1.6. (a) General mechanism for cationic RAFT process. (b) Oxidative photoredox cycle in *o*-PET-CCP.

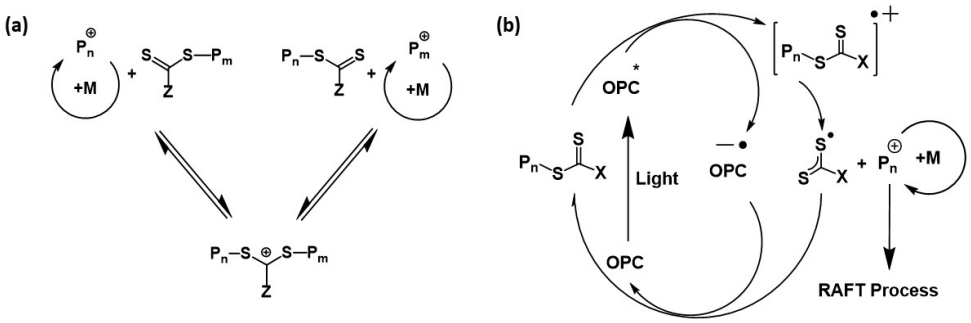

In 2016, Fors and coworkers reported an *o*-PET-CCP of vinyl ethers by using OPC **13a**.[40] The cooperation between CTAs and pyrylium salts enabled extraordinary temporal control over polymer chain growth with light, which was demonstrated by switching polymerization through alternating periods of light and dark. This polymerization also succeeded with a broad scope of vinyl ether monomers. The mechanism of this *o*-PET-CCP was investigated using a suite of spectroscopic and electrochemical analytical techniques (Scheme 1.6.b).[41] First, the RAFT chain transfer agent (CTA) is oxidized by an excited state pyrylium salt. After single electron oxidation, CTAs turn into their corresponding radical cation species, which spontaneously undergo mesolytic cleavage to form a reactive cation and a dithiocarbamate radical. The reactive cations initiate the polymerization of vinyl ethers and RAFT type chain transfer reaction is responsible for the control over chain growth. On the other hand, pyranyl radicals will reduce dithiocarbamate radical into corresponding anionic species, which deactivate cationic propagating chains by end capping. Based on the detailed understanding of this polymerization mechanism, Fors and coworkers were able to develop a mechanism-switch polymerization that converted between cation- or radical-based propagation.[42] And the same group also succeeded in realizing quantitative chain-end functionalization.[43]

Section 3: Introduction to Organic Photoredox-Mediated Ring-Opening Metathesis Polymerization (*o*-ROMP)

1.3.a Historical Perspective

Ring-opening metathesis polymerization (ROMP) is a type of chain-growth polymerization, which has emerged as a powerful and broadly applicable technique for synthesizing polymeric materials.[44] The origins of ROMP can be traced back to 1950s when various mixtures of metal salts were recognized for their reactivities toward olefin metathesis, a unique metal-mediated carbon-carbon double bond exchange process. Akin to other forms of olefin metathesis, the resultant polymer conserves all unsaturation associated with the cyclic olefin type monomer. Although there have been numerous reports of various metals used for ROMP, those based on Ru and Mo (Figure 1.4) have become most popular due to their excellent functional group tolerance, which has greatly expanded the monomer scope.[45] Importantly, careful adjustment of reaction conditions and catalysts choice can be used to achieve living polymerization that, afford polymers with controlled molecular weight, narrow polydispersity and high chain-end fidelity.

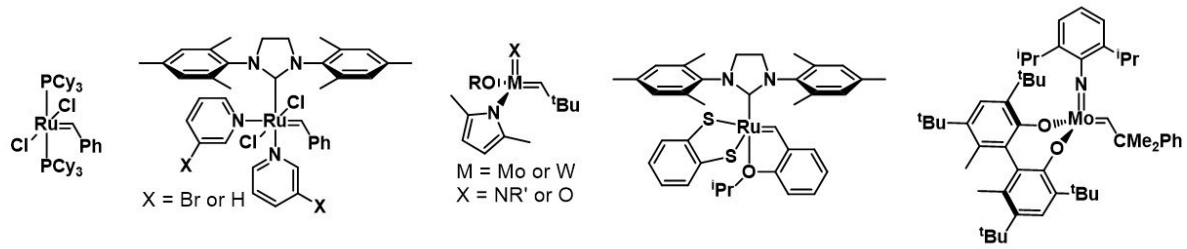

Figure 1.4. Select examples of well-defined metal-based ROMP initiators.

A general mechanism of ROMP based on Chauvin's original proposal is shown in Scheme 1.7. Initiation begins with the coordination of a transition-metal alkylidene complex to a cyclic olefin. A subsequent [2+2] cycloaddition affords a four-membered metallacyclobutane. This highly strained intermediate immediately undergoes a cycloreversion reaction to form a new metal-alkylidene species with exactly the same reactivity, although the resulting complex has

increased in size since it now incorporates one monomer unit. Additional monomers undergo this sequence of elementary steps during propagation to ultimately afford a high molecular weight polymer.

Scheme 1.7. Generalized Mechanism of Traditional ROMP using Metal Initiators

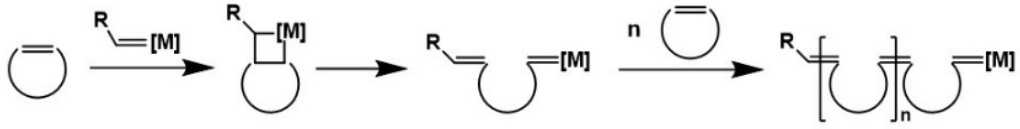

Due to the covalent attachment of metal initiator to the polymer chain, however, ROMP polymers can be very difficult to purify.[46] Living ROMP is commonly quenched through the addition of a specialized chemical reagent, which selectively removes the transition metal from the chain end and deactivates it from further propagation. However, these metallic by-products not only shorten the lifetime of bulk materials, but also limit the application of ROMP polymers in biomedical or microelectronic devices. Although there has been much effort devoted to improving purification procedure, these extra processes dramatically increase the length and cost of polymer production.

1.3.b A Metal-Free Electrochemical Approach

To address the need for metal-free alternatives to traditional ROMP, as well as add to general community efforts to develop "greener" controlled polymerization, our group envisioned an organic alternative to traditional metal-mediated ROMP. Inspired by Chiba's electrochemical approach to intermolecular cross metathesis between vinyl ethers and terminal olefins, we hypothesized that an "all-organic" electrochemical ROMP could also be possible. In Chiba's pioneering experiments, it was demonstrated that oxidation of vinyl ethers leads to the formation of a [2+2] radical cation complex, reminiscent of the metallacyclobutane intermediate in traditional

metal-mediated ROMP, that is subsequently reduced to give a cyclobutane (Scheme 1.8).[47] It is apparent from the ROMP mechanism that the success of traditional ROMP relies on the cycloreversion of the strained metallacyclobutane intermediate to give the propagating species. We postulated that outcompeting the reduction of [2+2] complex by rapid ring-opening of strained cyclic olefin could result in a new ROMP type polymerization with unique mechanism.

Scheme 1.8. Electrochemical Olefin Metathesis and Cyclobutane Formation

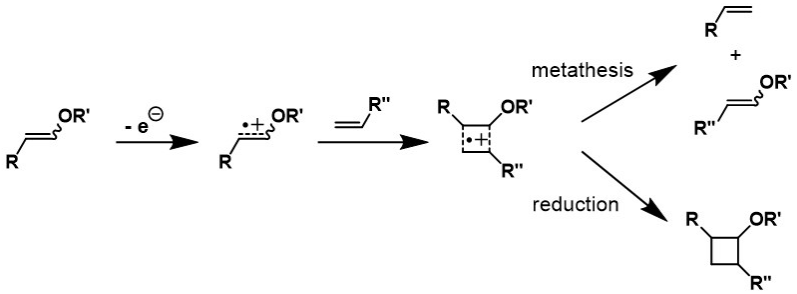

Specifically, we hypothesized that (Scheme 1.9), after the single-electron oxidation of vinyl ether (**A**), the reactive radical cation intermediate (**B**) could react with a strained cyclic olefin to form a [2+2] complex (**C**). Rapid ring-opening to release the ring strain would outcompete the reduction of **C**, thereby regenerating a reactive radical cation (**D**) with monomer incorporated. The active chain end would then propagate and ultimately afford ROMP polymer (**E**). Reduction of the radical cation chain end would eventually render a ROMP polymer (**F**) with vinyl ether end group.

Scheme 1.9. Hypothesized Mechanism of Redox-Mediated *o*-ROMP

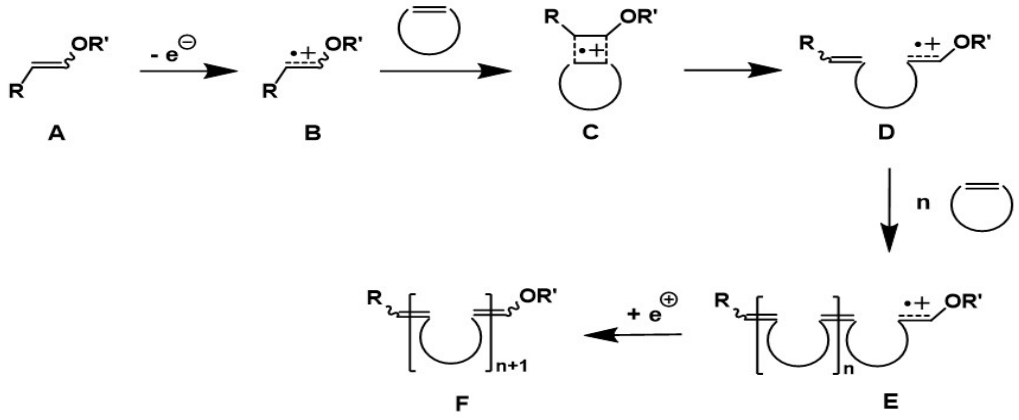

To investigate the direct oxidation of vinyl ethers and propensity for the generated radical cation to initiate ROMP, we conducted bulk electrolysis on solutions of norbornene **1** containing readily available vinyl ether initiators (**2a**, **2b** and **2c**) (Scheme 1.10).[48] We focused on using **1** as our initial screening monomer, since this structure possessed relatively high strain (~ 100 kJ/mol) among common ROMP monomers. Initial results were discouraging, as there was no detection of polymer in solution after bulk electrolysis for 3 hours. During the cleaning of the carbon fiber anode, however, we noticed the surface of anode was coated with a white precipitate that was also insoluble in methanol. Characterization of this deposited residue using ^{1}H-NMR spectroscopy revealed signals consistent with polynorbornene (PNB) prepared via traditional ROMP technique. It was also observed that the end group signal is consistent with vinyl ether after removal of any residual vinyl ether initiator through precipitation. Gel-permeation chromatography (GPC) analysis exhibited a number average molecular weight (M_n) of 11.8 kDa ($Đ$ = 2.2), which confirmed the macromolecular nature of the product. Although the yields were consistently low (only ~ 3%), these initial results confirmed that the anodic oxidation of vinyl ethers could initiate the polymerization of 1**,** likely via a ROMP-type mechanism.

Scheme 1.10. Electro-mediated *o*-ROMP and select vinyl ether initiators

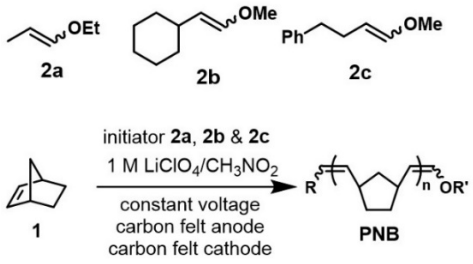

We attributed this low yield to the poor solubility of both **1** and PNB in the bulk electrolysis system that is, based on nitromethane (CH_3NO_2) and lithium perchlorate ($LiClO_4$). During electrolysis, the insolubility of PNB led to the deposition of growing polymer onto the anode surface, which prevented further oxidation of the vinyl ether initiator and resulted in a rapid

decrease in current. However, after screening various electrode materials and electrolyte/solvent combination, we realized that carbon fiber electrodes, $LiClO_4$, and $CH3NO_2$ were crucial for the success of electromediated *o*-ROMP. Other attempts to increase the yield, including the use of an ultrasonic bath, afforded small improvements (Table 1.2).

Table 1.2. Summary of results from the electro-mediated *o*-ROMP of monomer **1** and initiators **2a-c**

initiator	$[M]_0/[I]_0$[a]	M_n (kDa)[b]	$Đ$[c]	Yield (%)
2a	28/1	6.2	1.4	12
2b	28/1	4.8	1.5	14
2c	28/1	6.7	1.5	13

[a]Initial molar ratio of monomer and initiator. [b]Determined by GPC using multiangle laser light scattering (MALLS). [c]Dispersities determined by GPC.

1.3.c A Metal-Free Photochemical Approach

To circumvent the solubility issues encountered in the electrochemical set up, we questioned whether the vinyl ether radical cation could be accessed by another method. It is well known that the photoredox processes are susceptible to a broader solvent scope and homogeneous oxidation than their electrochemical counterparts. Photo-oxidants such as OPC **13** and ruthenium tris(bipyrimidine) have been used by the Nicewicz and Yoon groups respectively, for the photoredox-mediated synthesis of cyclobutanes (Scheme 1.11).[49] Assuming that a cyclic olefin would outcompete the reduction in favor of ring-opening, we envisioned that a photo-chemical ROMP could be possible.

Scheme 1.11. Photoredox-Mediated Cyclobutane Formation

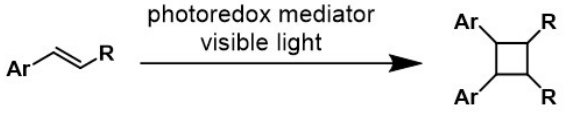

We chose pyrylium salts OPC **13** as our initial photocatalyst since it has been identified as good candidate for facilitating photooxidation and is completely organic.[48] As the oxidizing power of excited OPC **13** has been calculated to be 1.89 V vs SCE, this mediator was expected to be good oxidizers for vinyl ether initiators because the oxidation potentials of **2a-c** are in the range of 1.30 V to 1.43 V vs SCE. Our photochemical set up consisted of 3 mol% of catalyst loading relative to initiator, dichloromethane (CH_2Cl_2) as the solvent (monomer concentration ~ 1.9 M), and a 2-watt blue LED bulb (λ_{em} = 450 -480 nm) as the visible light source (Table 1.3).

Table 1.3. Summary of results from the photoredox-mediated *o*-ROMP of monomer **1**, initiators **2a-c**, and photoredox catalyst OPC **13** and Picture of Reaction Set-Up

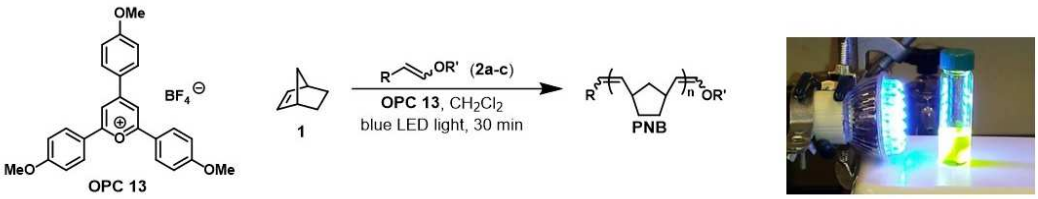

initiator	**[1]**$_0$: **[2]**$_0$: **[OPC 13]**$_0$[a]	[M]$_0$ (M)[b]	conversion[c] (%)	$M_{n,\,theo}$ [kDa]	$M_{n,\,exp}$ [kDa]	Đ
2c	97 : 1 : 0.03	1.9	88 (73)	8.0	15.1	1.7
2b	97 : 1 : 0.03	1.9	92 (80)	8.4	14.9	1.6
2a	106 : 1 : 0.03	2.0	87 (67)	9.0	15.8	1.6
2a	48 : 1 : 0.03	1.8	95 (78)	4.3	8.1	1.4
2a	491 : 1 : 0.03	5.3	51 (25)	23.6	22.2	1.5
2a	494 : 1 : 0.03	1.8	72 (50)	33.4	43.9	1.5
2a	1000 : 1 : 0.03	1.9	61 (47)	57.4	60.2	1.6

[a]Initial molar ratio of **1**, **2** and OPC **13**. [b]Initial concentration of **1**. [c]Conversion of **1**, as determined by ^{1}H-NMR analysis; isolated yields after precipitation given in parentheses. $M_{n,\,theo}$ is theoretical number average molecular weight calculated from initial **1** : **2** ratio and % conversion of **1**. $M_{n,\,exp}$ is experimental number average molecular weight determined by GPC using MALLS. Dispersities (*Đ*) determined by GPC.

Each initiator gave PNB in good yield via the photoredox pathway (Table 2). Although **2c** provides a distinguishable NMR handle, most of the polymerizations were carried out using **2a** since this vinyl ether initiator is commercially available. Varying the initial monomer to initiator loading provided a certain degree of control over the final M_n with moderate initiator. The dispersities of resultant PNB were found to vary between 1.4 and 1.7 across different experiments. We also discovered that successful polymerization could be carried out at high monomer concentration (5.3 M). This result suggests that bulk polymerizations using a liquid monomer may be possible in the future. Control experiments confirmed that the initiator, photoredox mediator, and light source were each required for successful polymerization.

During the course of the polymerization, we observed a gradual increase in M_n with increasing conversion of monomer, which is consistent with the chain growth nature of ROMP (Figure 1.5). The linearity was not as precise as traditional "living" ROMP, though there was a positive correlation. We attributed this to the relative rates of initiation and propagation in the photoredox method and, any number of early termination events.

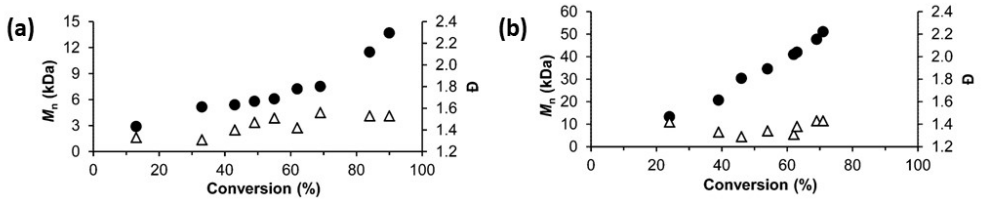

Figure 1.5. Plot of M_n (black dot) and $Đ$ (white triangle) vs % conversion of monomer using initial **1** : **2a** of (a) 100 : 1 and (b) 500 : 1.

We also discovered that light could be used to reversibly activate the vinyl ethers, which allowed a high degree of temporal control over the polymerization. We noticed that there were no significant changes in monomer conversion and molecular weight during the periods in which the light was off (Figure 1.6). And each re-exposure to light resulted in increased conversion and molecular weight. These results were consistent with the deactivation and reactivation of polymer

vinyl ether chain ends, rather than photoinitiation of new polymer chains. This level of temporal control is not possible in traditional metal-based ROMP system.

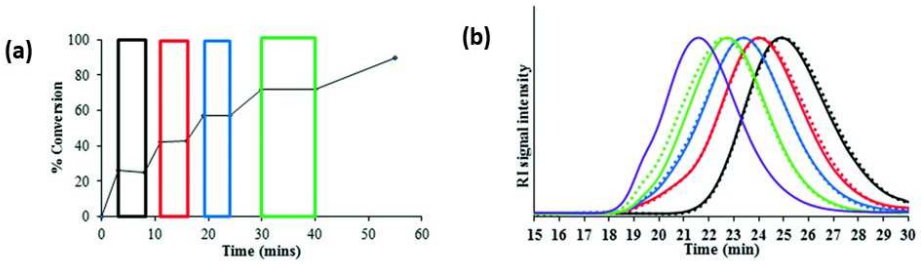

Figure 1.6. (a) Plot of percentage conversion of monomer over time (periods of dark are highlighted by rectangular boxes; (b) GPC traces for dark/light cycles (the solid lines represent GPC traces following exposure to blue LED light and the dotted lines refer to GPC traces of periods in the dark immediately following a period light; colors are correlated with those in left figure.

Notes and References to Chapter 1

[1] (a) Ouchi, M.; Sawamato, M. *Macromolecules*, **2017**, *50*, 2603. (b) Grubbs, R. B.; Grubbs, R. H. *Macromolecules*, **2017**, *50*, 6979. (c) Perrier, R. *Macromolecules*, **2017**, *50*, 7433.
[2] (a) Corrigan, N.; Yeow, J.; Judzewitsch, P.; Xu, J.; Boyer, C. *Angew. Chem. Int. Ed.*, **2019**, *58*, 5170. (b) Corrigan, N.; Shanmugam, S.; Xu, J.; Boyer, C. *Chem. Soc. Rev.*, **2016**, *45*, 6165. (c) Michaudel, Q.; Kottisch, V.; Fors, B. P. *Angew. Chem. Int. Ed.*, **2017**, *56*, 9670. (d) Chen, M.; Zhong, M.; Johnson, J. A. *Chem. Rev.*, **2016**, *116*, 10167. (e) Pan, X.; Tasdelen, M. A.; Laun, J.; Junkers, T.; Yagci, Y.; Matyjaszewski, K. *Prog. Polym. Sci.*, **2016**, *62*, 73. (f) Dadashi-Silab, S.; Doran, S.; Yagci, Y. *Chem. Rev.*, 2016, **116**, 10212.
[3] (a) Prier, C. K.; Rankic, D. A.; McMillan, D. W. C. *Chem. Rev.*, **2013**, *113*, 5322. (b) Narayanam, J. M. R.; C. R. J. Stephenson, *Chem. Soc. Rev.*, **2011**, *40*, 102.
[4] (a) Fors, B. P.; C. J. Hawker, *Angew. Chem. Int. Ed.*, **2012**, *51*, 8850. (b) Xu, J.; Jung, K.; Atme, A.; Shanmugam, S.; Boyer, C. *J. Am. Chem. Soc.*, **2014**, *136*, 5508.
[5] Romero, N. A.; Nicewicz, D. A. *Chem. Rev.*, **2016**, *116*, 10075.
[6] (a) Wang, J.-S.; Matyjaszewski, K. *J. Am. Chem. Soc.*, **1995**, *117*, 5614. (b) Kato, M.; Kamigaito, M.; Sawamoto, M.; Higashimura, T. *Macromolecules*, **1995**, *28*, 1721.
[7] Matyjaszewski, K. *Adv. Mater.*, **2018**, *30*, 1706441.
[8] (a) Treat, N. J.; Sprafke, H.; Kramer, J. W.; Clark, P. G.; Barton, B. E.; Read de Alaniz, J.; Fors, B. P.; C. J. Hawker, *J. Am. Chem. Soc.*, **2014**, *136*, 16096. (b) Miyake, G. M.; Theriot, J. C. *Macromolecules*, **2014**, *47*, 8255.
[9] Dadashi-Silab, S.; Pan, X.; Matyjaszewski, K. *Chem. Eur. J.*, **2017**, *23*, 5972.
[10] Pan, X.; Fang, C.; Fantin, M.; Malhotra, N.; So, W. Y.; Peteanu, L. A.; Isse, A. A.; Gennaro, A.; Liu, P.; Matyjaszewski, K. *J. Am. Chem. Soc.*, **2016**, *138*, 2411.
[11] Liang, Y.; Bergbreiter, D. E. *Polym. Chem.*, **2016**, *7*, 2161.
[12] (a) Sartor, S. M.; McCarthy, B. G.; Person, R. M.; Miyake, G. M.; Damrauer, N. H. *J. Am. Chem. Soc.*, **2018**, *140*, 4778. (b) Lim, C.-H.; Ryan, M. D.; McCarthy, B. G.; Theriot, J. C.; Sartor, S. M.; Damrauer, N. H.; Musgrave, C. B.; Miyake, G. M. *J. Am. Chem. Soc.*, **2017**, *139*, 348. (c) Pearson, R. M.; Lim, C.-H.; McCarthy, B. G.; Musgrave, C. B.; Miyake, G. M. *J. Am. Chem. Soc.*, **2016**, *138*, 11399. (d) Theriot, J. C.; Lim, C.-H.; Yang, H.; Ryan, M. D.; Musgrave, C. B.; Miyake, G. M. *Science*, **2016**, *352*, 1082-1086. (e) McCarthy, B. G.; Pearson, R. M.; Lim, C.-H.; Sartor, S. M.; Damrauer, N. H.; Miyake, G. M. *J. Am. Chem. Soc.*, **2018**, *140*, 5088.
[13] Cole, J. P.; Federico, C. R.; Lim, C.-H.; Miyake, G. M. *Macromolecules*, **2019**, *52*, 747.
[14] McCarthy, B. G.; Miyake, G. M. *ACS Macro Lett.*, **2018**, *7*, 1016.
[15] (a) Huang, Z.; Gu, Y.; Liu, X.; Zhang, L.; Cheng, Z.; Zhu, X. *Macromol. Rapid Commun.*, **2017**, *38*, 1600461. (b) Kutahya, C.; Allushi, A.; Isci, R.; Kreutzer, J.; Ozturk, T.; Yilmaz, G.; Yagci, Y. *Macromolecules*, **2017**, *50*, 6903.
[16] (a) Allushi, A.; Kutahya, C.; Aydogan, C.; Kreutzer, J.; Yilmaz, G.; Yagci, Y. *Polym. Chem.*, **2017**, *8*, 1972. (b) Kutahya, C.; Aykac, F. S.; Yilmaz, G.; Yagci, Y. *Polym. Chem.*, **2016**, *7*, 6094. (c) Liu, X.; Zhang, L.; Cheng, Z.; Zhu, X. *Polym. Chem.*, **2016**, *7*, 689.
[17] Bian, C.; Zhou, Y.-N.; Guo, J.-K.; Luo, Z.-H. *Macromolecules*, **2018**, *51*, 2367.
[18] Furst, L.; Matsuura, B. S; Narayanam, J. M. R.; Tucker, J. W.; Stephenson, C. R. J. *Org. Lett.*, **2010**, *12*, 3104.
[19] (a) Theriot, J. C.; McCarthy, B. G.; Lim, C.-H.; Miyake, G. M. *Macromol. Rapid Commun.*, **2017**, *38*, 1700040. (b) Ryan, M. D.; Theriot, J. C.; Lim, C.-H.; Yang, H.; Lockwood, A. G.; Garrison, N. G.; Lincoln, S. R.; Musgrave, C. B.; Miyake, G. M. *J. Polym. Sci., Part A: Polym. Chem.*, **2017**, *55*, 3017.

[20] (a) Wang, J.; Yuan, L.; Wang, Z.; Rahman, M. A.; Huang, Y.; Zhu, T.; Wang, R.; Chen, J.; Wang, C.; Chu, F.; Tang, C. *Macromolecules*, **2016**, *49*, 7709. (b) Li, S.; Mohamed, A. I.; Pande, V.; Wang, H.; Cuthbert, J.; Pan, X.; He, H.; Wang, Z.; Viswanathan, V.; Whitacre, J. F.; Matyjaszewski, K. *ACS Energy Lett.*, **2018**, *3*, 20.
[21] Pan, X.; Lamson, M.; Yan, J.; Matyjaszewski, K. *ACS Macro Lett.*, **2015**, *4*, 192.
[22] Discekici, E. H.; Amant, A. H. St.; Nguyen, S. N.; Lee, I.-H.; Hawker, C. J.; Read de Alaniz, J. *J. Am. Chem. Soc.*, **2018**, *140*, 5009.
[23] Chiefari, J.; Chong, Y. K.; Ercole, F.; Kristina, J.; Jeffery, J.; Le, T. P. T.; Mayadunne, R. T. A.; Meijs, G. F.; Moad, C. L.; Moad, G.; Rizzardo, E.; Thang, S. H. *Macromolecules*, **1998**, *31*, 5559.
[24] Xu, J.; Shanmugam, S.; Duong, H. T.; Boyer, C. *Polym. Chem.*, **2015**, *6*, 5615.
[25] Shanmugam, S.; J. Xu, J.; Boyer, C. *Macromolecules*, **2016**, *49*, 9345.
[26] Shanmugam, S.; J. Xu, J.; Boyer, C. *Macromolecules*, **2017**, *50*, 1832.
[27] Yeow, J.; Chapman, R.; Xu, J.; Boyer, C. *Polym. Chem.*, **2017**, *8*, 5012.
[28] Wu, C.; Corrigan, N.; Lim, C.-H.; Jung, K.; Zhu, J.; Miyake, G. M.; Xu, J.; Boyer, C. *Macromolecules*, **2019**, *52*, 236.
[29] Wu, C.; Chen, H.; Corrigan, N.; Jung, K.; Kan, X.; Li, Z.; Liu, W.; Xu, J.; Boyer, C. J. Am. Chem. Soc.,
[30] Xu, J.; Shanmugam, S.; Boyer, C. *ACS Macro Lett.*, **2015**, *4*, 926.
[31] Chen, M.; MacLeod, M. J.; Johnson, J. A. *ACS Macro Lett.*, **2015**, *4*, 565.
[32] Chen, M.; Deng, S.; Gu, Y.; Lin, J.; MacLeod, M. J.; Johnson, J. A. *J. Am. Chem. Soc.*, **2017**, *139*, 2257.
[33] (a) Chu, Y.; Huang, Z.; Liang, K.; Guo, J.; Boyer, C.; Xu, J. *Polym. Chem.*, **2018**, *9*, 1666. (b) Chu, Y.; Corrigan, N.; Wu, C.; Boyer, C.; Xu, J. *ACS Sustainable Chem. Eng.*, **2018**, *6*, 15245. (c) Shanmugam, S.; Xu, S.; Adnan, N. N. M.; Boyer, C. *Macromolecules*, **2018**, *51*, 779.
[34] Lee, I.-H.; Discekici, E. H.; Anastasaki, A.; Read de Alaniz, J.; Hawker, C. J. *Polym. Chem.*, **2017**, *8*, 3351.
[35] Xu, J.; Shanmugam, S.; Fu, C.; Aguey-Zinsou, K.-F.; Boyer, C. *J. Am. Chem. Soc.*, **2016**, *138*, 3094.
[36] Xu, J.; Fu, C.; Shanmugam, S.; Hawker, C. J.; Moad, G.; Boyer, C. *Angew. Chem. Int. Ed.*, **2017**, *56*, 8376.
[37] Huang, Z.; Noble, B. B.; Corrigan, N.; Chu, Y.; Satoh, K.; Thomas, D. S.; Hawker, C. J.; Moad, G.; Kamigaito, M.; Coote, M. L.; Boyer, C.; Xu, J. *J. Am. Chem. Soc.*, **2018**, *140*, 13392.
[38] Aoshima, S.; Kanaoka, S. *Chem. Rev.,* **2009**, *109*, 5245.
[39] (a) Uchiyama, M.; Satoh, K.; Kamigaito, M. *Angew. Chem. Int. Ed.*, **2015**, *54*, 1924. (b) Sugihara, S.; Konegawa, N.; Maeda, Y. *Macromolecules*, **2015**, *48*, 5120.
[40] Kottisch, V.; Michqudel, Q.; Fors, B. P. *J. Am. Chem. Soc.*, **2016**, *138*, 15535.
[41] Michqudel, Q.; Chauviré, T.; Kottisch, V.; Supej, M. J.; Stawiasz, K. J.; Shen, L.; Zipfel, W. R.; Abruña, H. D.; Freed, J. H.; Fors, B. P. *J. Am. Chem. Soc.*, **2017**, *139*, 15530.
[42] Kottisch, V.; Michqudel, Q.; Fors, B. P. *J. Am. Chem. Soc.*, **2017**, *139*, 10665.
[43] Kottisch, V.; Supej, M. J.; Fors, B. P. *Angew. Chem. Int. Ed.*, **2018**, *57*, 1.
[44] Bielawski, C. W.; Grubbs, R. H. *Prog. Polym. Sci.,* **2007**, *32*, 1.
[45] (a) Chaunvin, Y. *Angew. Chem., Int. Ed.,* **2006**, *45*, 3740. (b) Schrock, R. R. *Acc. Chem. Res.,* **1986**, *19*, 342. (c) Schrock, R. R. *Chem. Rev.,* **2009**, *109*, 3211. (d) Vougioukalakis, G. C.; Grubbs, R. H. *Chem. Rev.,* **2010**, *110*, 1746.
[46] Vougioukalakis, G. C. *Chem.—Eur. J.,* **2012**, *18*, 8868.

[47] (a) Chiba, K.; Miura, T.; Kim, S.; Kitano, Y.; Tada, M. *J. Am. Chem. Soc.,* **2001**, *123*, 11314. (b) Miura, T.; Kim, S.; Kitano, Y.; Tada, M.; Chiba, K. *Angew. Chem., Int. Ed.* **2006**, *45*, 1461.
[48] Ogawa, K. A.; Goetz, A. E.; Boydston, A. J. *J. Am. Chem. Soc.,* **2015**, *137*, 1400.
[49] (a) Du, J.; Skubi, K. L.; Schultz, D. M.; Yoon, T. P. *Science,* **2014**, *344*, 392. (b) Riener, M.; Nicewicz, D. A. *Chem. Sci.,* **2013**, *4*, 2625. (c) Lu, Z.; Yoon, T. P. *Angew. Chem., Int. Ed.,* **2012**, *51*, 10329.

Chapter 2. Multidirectional Photoredox-Mediated Ring-Opening Metathesis Polymerization (ROMP) Grafting from Organic Initiators[1]

Section 1: Introduction

2.1.a Metallic Initiators versus Organic Initiators

To synthesize ROMP polymer with different architectures, various multifunctional metallic initiators, which ROMP is grafted from, has been prepared.[1-8] The challenge encountered in the preparation of those well-defined initiators usually includes 1) the design of appropriate multifunctional ligand and 2) low yields of cross-metathesis between ligand and metal precursors. Undoubtedly, the design and synthesis of multifunctional metallic macroinitiators will be more difficult compared to corresponding small-molecular analogue.[9]

On the other hand, the organic photoredox-mediated ROMP (*o*-ROMP) utilizes vinyl ethers as initiators, which are easier to install relative to metallic counterpart.[10-13] We envisioned the use of vinyl ether initiators to provide unique synthetic routes to multi-topic initiators, such as those that could lead to bidirectional polymer chain growth, multi-arm star polymers, or graft-from brush polymers. A potential caveat of the vinyl ether initiators is that high effective concentrations of initiator sites could lead to unwanted intramolecular reactions between oxidized and neutral species.[14-15] To [1]investigate the feasibility of organocatalyzed ROMP from multi-topic initiators, we evaluated a series of divinyl ethers in bidirectional ROMP.

[1] Reproduced with permission from Lu, P.; Alrashdi, N. M.; Boydston, A. J. "Bidirectional Metal-Free ROMP from Difunctional Organic Initiators" *J. Polym. Sci., Part A: Polym. Chem.* **2017**, *55*, 2977. Copyright 2017 Wiley Periodicals, Inc.

Section 2: Results and Discussion

2.2.a Grafting o-ROMP from Difunctional Initiators

We first prepared and investigated two pseudo-isomeric divinyl ether initiators (**1** and **2**, Figure 2.1). Our intention was to preserve the spacing between reactive sites of the vinyl ether moieties while varying the nature of the monomer incorporation. Specifically, initiator **1** would incorporate monomers via insertion at the center of the outwardly-growing polymer, whereas initiator **2** would propagate via an active chain end mechanism.

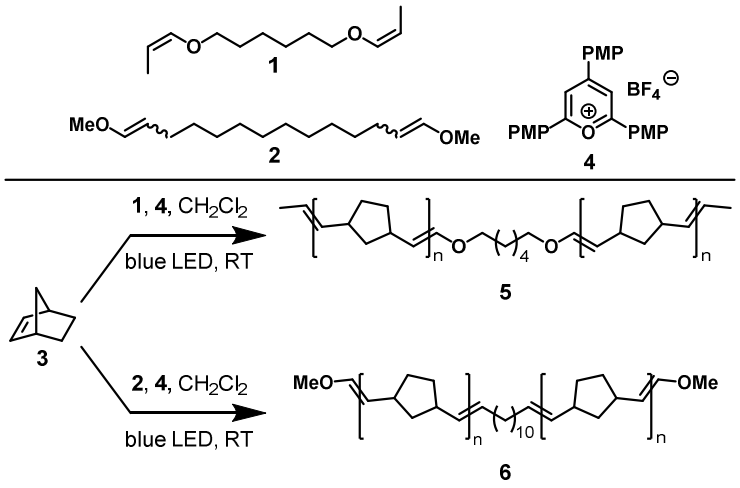

Figure 2.1. Small-molecular divinyl ether initiators and pyrylium photoredox catalyst used in this study (top). Organocatalyzed ROMP of norbornene (bottom).

Each initiator was found to undergo organocatalyzed ROMP of norbornene (**3**) under our previously reported conditions using 2,4,6-tris(4-methoxyphenyl)pyrylium tetrafluoroborate (**4**) as a photoredox catalyst. Averaged data from three parallel runs are summarized in Table 2.1. Using an initial monomer to vinyl ether molar ratio ($[\mathbf{3}]_0/[VE]_0$) of 50:1, initiator **1** provided polynorbornene **5** with excellent agreement between theoretical and experimental M_n values (entry 1). Notably, these initiator efficiencies, which are near unity, are considerably higher than observed for organocatalyzed ROMP using ethyl propenyl ether as initiator under similar conditions. In comparison with **1**, initiator **2** also proceeded with high conversion of monomer (entry 2) although

the initiator efficiency was found to be lower than for **1**, and more consistent with previous polymerizations using ethyl propenyl ether. Attempts to identify products of deleterious reaction pathways from the initiators were met with limited success.

Table 2.1. Summary of Results for Bidirectional *o*-ROMP from **1** and **2**.

Entry	Initiator	$[\mathbf{3}]_0/[VE]_0$	Time (min)	Conversion[a] (%)	$M_{n,\,theo}$[b] (kDa)	$M_{n,\,GPC}$[c] (kDa)	$M_{w,\,GPC}$[c] (kDa)	$Đ$[d]	IE[e] (%)
1	**1**	50	75	82 ± 4	7.9 ± 0.4	8.0 ± 0.9	10.3 ± 0.5	1.29 ± 0.08	98 ± 7
2	**2**	50	75	83 ± 4	8.1 ± 0.3	12.3 ± 2.2	14.7 ± 2.7	1.20 ± 0.01	67 ± 12
3	**1**	500	35	33%	31.2	46.0	54.4	1.2	68

[a] Monomer conversion as judged by ^{1}H NMR spectroscopy of crude reaction mixture. [b] Theoretical number-average molecular weight based upon initial monomer to initiator loading and monomer conversion. [c] Determined by gel-permeation chromatography using in-line multi-angle laser light scattering and RI detection. [d] Molecular weight dispersity. [e] Initiator efficiency = $M_{n,\,theo}/M_{n,\,GPC}$. Rows 1 and 2 reflect average of three runs, error = one standard deviation.

Despite the differences in initiator efficiency, we found that **1** and **2** gave comparable rates of polymerization (Figure 2.2). This suggested to us that since **2** suffers from some nonproductive initiator consumption (lower initiator efficiency), the rate of monomer incorporation with **2** is likely higher than for **1**. We speculate that disparate steric access to the active vinyl ether site is the cause of the different propagation rates.

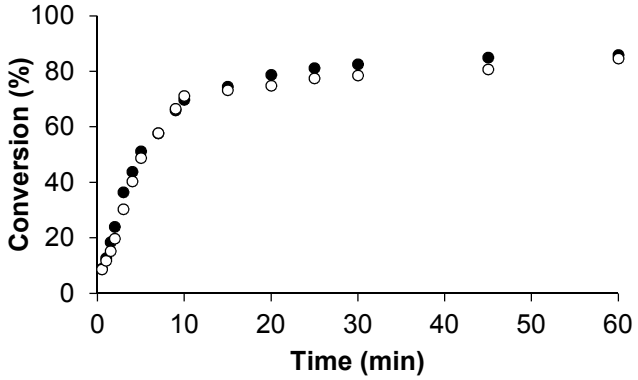

Figure 2.2. Conversion versus time for organocatalyzed ROMP from initiators **1** (black) and **2** (white)

The vinyl ether moieties in polymer **5** provide opportunities for post-polymerization modification and controlled degradation. In our studies, we were able to confirm the bidirectional chain growth from initiator **1** via hydrolysis experiments. We first prepared a higher molecular weight sample (Table 1, entry 3, M_n = 46.0 kDa, $Đ$ = 1.2) such that the daughter fragments would be of sufficient molecular weight for analysis. After subjecting this sample of polymer **5** to vinyl ether hydrolysis using Amberlyst 15 ion-exchange resin, we found that the resulting polynorbornene product had a monomodal molecular weight distribution and M_n = 24.0 kDa ($Đ$ = 1.1), roughly half that of the initial polymer (Figure 2.3). These results are consistent with ca. equal chain lengths having been synthesized from each initiator site.

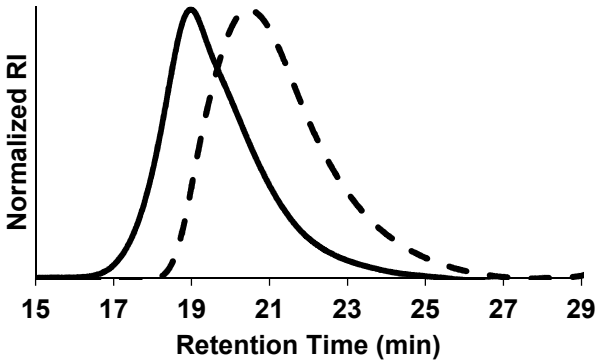

Figure 2.3. GPC traces of polymer 5 (M_n = 45 kDa) as isolated via precipitation (solid) and after hydrolysis (dashed, M_n = 24 kDa).

2.2.b. Grafting o-ROMP from Polyether-based Macroinitiators

Motivated by the success of the bidirectional chain growth, we considered broader applications in the synthesis of degradable triblock copolymers. Toward this end, we prepared a ditopic initiator (**7**) from poly(propylene glycol) (PPG) as shown in Figure 2.4 (M_n = 1.0 kDa). Organocatalyzed ROMP proceeded smoothly with 67% monomer conversion to yield triblock copolymer **8** having M_n = 15.9 kDa ($Đ$ = 1.2) based upon GPC analysis. The calculated initiator

efficiency was only 37%, although we observed a monomodal molecular weight distribution by GPC (Figure 2.5, left). Upon hydrolysis, GPC analysis revealed a monomodal product peak with M_n = 5.9 kDa ($Đ$ = 1.3), slightly less than half that of the original polymer (minus the PPG block). Additionally, a low molecular peak was observed that was consistent with the retention time of the PPG initiator. These results were consistent with roughly uniform polymer growth from each initiator site.

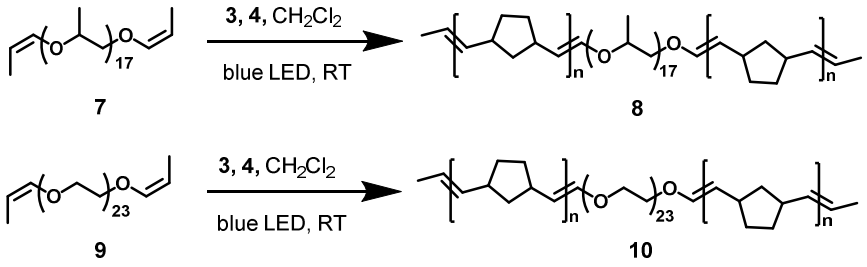

Figure 2.4. *o*-ROMP from polyether-based macroinitiators.

Using a similar approach, we also prepared difunctional initiator **9** based upon poly(ethylene glycol) (PEG). Again, organocatalyzed ROMP provided an ABA triblock copolymer (**10**) after moderate monomer conversion. GPC analysis of **10** (Figure 2.5, right) after isolation by precipitation revealed M_n = 8.6 kDa (Đ = 1.5). After hydrolysis with Amberlyst 15 resin, the resulting polymer was found to have M_n = 5.1 kDa (Đ = 1.6).

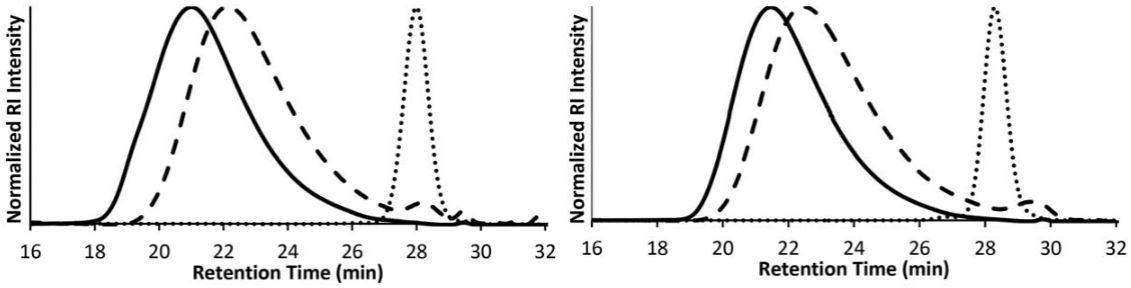

Figure 2.5. GPC traces of macroinitiators (dotted), copolymers (solid), and hydrolyzed polymers (dashed). Left, GPC traces for **7**, **8**, and hydrolysis of **8**. Right, GPC traces for **9**, **10**, and hydrolysis of **10**.

2.2.c Grafting o-ROMP from Polystyrene-based Macroinitiators

We turned our attention toward grafting from a statistical copolymer. Toward this end, macroinitiator was prepared by a sequence of metal-mediated ATRP, dehalogenation of chain-end, and isomerization of side-chain olefins (Figure 2.6). Analysis of by GPC (Figure 2.7) revealed M_n = 2.2 kDa ($Đ$ = 1.1) and ^{1}H-NMR analysis was consistent with an average of three vinyl ether moieties per chain.

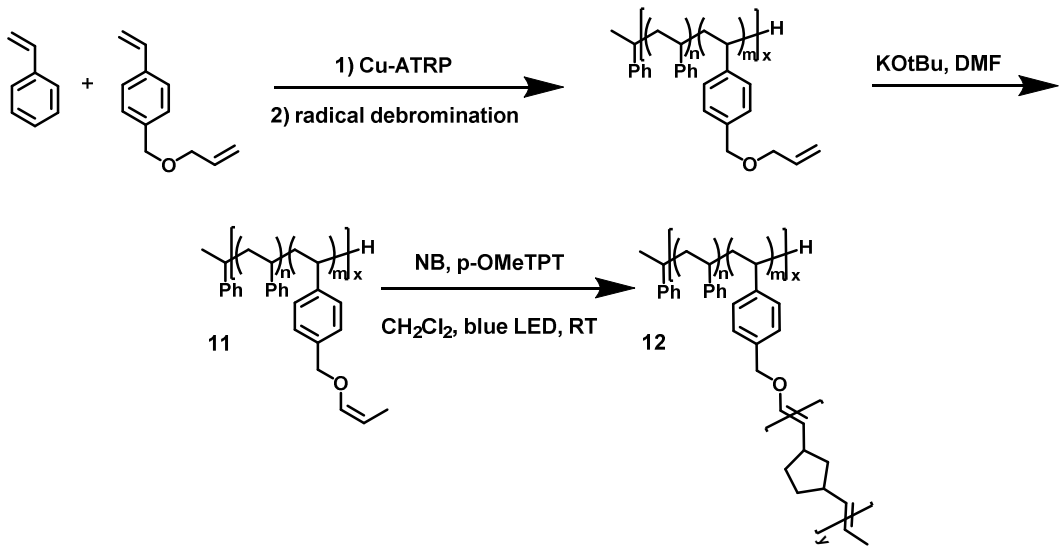

Figure 2.6. Synthesis of polystyrene-based macroinitiators and corresponding *o*-ROMP.

When subjected to *o*-ROMP conditions, polymer was obtained with 64% monomer conversion. The isolated polymer was found to have M_n = 28.2 kDa ($Đ$ = 1.6) by GPC analysis (Figure 2.7). After treatment with Amberlyst 15 ion-exchange resin, the resulting polymer was found to have a reduced molecular weight of M_n = 18.3 kDa ($Đ$ = 1.7). Assuming complete hydrolysis of all vinyl ether moieties, the molecular weight of cleaved polynorbornene daughter fragments are consistent with about 53% of the vinyl ether moieties having initiated *o*-ROMP.

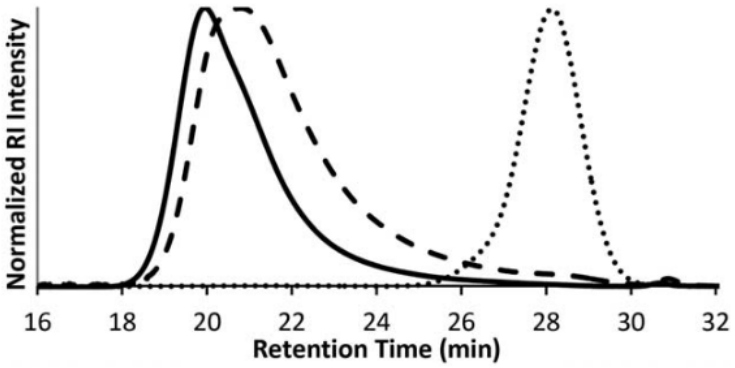

Figure 2.7. GPC traces of macroinitiators (dotted), copolymers (solid), and hydrolyzed polymers (dashed). GPC traces for

Section 3: Conclusions

In conclusion, we have demonstrated bidirectional polymer growth in *o*-ROMP from difunctional initiators. Evaluation of inwardly growing polymers versus outwardly growing polymers revealed that incorporation of monomers at chain end and chain-centered active sites were successful. The ability to grow polymer chains from internal active sites enabled rapid access to cleavable copolymers based upon PPG, PEG, and polystyrene macroinitiators. The relative ease with which vinyl ether moieties can be installed on potential initiator structures holds promise for access to a broader diversity of *o*-ROMP nanostructures. Herein, we established the feasibility and first steps toward this end.

Section 4: Experimental

General Consideration. Dimethylformamide (DMF), dimethyl sulfoxide (DMSO), Dichloromethane (CH_2Cl_2), and tetrahydrofuran (THF) were obtained from a solvent purification system. For polymerization of norbornene, CH_2Cl_2 was dried over 4Å molecular sieves before use. All polymerization were carried out in standard borosilicate glass vials with magnetic stirring. Irradiation of photochemical reactions was done using a 2 W Miracle blue LED indoor gardening

bulb purchased from Amazon. Norbornene was sublimed prior to use. All other reagents and solvents were obtained from commercial sources and used as received unless otherwise noted. ^{1}H and ^{13}C NMR spectra were recorded on Bruker AVance 300 MHz or 500 MHz spectrometers. Chemical shifts are reported in delta (δ) units, expressed in parts per million (ppm) downfield from tetramethylsilane using the residual protio-solvent as an internal standard (CDCl3, ^{1}H: 7.26 ppm and ^{13}C: 77.0 ppm). Data are reported as follows: chemical shift, multiplicity (s = singlet, d = doublet, dd = doublet of doublet, dt = doublet of triplets, q = quartet, m = multiplet, br = broad peak), coupling constants (Hz) and integration. Gel Permeation Chromatography (GPC) was performed using a GPC setup consisting of: an Agilent pump, 3 in-line columns, and Wyatt light scattering and refractive index detectors with THF as the mobile phase. Number average molecular weight (M_n) and weight average molecular weight (M_w) were calculated from light scattering. The pyrylium tetrafluoroborate was prepared according to literature procedure.[16]

Synthesis of Initiator 1. To a suspension of NaH (2.8 grams, 69.96 mmol) in DMF (20 mL) at 0 °C was added a DMF solution of hexanediol dropwise (20 mL, 1.06 M, 21.2 mmol). The reaction mixture was stirred at room temperature for 30 mins. Then allyl bromide (4 mL, 46.5 mmol) was added dropwise into the reaction at 0 °C. The reaction was warmed to room temperature. After 17 hours, deionized water (5 mL) was added dropwise into the reaction at 0 °C to quench excess NaH. More deionized water (100 mL) was poured into the reaction and the suspension was extracted with Et_2O (4*50 mL). The combined organic layer was dried with Na_2SO_4. The solvent was evaporated to give the crude product as a yellow oil which was purified by flash chromatography (10 : 1 Hexane : Ether eluent). The spectral data matched those previously reported.[17]

The allyl ether obtained from previous steps (1.1 grams, 5.5 mmol) in DMSO (30 mL) at 0 °C was added potassium tert-butoxide (5.0 grams, 40.9 mmol) in single portion. The reaction was warmed to room temperature. After 6 hours, deionized water (5 mL) was added dropwise into the reaction at 0 °C to quench excess KOtBu. More deionized water (100 mL) was poured into the reaction and the suspension was extracted with Et_2O (4*50 mL). The combined organic layer was dried with Na_2SO_4. The solvent was evaporated to give the crude product as a yellow oil which was purified by passing through a silica plug using hexane. The spectral data matched those previously reported.[17]

Synthesis of Initiator 2. To the suspension of 1,12-dodecanediol (2.02 grams, 10 mmol) in DCM (30 mL) was added 2,2,6,6-Tetramethyl-1-piperidinyloxy (TEMPO) (313 mg, 2 mmol) and (Diacetoxyiodo) benzene (7.09 grams, 22 mmol). After 20 hours, the reaction was diluted with DCM (30 mL) and the solution was washed with saturated $Na_2S_2O_3$ aqueous solution (60 mL). The water phase was then extracted with DCM (3*20 mL). The combined organic layer was dried with Na2SO4. The solvent was evaporated to give the crude product which was purified by flash chromatography (8 : 1 Hexane : Ethyl Acetate). The spectral data matched those previously reported.[18]

A solution of potassium tert-butoxide (2.97 grams, 24.3 mmol) in 8 mL of THF was slowly added to a solution of (methoxymethyl)triphenylphosphonium chloride (8.3 grams, 24.3 mmol) in 30 mL of THF. After stirring the solution for 1 hour, a solution of the dialdehyde (1.6 grams, 8.1 mmol) in 10 mL THF was added dropwise and allowed to stir at room temperature for 2 hours. The solution was diluted with ether and washed with deionized water. The organic phase was collected

and dried with Na_2SO_4. The solvent was evaporated and the crude product was dissolved in hexane. The precipitates was filtered and the filtrate was concentrated. The residual triphenyl phosphine was removed by stirring overnight with 1.5 mL of methyl iodide and filtration through a plug of silica with diethyl ether as eluent. The product was prepared according to above procedure in 50% yield (2:3 *cis* to *trans* ratio). ^{1}H NMR (500 MHz, $CDCl_3$) δ = 6.27 (d, *J* = 12 Hz, 1H, *trans*) 5.85 (d, *J* = 6 Hz, 0.7H, *cis*) 4.72 (dt, J = 12 Hz, 7.5 Hz, 1H, *trans*) 4.33 (dt, J = 6 Hz, 7.5 Hz, 0.7H, *cis*) 3.56 (s, 2H, *cis*) 3.49 (s, 3H, *trans*) 2.04 (q, *J* = 7 Hz, 1.4H, *cis*) 1.90 (q, *J* = 7 Hz, 2.6H, *trans*) 1.22-1.35 (m, 16H, *cis/trans*); ^{13}C NMR (125 MHz, $CDCl_3$) δ = 147.1, 146.1, 107.3, 103.4, 59.5, 56.0, 30.9, 30.0, 29.8, 29.6, 29.4, 29.2, 27.8, 24.0; GC-MS *(m/z)* calcd for $C_{16}H_{30}O_2$, 254.2; found, 254.3.

Synthesis PPG Divinyl Ether 7. To a suspension of NaH (3.0 grams, 75.00 mmol) in DMF (20 mL) at 0 °C was added a DMF solution of PPG-diol dropwise (10 mL, 0.50 M, 5.00 mmol). The reaction mixture was stirred at room temperature for 30 mins. Then allyl bromide (4.3 mL, 50 mmol) was added dropwise into the reaction at 0 °C. The reaction was warmed to room temperature. After 24 hours, deionized water (5 mL) was added dropwise into the reaction at 0 °C to quench excess NaH. More deionized water (100 mL) was poured into the reaction and the suspension was extracted with Et_2O (4*50 mL). The combined organic layer was dried with Na_2SO_4. The solvent was evaporated to give the crude product as a yellow oil which was purified by flash chromatography (20 : 1 DCM : Methanol). ^{1}H-NMR (500 MHz, $CDCl_3$) δ = 5.93-5.85 (m, 2H) 5.24 (d, *J* = 17.5 Hz, 2H) 5.11 (d, *J* = 10.5 Hz, 2H) 4.05-4.02 (m, 4H) 3.75-3.25 (br, 52H) 1.14-1.06 (br, 52H).

To a solution of PPG-diallyl ether (2.7 grams, 2.7 mmol) in DMF (20 mL) at 0 °C was added potassium tert-butoxide (2.0 grams, 16.32 mmol) in single portion. The reaction was warmed to room temperature. After 24 hours, deionized water (5 mL) was added dropwise into the reaction at 0 °C. More deionized water (100 mL) was poured into the reaction and the suspension was extracted with Et_2O (4*50 mL). The combined organic layer was dried with Na_2SO_4. The solvent was evaporated to give the crude product as a yellow oil which was purified by flash chromatography (15 : 1 DCM : Methanol). ^{1}H-NMR (300 MHz, $CDCl_3$) δ = 6.05-5.97 (m, 2H) 4.40-4.29 (m, 2H) 3.89-3.77 (m, 2H) 3.62-3.26 (br, 58H) 1.54 (dd, *J* = 6.9 Hz, 1.8Hz, 6H) 1.19 (dd, *J* = 6.6Hz, 2.4Hz, 6H) 1.15-1.07 (br, 54H).

Synthesis of PEG Divinyl Ether 9. To a suspension of NaH (3.0 grams, 75.00 mmol) in DMF (20 mL) at 0 °C was added a DMF solution of PEG-diol dropwise (10 mL, 0.50 M, 5.00 mmol). The reaction mixture was stirred at room temperature for 30 mins. Then allyl bromide (4.3 mL, 50 mmol) was added dropwise into the reaction at 0 °C. The reaction was warmed to room temperature. After 24 hours, deionized water (5 mL) was added dropwise into the reaction at 0 °C to quench excess NaH. More deionized water (100 mL) was poured into the reaction and the suspension was extracted with CH_2Cl_2 (4*50 mL). The combined organic layer was dried with Na_2SO_4. The solvent was evaporated to give the crude product as a yellow solid which was purified by flash chromatography (20 : 1 CH_2Cl_2 : Methanol). ^{1}H-NMR (500 MHz, $CDCl_3$) δ = 5.93-5.85 (m, 2H) 5.20 (d, *J* = 17.5 Hz, 2H) 5.11 (d, *J* = 10.5 Hz, 2H) 3.98-3.91 (m, 4H) 3.62-3.54 (br, 92H). To a solution of PEG-diallyl ether (2.7 grams, 2.7 mmol) in DMF (20 mL) at 0 °C was added potassium tert-butoxide (2.0 grams, 16.32 mmol) in single portion. The reaction was warmed to room temperature. After 24 hours, deionized water (5 mL) was added dropwise into the reaction

at 0 °C. More deionized water (100 mL) was poured into the reaction and the suspension was extracted with CH_2Cl_2 (4*50 mL). The combined organic layer was dried with Na_2SO_4. The solvent was evaporated to give the crude product as a yellow solid which was purified by flash chromatography (15 : 1 CH_2Cl_2 : Methanol). ^{1}H-NMR (300 MHz, $CDCl_3$) δ = 6.01-5.91 (m, 2H) 4.43-4.31 (m, 2H) 3.89-3.82 (m, 6H) 3.66-3.61 (br, 92H) 1.54 (dd, *J* = 6.9 Hz, 1.8Hz, 6H).

Synthesis of Polystyrene Macroinitiator. 4-Vinylbenzyl alcohol was first obtained according to literature procedure. To a suspension of NaH (2.7 grams, 67 mmol) in DMF (75 mL) at 0 °C was added a DMF solution of 4-vinylbenzyl alcohol dropwise (20 mL, 2.23M, 44.5 mmol). The reaction mixture was stirred at room temperature for 30 mins. Then allyl bromide (4.25 mL, 49 mmol) was added dropwise into the reaction at 0 °C. The reaction was warmed to room temperature. After 17 hours, deionized water (5 mL) was added dropwise into the reaction at 0 °C to quench excess NaH. More deionized water (100 mL) was poured into the reaction and the suspension was extracted with Et_2O (4*50 mL). The combined organic layer was dried with Na_2SO_4 and then decanted. The solvent was evaporated to give the crude product as a colorless oil which was purified by flash chromatography (10 : 1 Hexane : Ether eluent). The product was prepared according to above procedure in 80% yield. ^{1}H NMR (300 MHz, $CDCl_3$) δ = 7.42 (d, *J* = 8.1 Hz, 2H) 7.33 (d, *J* = 8.1 Hz, 2H) 6.74 (dd, *J* = 17.4 Hz, 10.8 Hz, 1H) 6.04-5.92 (m. 1H) 5.76 (dd, *J* = 17.7 Hz, 1H) 5.37-5.21 (m, 3H) 4.53 (s, 2H) 4.05 (d, *J* = 5.7 Hz, 2H); ^{13}C NMR (75 MHz, $CDCl_3$) δ = 138.1, 137.1, 136.7, 134.9, 128.0, 126.3, 117.2, 113.8, 71.9, 71.2;

In a nitrogen-filled drybox, initiator 1-bromoethyl benzene (51.7 mg, 0.279 mmol, 1.0 equiv.), styrene (2.6 ml, 22.7 mmol, 80 equiv.), monomer 11 (976.8 mg, 5.6 mmol, 20 equiv.), dry toluene

(2 ml) and a magnetic stir bar were added into a 20 ml scintillation vial. A solution of CuBr (20.2 mg, 0.14 mmol, 0.5 equiv.) and PMDETA (24.2 mg, 0.14 mmol, 0.5 equiv.) in toluene (1.0 ml) was then added to the reaction mixture. The vial was sealed with a Teflon-lined screw cap and the reaction solution was stirred at 90 °C for 3 hours. Then the reaction mixture was open to air after the vial cooled back to room temperature. The viscous solution was diluted with CH_2Cl_2 and the solution was filtered through a neutral alumnia plug. The solvent was concentrated down to about 3 ml under reduced pressure. The solution was then added dropwise into an excess of cold MeOH causing the polymer to precipitate from solution. The precipitated polymer was collected by filtration and dried under reduced pressure. The polymer was isolated in 20% yield according to above procedure. ^{1}H NMR (300 MHz, $CDCl_3$) δ = 7.35-6.28 (br, 87H) 6.09-5.85 (br, 3H) 5.42-5.12 (br, 6H) 4.60-4.25 (br, 6H) 4.15-3.80 (br, 6H) 2.60-0.90 (br, 54H);

In a nitrogen-filled drybox, the copolymer obtained in previous step, dry toluene (2 ml) and a magnetic stir bar were added into a 20 ml scintillation vial. A solution of CuBr (7.2 mg, 0.05 mmol) and PMDETA (8.7 mg, 0.05 mmol) in toluene (1.0 ml) was then added to the reaction mixture. The vial was sealed with a rubber septa. Then tributyltin hydride (80 μl) was added into the reaction mixture by syringe. The reaction solution was stirred at 90 °C for 5 hours. Then the reaction mixture was open to air after the vial cooled back to room temperature. The viscous solution was diluted with CH_2Cl_2 and the solution was filtered through a neutral alumnia plug. The solvent was concentrated down to about 3 ml under reduced pressure. The solution was then added dropwise into an excess of cold MeOH causing the polymer to precipitate from solution. The precipitated polymer was collected by filtration and dried under reduced pressure. The polymer was isolated in 90% yield according to above prodecure. ^{1}H NMR (300 MHz, $CDCl_3$) δ = 7.35-

6.28 (br, 87H) 6.09-5.85 (br, 3H) 5.42-5.12 (br, 6H) 4.60-4.25 (br, 6H) 4.15-3.80 (br, 6H) 2.60-0.90 (br, 54H);

The copolymer obtained in the previous step was dissolved in dry DMF (20 ml) at 0 °C and then potassium tert-butoxide (240 mg, 1.96 mmol) was added in a single portion. The reaction was warmed to room temperature. After 20 hours, the reaction solution was filtered through a neutral alumnia plug. The solvent was concentrated down at reduced pressure. Then the polymer was dissolved into 3 ml CH_2Cl_2 and the polymer was precipitated by adding the CH_2Cl_2 solution dropwise into cold MeOH. The polymer was collected by filtration and dried under reduced pressure. The polymer was isolated in 80% yield according to above procedure. ^{1}H NMR (300 MHz, $CDCl_3$) δ = 7.35-6.28 (br, 87H) 6.11-5.93 (br, 3H) 4.82-4.58 (br, 6H) 4.51-4.35 (br, 3H) 2.45-1.15 (br, 63H);

General Procedure for *o*-ROMP. To a 2-dram vial containing a magnetic stirbar was added pyrylium salts **4** (1.3 mg, 0.003 mmol) followed by norbornene. CH2Cl2 was then added, followed by corresponding initiators (0.045 mmol). The vial was then sealed with a PTFE-lined cap and irradiated with blue LEDs (λ = 450–480 nm, 2 W) at a distance of 2.0 cm. Aliquots were taken for analysis to determine the conversion of norbornene by ^{1}H-NMR spectroscopy. The contents of the vial were then diluted with CH_2Cl_2 and filtered over neutral alumna to remove **4**. The filtrate was then partially concentrated and then added slowly into an excess of cold methanol, causing the polymer to precipitate. The solids were collected by filtration, washed with methanol, and then dried under reduced pressure to give the final polymer.

General Procedure for Hydrolysis Studies. To a 4-dram vial containing a magnetic stirbar was added polynorbornene followed by THF (polymer concentration = 5 mg/mL). Then, Amberlyst 15 ion-exchange resin was added. The vial was sealed with a PTFE-lined cap and transferred into an oil-bath preheated to 45 °C. The hydrolysis process was monitored by GPC and judged to have reached maximum conversion when there was no shift of retention time for solution aliquot.

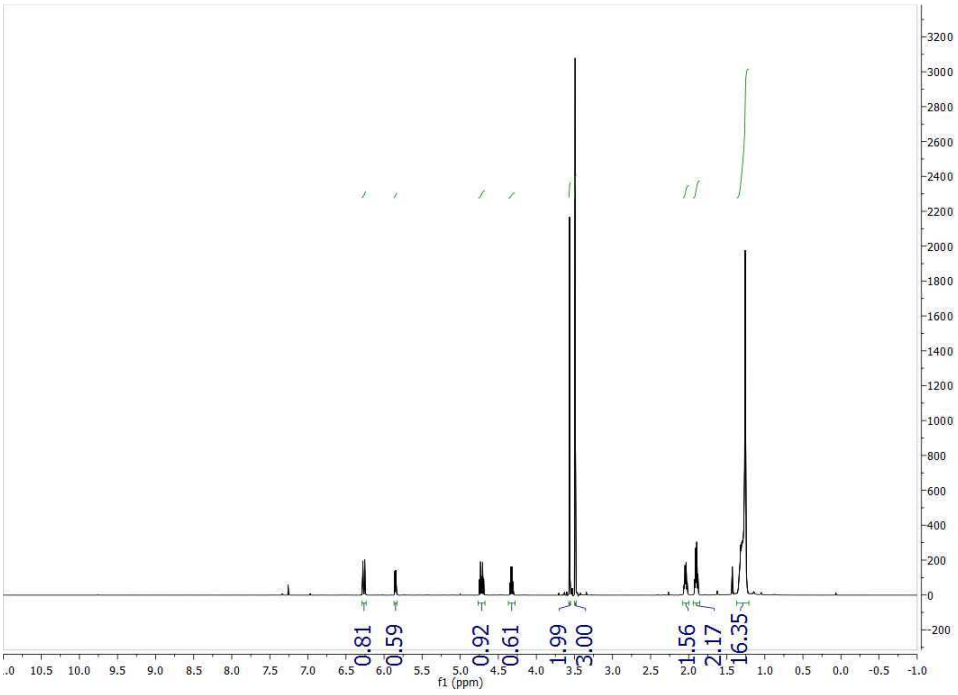

Figure 2.8. ^{1}H-NMR spectrum of initiator **2**

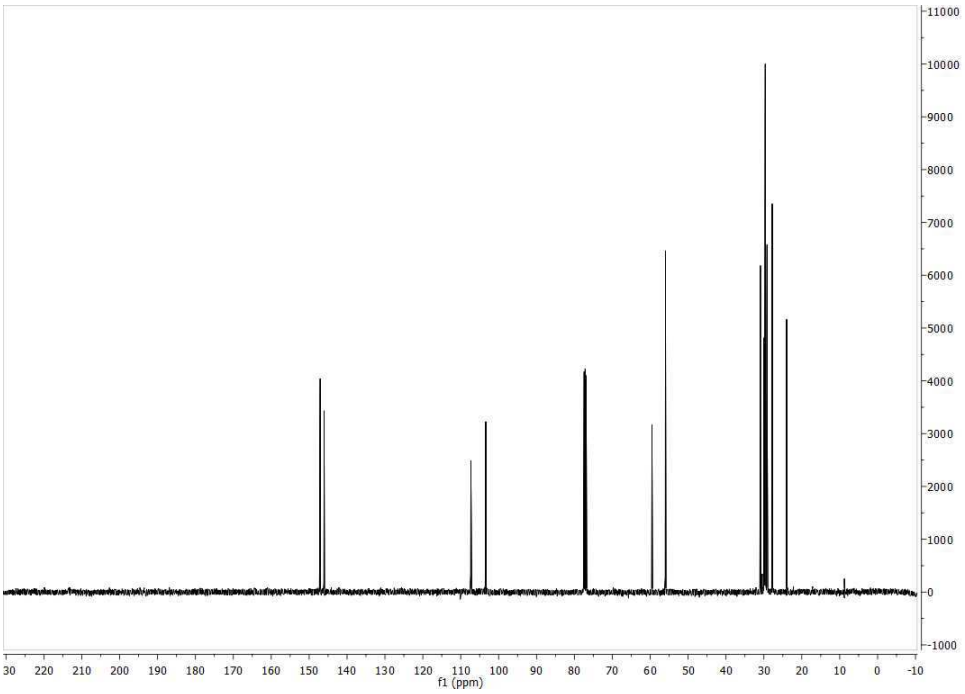

Figure 2.9. ^{13}C-NMR spectrum of initiator **2**

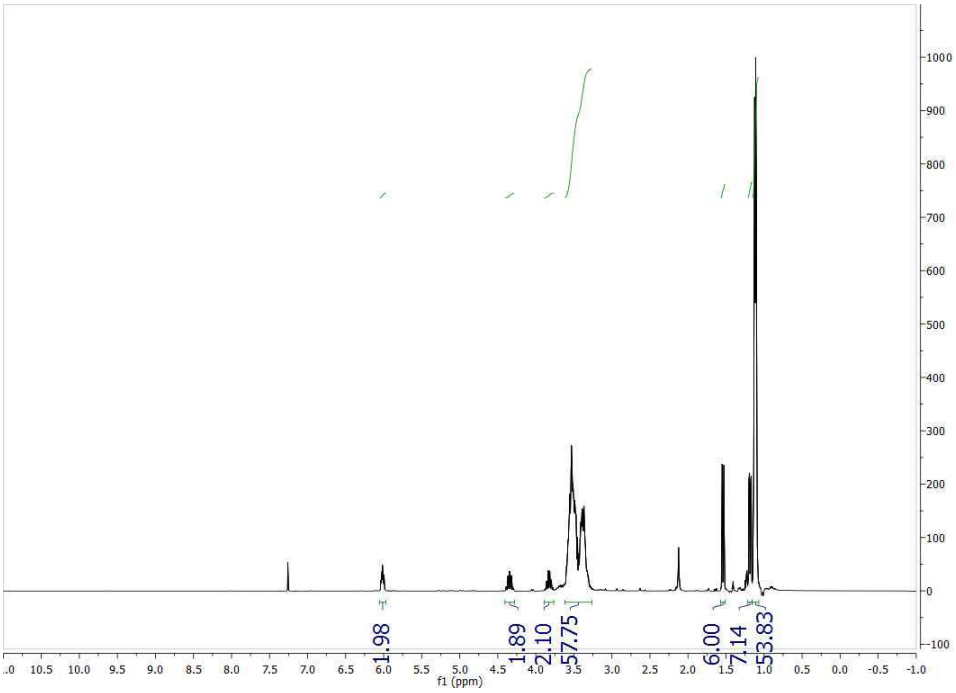

Figure 2.10. ^{1}H-NMR spectrum of macroinitiator **7**

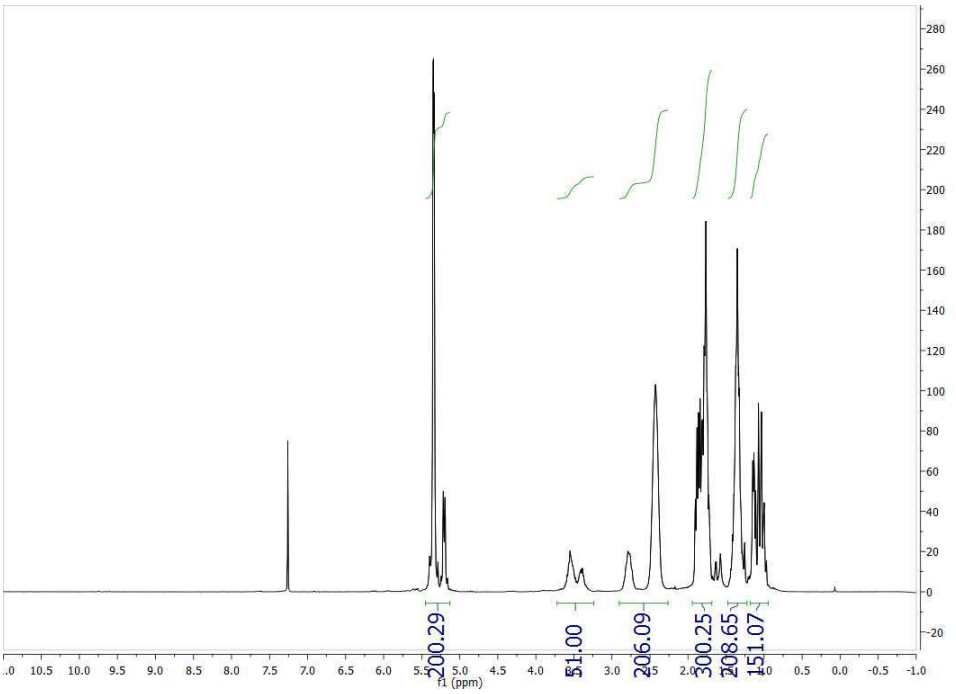

Figure 2.11. [1]H-NMR spectrum of triblock copolymer **8**

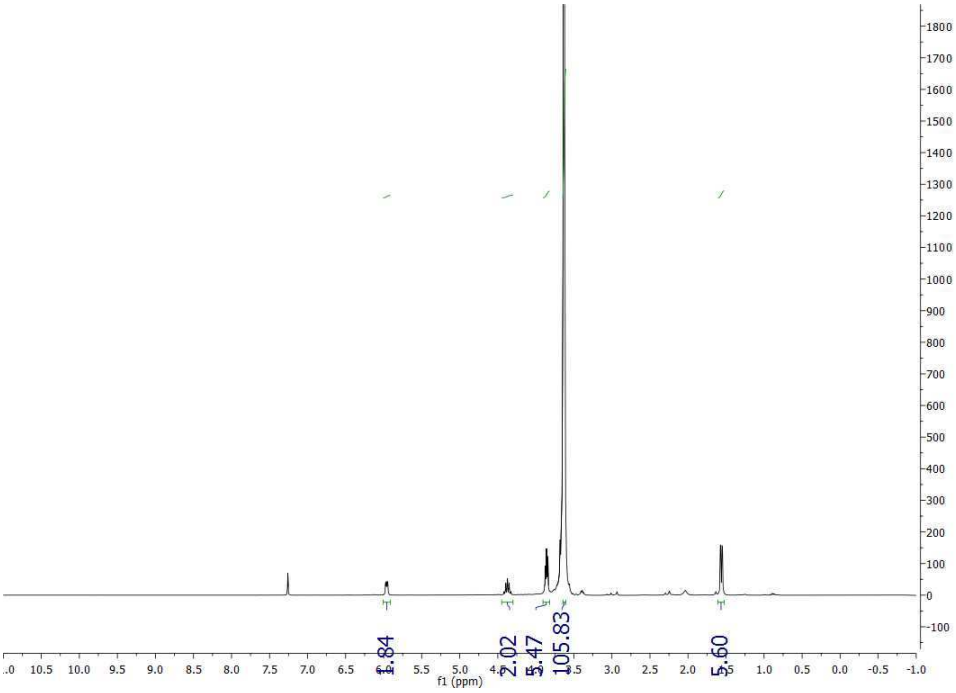

Figure 2.12. [1]H-NMR spectrum of macroinitiator **9**

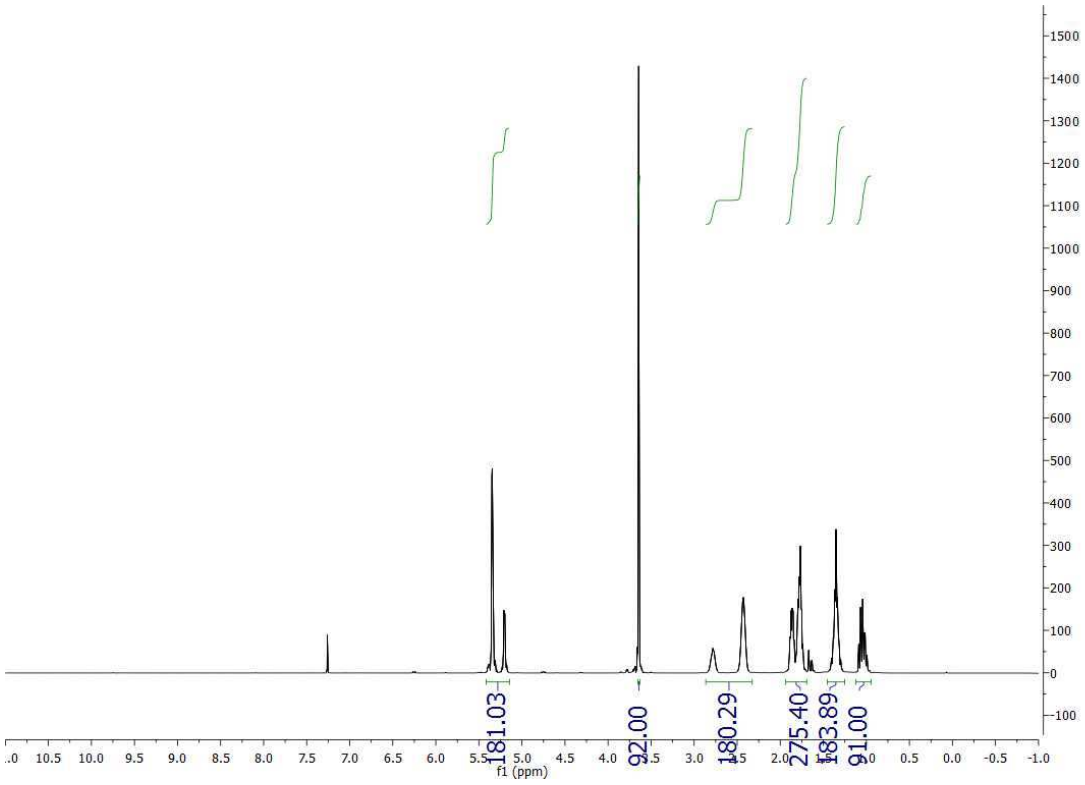

Figure 2.13. [1]H-NMR spectrum of triblock copolymer **10**

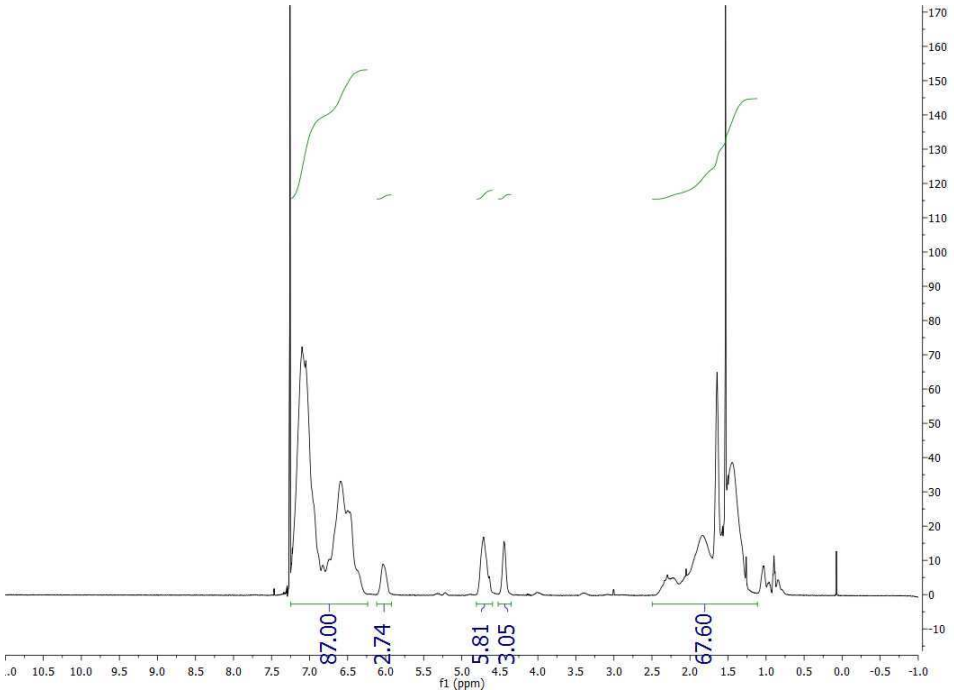

Figure 2.14. [1]H-NMR spectrum of macroinitiator **11**

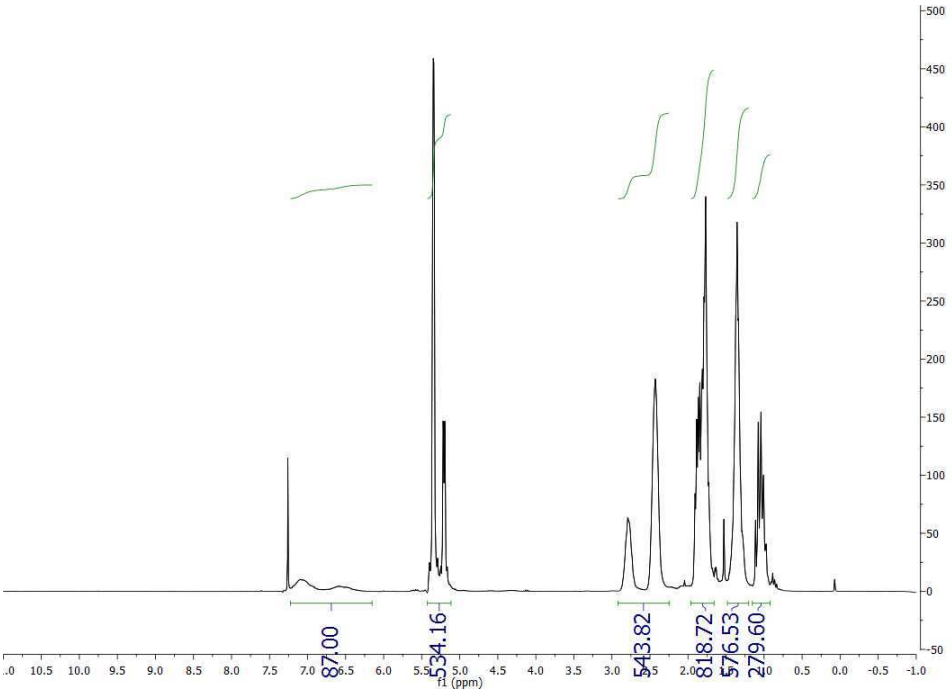

Figure 2.15. ^{1}H-NMR spectrum of graft-copolymer **12**

Notes and References for Chapter 2

[1] Risse, W.; Wheeler, D. R.; Cannizzo, L. F.; Grubbs, R. H. *Macromolecules*, **1989**, *22*, 3205.
[2] Fox, H. H.; Lee, J.-K.; Park, L. Y.; Schrock, R. R. *Organometallics*, **1993**, *12*, 759.
[3] Weck, M.; Schwab, P.; Grubbs, R. H. *Macromolecules*, **1996**, *29*, 1789.
[4] Garber, S. B.; Kingsbury, J. S.; Gray, B. L.; Hoveyda, A. H. *J. Am. Chem. Soc.*, **2000**, *122*, 8168.
[5] Schrock, R. R.; Gabert, A. J.; Singh, R.; Hock, A. S. *Organometallics*, **2005**, *24*, 5058.
[6] Mayershofer, M. G.; Nuyken, O.; Buchmeiser, M. R. *Macromolecules*, **2006**, *39*, 2452.
[7] Mayershofer, M. G.; Nuyken, O.; Buchmeiser, M. R. *Macromolecules*, **2006**, *39*, 3484.
[8] Kim, K. O.; Shin, S.; Kim, J.; Choi, T.-L. *Macromolecules*, **2014**, *47*, 1351.
[9] Castle, T. C.; Khosravi, E.; Hutchings, L. R.; *Macromolecules*, **200**6, *39*, 5639.
[10] Ogawa, K. A.; Goetz, A. E.; Boydston, A. J. *J. Am. Chem. Soc.,* **2015**, *137*, 1400.
[11] Goetz, A. E.; Boydston, A. J. *J. Am. Chem. Soc.,* **2015**, *137*, 7572.
[12] Goetz, A. E.; Pascual, L. M. M.; Dunford, D. G.; Ogawa, K. A.; Knorr, D. B., Jr.; Boydston, A. J. *ACS Macro Lett.,* **2016**, *5*, 579.
[13] Pascual, L. M. M.; Goetz, A. E.; Roehrich, A. M.; Boydston, A. J. *Macromol. Rapid Commun.* **2017**, *38*, 1600766.
[14] Moeller, K. D. *Synlett*, **2009**, *8*, 1208.
[15] Sutterer, A.; Moeller, K. D. *J. Am. Chem. Soc.*, **2000**, *122*, 5636.
[16] Martinu, M.; Steckhan, E.; Esch, T. *Chem. Ber.,* **1993**, *126*, 1671.
[17] Su, C.; Williard, P. G. *Org. Lett.,* **2010**, *12*, 5378.
[18] Shirouzu, T.; Watari, K.; Ono, M.; Koizumi, K.; Saiki, I.; Tanaka, C.; van Soest, R. W. M.; Miyamoto, T. *J. Nat. Prod.,* **2013**, *76*, 1337.

Chapter 3. Integration of Organic Photoredox-Mediated Ring-Opening Metathesis Polymerization (*o*-ROMP) and Organocatalyzed Ring-Opening Polymerization (*o*-ROP) through Bifunctional Initiators[1]

Section 1: Introduction

3.1.a Preparation of Block Copolymers through Bifunctional Initiators

The unique physicochemical properties of block copolymers make them attractive materials for a wide range of applications,[1] such as thermoplastic elastomers,[2] substrates for lithographic patterning,[3] and micelles for drug delivery systems.[4] Since block copolymers have applications in a broad array of areas, there has been tremendous effort focusing on their preparation. Traditionally, there are three different ways to prepare well-defined block copolymers: 1) polymer-polymer chain coupl[2]ing of different segments;[5-9] 2) sequential addition of different monomers that can be polymerized by the same mechanism;[10-12] and 3) sequential or simultaneous polymerization of monomers that convert via different mechanisms, often realized by either post-modification techniques or bifunctional initiator approaches.[13-15] Although each method has unique strengths, we were attracted by the ability of dual polymerizations to create disparate block compositions arising from unique polymerization mechanisms of each block. For example, using a hetero-bifunctional initiator is an attractive method for growing a unique polymer segment from each initiator moiety. Moreover, since bifunctional initiators bear two initiation sites for two distinct polymerizations, block copolymers can be envisioned from 1) polymerization of

[1] Reproduced with Permission from Lu, P.; Boydston, A. J. "Integration of metal-free ring-opening metathesis polymerization and organocatalyzed ring-opening polymerization through a bifunctional initiator" *Polym. Chem.* 2019, Advance Article. Copyright 2018 Royal Society of Chemistry.

an A-block, isolation of the resulting macroinitiator, and subsequent polymerization of a B-block; 2) one-pot sequential polymerizations of each block; and 3) simultaneous (orthogonal) polymerizations of two monomer classes, provided the reactive species of the different polymerizations are co-compatible. Thus far, numerous bifunctional initiators combining different polymerization methods (e.g., ATRP, RAFT, ROP, ROMP) have been synthesized and used to prepare well-defined block copolymers.[16-20]

For example, a collaborative effort between the Miyake and Boyer groups showcased a combination of *o*-ATRP and *o*-PET-RAFT via a bifunctional initiator (**BI 1** in Figure 1), which allowed access to block copolymers using a single photocatalyst (OPC **2a**).[21] In order to incorporate a broader monomer scope than vinyl monomers, Boyer group and Yagci group independently developed several different kinds of bifunctional initiators (Figure 3.1), which succeeded in integrating ring opening polymerization (ROP) with *o*-PET-RAFT (**BI 2**) and *o*-ATRP (**BI 3**).[22-23] The resulted block copolymer may have potential biomedical application due to the presence of biocompatible blocks (polyester and polycarbonate) from ROP process.

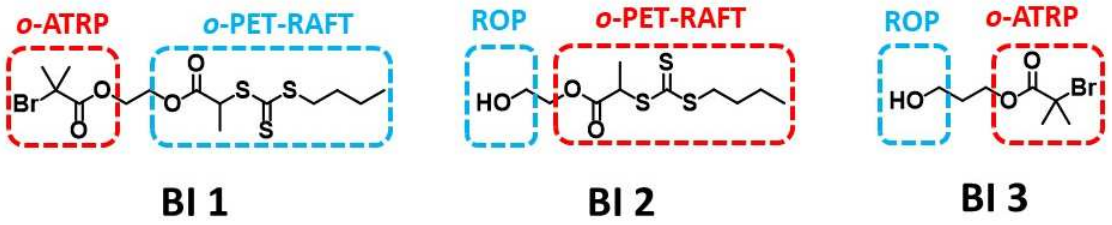

Figure 3.1. Chemical structures of bifunctional initiators BI 1, BI 2, and BI 3.

With the recent introduction of *o*-ROMP,[24-29] we became curious whether this method could be integrated with other polymerizations to provide an entirely organocatalyzed approach to block copolymers via dual polymerization from bifunctional initiators. Although appropriate bifunctional initiators could be obtained from standard synthetic outlay, a potential challenge was the fact that *o*-ROMP exhibits much lower

functional compatibility in comparison with traditional metal-mediated ROMP.[27] Therefore, the exploration of compatibility is necessary, and the current study illustrates efficient, successful advances.

Section 2: Results and Discussion

Scheme 3.1. Synthetic route toward functional block copolymers from bifunctional initiator **1**

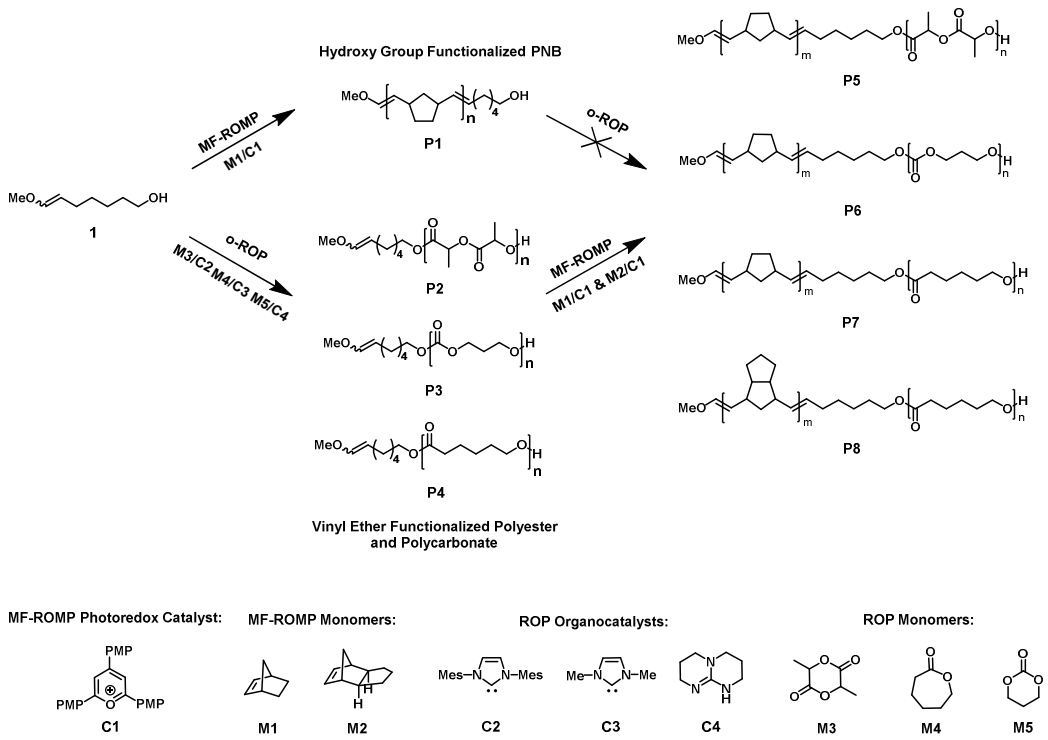

3.2.a Grafting o-ROMP from Bifunctional Initiators

o-ROMP is a type of controlled polymerization mediated by organic photoredox catalysts. Instead of using metal-alkylidene initiators, *o*-ROMP utilizes vinyl ethers as organic initiators that are reversibly activated through one-electron oxidation. To complement this polymerization, we selected organocatalyzed-ROP (*o*-ROP), which can be mediated by nucleophilic organocatalysts.[30-32] Besides their metal-free merits, the combination of *o*-ROMP and *o*-ROP also offer backbone compositions that display highly disparate physicochemical properties.[33]

To investigate the feasibility of integrated *o*-ROMP and *o*-ROP from a single unit, we first prepared a bifunctional initiator bearing a vinyl ether at one terminus and a hydroxyl group at the other (**1**). We chose norbornene (**M1**) and exo-dihydrodicyclopentadiene (**M2**) as *o*-ROMP monomers and three different *o*-ROP monomers, specifically *rac*-lactide (**M3**), $\mathcal{E}$-caprolactone (**M4**), and cyclic trimethylene carbonate (**M5**) (Scheme 3.1).

The MF-ROMP of norbornene from bifunctional initiator **1** achieved decent conversion (55%). The resulting hydroxy end-capped polymer (**P1**) was isolated and then used as a macroinitiator for *o*-ROP. The following *o*-ROP from **P1** was met with limited success and we observed unreacted macroinitiator as determined by SEC analysis. The combination of low *o*-ROMP conversion and incomplete chain extension from some fractions of **P1** indicated to us that the hydroxyl groups might undergo side reactions with activated vinyl ethers during *o*-ROMP.[27] It was demonstrated by Moeller and coworkers that single-electron oxidation of nucleophilic vinyl ethers will reverse their polarity to form electrophilic radical cations, which can be trapped by nucleophiles, such as alcohols.[34-36] In a previous report by Moeller and coworkers, it was discovered that compound **1** indeed resulted in products of methanol trapping of the radical cation.[37, 38]

3.2.b Grafting o-ROMP from Macroinitiators

Upon switching the order of the polymerizations, bifunctional initiator **1** was found to facilitate *o*-ROP of each corresponding monomer and polymerizations reached high conversions (97% for **M3**, 88% for **M4**, and 99% for **M5**). In each case, we used an organocatalyst that had been previously reported to facilitate *o*-ROP of the specific monomer.[39, 40] The isolated macroinitiators (**P2**, **P3**, and **P4**) were then each used in attempted

o-ROMP to form diblock copolymers. Each macroinitiator was found to participate in *o*-ROMP of norbornene (**M1**) with moderate to high conversion (Table 3.1), and SEC analysis of each crude product revealed monomodal molecular weight distributions consistent with high fidelity of chain extension. Since the T_g of the PNB blocks were close to the T_m of the polycaprolactone (PCL) blocks, we switched to **M2** for the *o*-ROMP. Homopolymers of **M2** (PDCPD-H_2) are reported to have a T_g near 130 °C.[25] DSC analysis clearly indicated thermal transitions characteristic of each block, which provided further support for successful preparation of block copolymers.

Table 3.1. Characterization of block copolymers by *o*-ROMP grafting from isolated macroinitiators

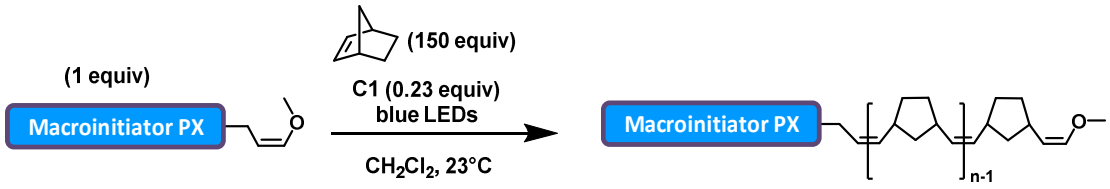

Entry	**PX**	$M_{n,\,GPC}$ of **PX** (kDa)	*o*-ROMP conversion[f] (%)	$M_{n,\,GPC}$ of Block Copolymer[e] (kDa)	$Đ_{GPC}$[e]	PNB wt %[f]	thermal transition[g] (°C)
1	**P2**[b]	9.8	70	25.4	1.49	67	T_g: 35 and 55
2	**P3**[c]	19.7	64	32.3	1.45	33	T_g: 35 T_m: 56
3[a]	**P3**	19.7	60	38.5	1.39	44	T_g: 130 T_m: 56
4	**P4**[d]	16.1	85	33.6	1.69	50	T_g: -27 and 35

[a]M2 was used as monomer for *o*-ROMP, [b][M3]/[1]/[C2]: 50/1/1.5, [c][M4]/[1]/[C3]: 200/1/1, [d][M5]/[1]/[C4]: 200/1/0.01, [e]Determined by gel permeation chromatography using in-line multiangle laser scattering and RI detection. Molecular weight dispersity (Đ) = M_w/M_n, [f]Calculated by ^{1}H-NMR analysis, [g]Determined by DSC.

3.2.c Development of One-Pot Process Integrating o-ROMP and o-ROP

The successful preparation of block copolymers from macroinitiators encouraged us to explore a one-pot method for tandem *o*-ROP and *o*-ROMP (Scheme 3.2). Notably, *o*-ROMP in the presence of monomeric lactide, caprolactone, or propylene carbonate failed to reach good conversion (see Experimental section). Presumably, the *o*-ROP monomeric species display greater nucleophilicity than their corresponding polymeric repeat units, which could be ascribed to steric encumbrance in the latter. Considering these observations, we did not pursue further a simultaneous dual polymerization. Additionally, these results indicated to us that high conversion of the *o*-ROP monomer would be required for success in the subsequent *o*-ROMP. Since TBD could be used as an organocatalyst for each of the *o*-ROP monomers (**M3**, **M4**, and **M5**), it was chosen for the *o*-ROP process in this one-pot method.[41] In each polymerization, the *o*-ROP reactants and organocatalyst were combined in CH_2Cl_2 and stirred at room temperature. Aliquots were withdrawn for ^{1}H NMR and SEC analyses. Once maximum conversion of the *o*-ROP monomer was observed by ^{1}H NMR spectroscopy, the *o*-ROMP monomer and photoredox catalyst were added to the solution in a single portion. Key results are summarized in Table 3.2.

Scheme 3.2. One-pot, two-step process for preparation of functional block copolymers integrating *o*-ROMP and *o*-ROP

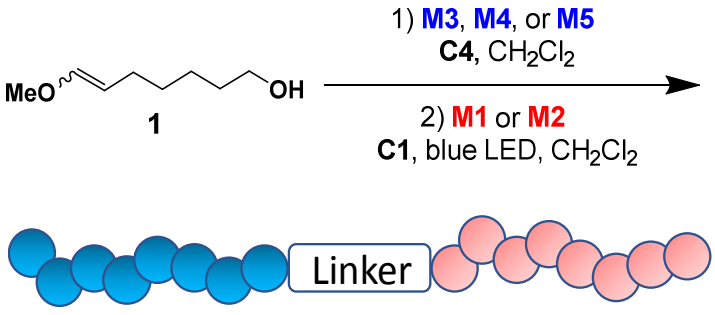

As alluded to previously, the success of the *o*-ROMP in the second polymerization was found to be dependent upon the monomer conversion achieved in the first (o-ROP) polymerization.

When *rac*-lactide (**M3**) and cyclic trimethylene carbonate (**M5**) were chosen as monomers for the *o*-ROP process, high conversions were achieved and thus the following *o*-ROMP process showed excellent conversion of norbornene (**M1**) as well (Table 3.2, entries 1 – 6). However, when $\mathcal{E}$-caprolactone (**M4**) was selected as the *o*-ROP monomer, its conversion could not be raised greater than 78%, which stifled monomer conversion in the following *o*-ROMP process. We also found that slightly increasing the loading of the *o*-ROMP photoredox catalyst (**C1**) to compensate for consumption by the TBD significantly increased conversion in the *o*-ROMP. It is noteworthy that TBD has been reported to dramatically decrease the rate of traditional Ru-mediated ROMP.[19]

With successful methods for block copolymer synthesis at hand, we next focused on compositional and thermal characterization. SEC analyses (Figure 3.2.A) were consistent with successful chain extension and high initiator efficiency in the formation of the second block. In each case, a monomodal distribution with increased molecular weight was observed for the block copolymer sample in comparison with the corresponding macroinitiator intermediate. Analysis by ^{1}H NMR spectroscopy clearly revealed signals consistent with each polymer block (Figure 3.2.B). Based upon signal integrations, the composition of each block copolymer was found to correlate well with the monomer feed ratios and conversions, indicating that initiation effiency was high for each polymerization type. Copolymer compositions determined from TGA were also found to be consistent with ^{1}H NMR data. This was especially evident for **P5** and **P6**, which contain polylactide (PLA) and poly(trimethylene carbonate) (PTMC) blocks, because there was a plateau region in each TGA plot (Figure 3.2.C). In general, thermal properties of block copolymers of the same composition were agnostic to either a two-post or one-pot method of synthesis (Figure 3.2.D). One exception was PCL-b-PDCPD-H_2 (**P8**), which could be explained by different block lengths based upon the method of synthesis. Specifically, **P8** prepared from macroinitiator **P4**

displayed distinguishable thermal transitions by DSC, whereas **P8** prepared via the one-pot method only showed thermal transitions for the PCL block (Figure 3.2.D, orange line). Again, this is likely ascribed to relatively shorter PDCPD-H_2 blocks from the one-pot method,[42] which originated from lower **M2** conversion and therefore inhibition of *o*-ROMP.

Table 3.2. One-pot preparation of block copolymers by MF-ROMP and o-ROP

en-try	mono-mers	*o*-ROP		*o*-ROMP		M_n after o-ROP (kDa)	M_n after *o*-ROMP (kDa)	$Đ$
		[M*X*]:[**1**]:[**C4**]	conve-rsion (%)	[M*X*]:[**1**]:[**C1**]	conve-rsion (%)			
1	**M3/M1**	50 : 1.0 : 0.1	99	100 : 1.0 : 0.3	83	6.2	15.2	1.30
2	**M3/M1**	75 : 1.0 : 0.1	99	100 : 1.0 : 0.3	85	8.6	17.8	1.60
3	**M3/M1**	100 : 1.0 : 0.1	98	100 : 1.0 : 0.3	79	20	30.3	1.24
4	**M3/M1**	150 : 1.0 : 0.1	98	150 : 1.0 : 0.3	60	30	40.1	1.28
5	**M5/M1**	100 : 1.0 : 0.1	99	100 : 1.0 : 0.3	86	13	24.8	1.79
6	**M5/M1**	200 : 1.0 : 0.1	99	100 : 1.0 : 0.3	75	18	25.6	1.72
7	**M4/M1**	50 : 1.0 : 0.4	78	100 : 1.0 : 0.5	41	7.5	13.6	1.35
8	**M4/M2**	50 : 1.0 : 0.4	78	100 : 1.0 : 0.5	35	7.5	10.3	1.46

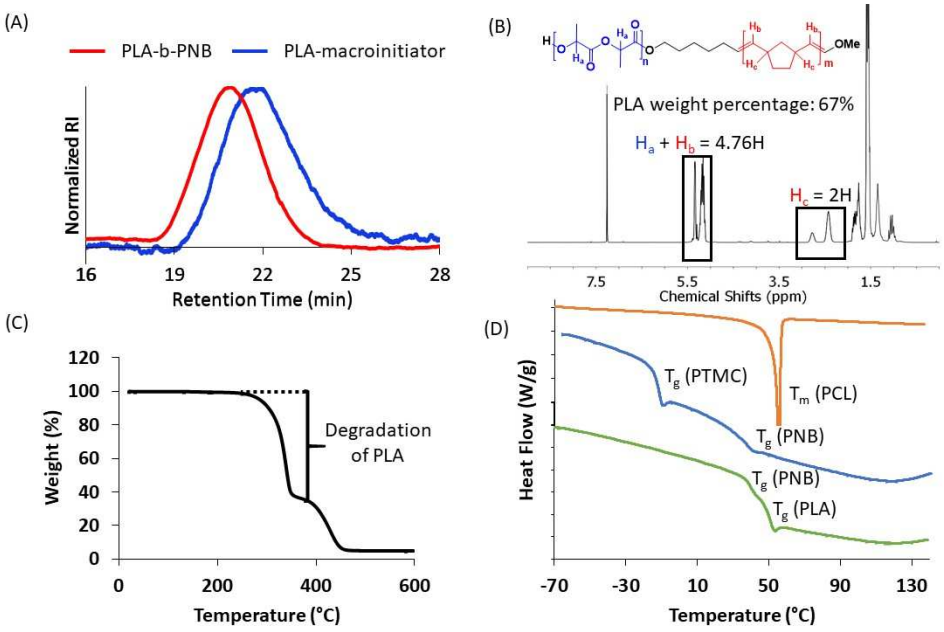

Figure 3.2. (A) SEC overlay of PLA-macroinitiator and PLA-*b*-PNB (entry 3 from Table 3.2), (B) ^{1}H-NMR spectrum of PLA-*b*-PNB (entry 3 from Table 3.2) and (C) TGA plot of PLA-*b*-PNB (entry 3 from Table 3.2) with 64 wt% of PLA block, (D) DSC thermograms (exotherm up) of block

copolymers made from one-pot process (under nitrogen with a scanning rate of 5 °C/min). Orange line: entry 8 from Table 3.2; Blue line: entry 5 from Table 3.2; Green line: entry 4 from Table 3.2.

Section 3: Conclusions

In conclusion, we successfully demonstrate an expanded utility of *o*-ROMP by preparation of block copolymers via an integration of *o*-ROMP and *o*-ROP from a bifunctional initiator. With the separation of intermediate macroinitiators after *o*-ROP, grafting-from *o*-ROMP efficiently afforded diblock copolymers in high efficiency. Furthermore, a one-pot process was developed and that allowed for easy access block copolymers without isolation of intermediate macroinitiators. We anticipate useful variations of integrated *o*-ROMP to provide entirely metal-free copolymers for a range of applications.

Section 4: Experimental

General Consideration. Dimethylformamide (DMF), dichloromethane (CH_2Cl_2), tetrahydrofuran (THF) were obtained from a solvent purification system. For MF-ROMP procedure, CH_2Cl_2 was dried over 4Å molecular sieves before use. Norbornene was sublimed prior to use. 3,6-dimethyl-1,4-dioxane-2,5-dione (rac-LA) was recrystallized from dry toluene (×3) prior to use and stored at -20 °C under inert atmosphere. Ɛ-caprolactone (CL) was distilled over CaH_2 (×2) and stored under inert atmosphere. The pyrylium tetrafluoroborate was prepared according to literature procedure.[43] 1,3-(2,4,6-trimethylphenyl)imidazolium chloride and 1,3-dimethylimidazolium iodide were prepared according to previous literature procedure.[44, 45] Initiator **1** was prepared as previously described.[46] All other reagents and solvents were obtained from commercial sources and used as received unless otherwise noted. All polymerizations were carried out in standard borosilicate glass vials with magnetic stirring. Irradiation of photochemical reactions was done using a 2W Miracle Blue LED indoor gardening bulb purchased from Amazon. ^{1}H and ^{13}C NMR spectra were

recorded on Bruker AVance 300 MHz or 500 MHz spectrometers. Chemical shifts are reported in delta (δ) units, expressed in parts per million (ppm) downfield from tetramethylsilane using the residual protio-solvent as an internal standard ($CDCl_3$, ^1H: 7.26 ppm and ^{13}C: 77.0 ppm). Data are reported as follows: chemical shift, multiplicity (s = singlet, d = doublet, dd = doublet of doublet, dt = doublet of triplets, q = quartet, m = multiplet, br = broad peak), coupling constants (Hz) and integration. Gel Permeation Chromatography (GPC) was performed using a GPC setup consisting of: an Agilent pump, 3 in-line columns, and Wyatt light scattering and refractive index detectors with THF as the mobile phase. Number average molecular weight (M_n) and weight average molecular weight (M_w) were calculated from refractive index data and light scattering, respectively, using Astra software from Wyatt Technology Corp. Thermogravimetric analysis (TGA) was performed on a TA TGA Q50 under nitrogen from room temperature to 600 °C at a rate of 5 °C/min. Differential Scanning Calorimetry (DSC) was performed on a TA DSC Q250 calorimeter under nitrogen. Heat flow as watts from the second heating was recorded and reported after normalizing by mass of the sample (W/g).

General Procedure for o-ROMP from Macroinitiator

To a 2-dram vial containing a magnetic stir bar was added pyrylium salt (1.3 mg, 0.003 mmol) followed by corresponding macroinitiator (0.01 mmol) and norbornene (141 mg, 1.50 mmol). CH_2Cl_2 was then added. The vial was sealed with a PTFE-lined cap and irradiated with blue LEDs (λ = 450 nm, 2 W) at a distance of 2.0 cm. Aliquots were taken for analysis to determine the conversion of norbornene by ^1H-NMR spectrometry. The contents of the vial were then diluted with CH_2Cl_2 and filtered over neutral alumina to remove pyrylium salts. The filtrate was then partially concentrated and then added slowly into an excess of methanol, causing the polymer to

precipitate. The solids were collected by filtration, washed with methanol, and then dried under reduced pressure to give the final polymer.

General Procedure for "one-pot" Block Copolymer Synthesis

All organocatalytic ring-opening polymerizations were set up inside glove box at ambient temperature. To a 2-dram vial containing a magnetic stir bar was added TBD (0.3 mg, 0.002 mmol) followed by adding bifunctional initiator **1** (3.0 mg, 0.02 mmol). CH_2Cl_2 was then added, followed by corresponding monomer. The vial was sealed with a PTFE-lined cap and aliquots were taken for determining monomer conversion. After there was no more increase of monomer conversion, the vial was pumped out of glove box and the reaction was open to air. The contents of the vial were then diluted with CH_2Cl_2 and pyrylium salts (3.0 mg, 0.006 mmol) were then added. Aliquots were taken for analysis to determine the molecular weight of macroinitiator. Norbornene was then added and the vial was sealed again with a PTFE-lined cap. At room temperature, the reaction was irradiated with blue LEDs (λ = 450 nm, 2 W) with a distance of 2.0 cm. Aliquots were taken for analysis to determine the conversion of norbornene by ^{1}H-NMR spectrometry. The contents of the vial were then diluted with CH_2Cl_2 and filtered over neutral alumina to remove pyrylium salts. The filtrate was then partially concentrated and then added slowly into an excess of methanol, causing the polymer to precipitate. The solids were collected by filtration, washed with methanol, and then dried under reduced pressure to give the final polymer.

Determination of MF-ROMP monomer conversion

For tracking the conversion of monomer by ^{1}H-NMR spectroscopy (in $CDCl_3$), the following signals were used,

For **M1** (norbornene), the monomer signal at δ = 5.97 ppm (2H) was integrated against the polymer signal at δ = 2.90 to 2.30 ppm (2H total after subtracting monomer peak at 2.83 ppm).

For **M2** (exo-dihydroDCPD), the monomer signal at δ = 0.95 ppm (2H) was integrated against the polymer signal at δ = 1.18 ppm (1H).

Table 3.3. Effect of Additives on Polymerization of norbornene to polynorbornene

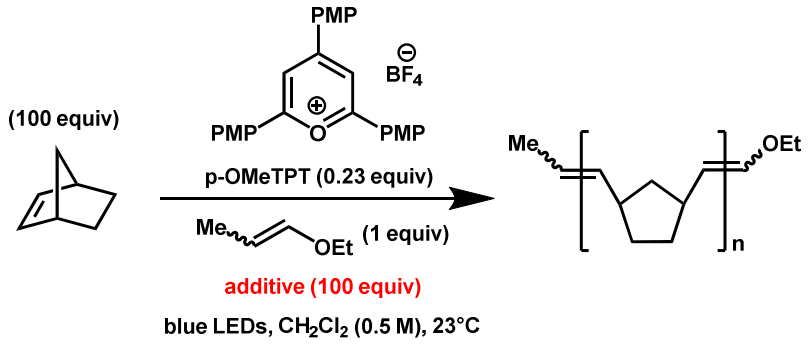

additive	equivalents[a]	conversion (%)[b]
N/A	0	86
rac-lactide (M2)	100	54
caprolactone (M3)	100	45
cyclic trimethylene carbonate (M4)	100	58

[a]Relative to enol ether initiator. [b]Determined using 1H-NMR spectroscopy by comparison of monomer and polymer peaks. PMP = p-methoxyphenyl. All reaction times = 90 min.

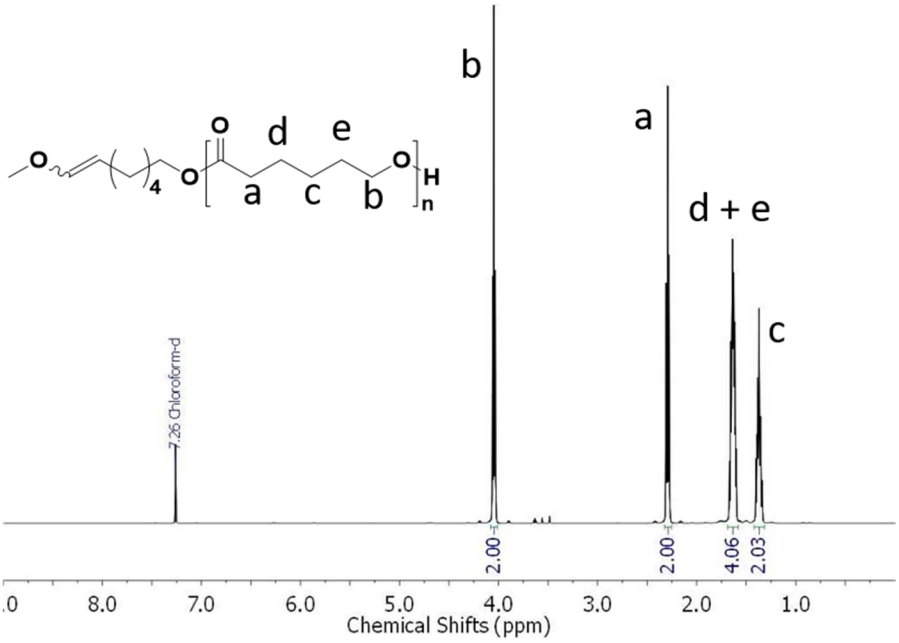

Figure 3.3. [1]H-NMR spectrum PCL macroinitiator

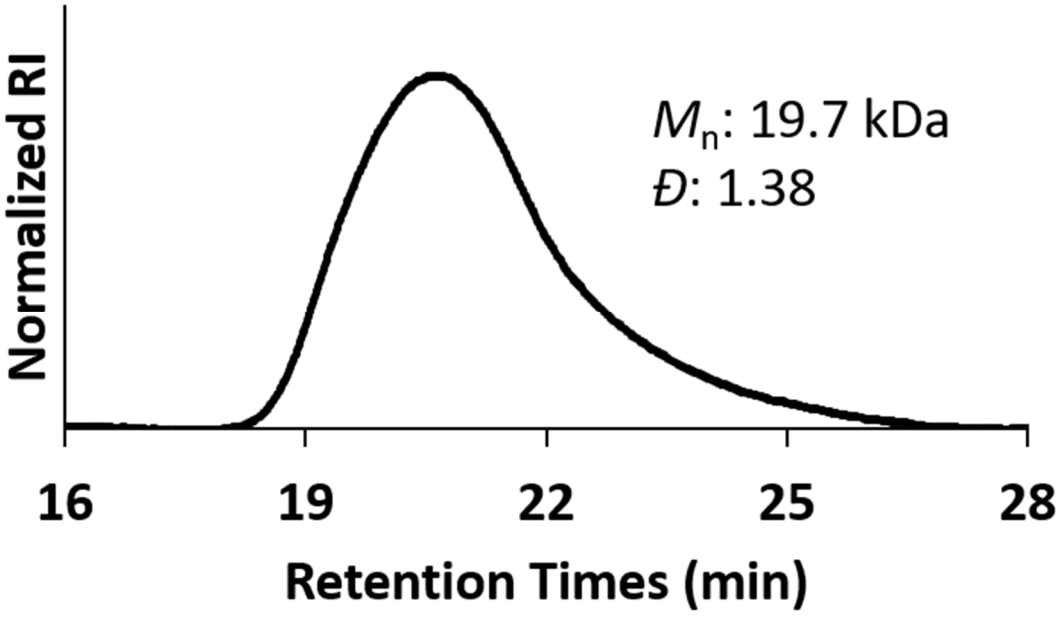

Figure 3.4. SEC chromatogram of PCL macroinitiator

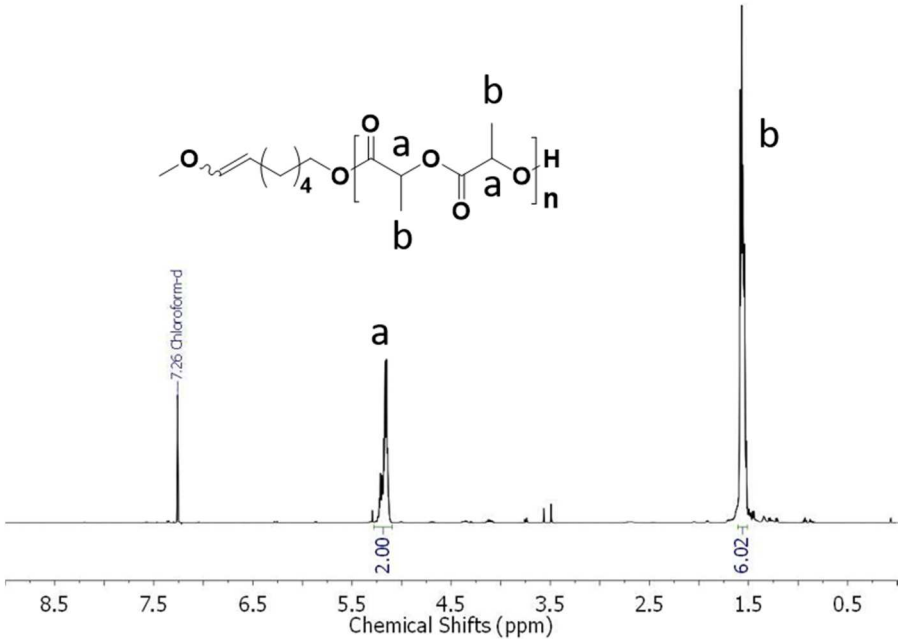

Figure 3.5. ^{1}H-NMR spectrum PLA macroinitiator

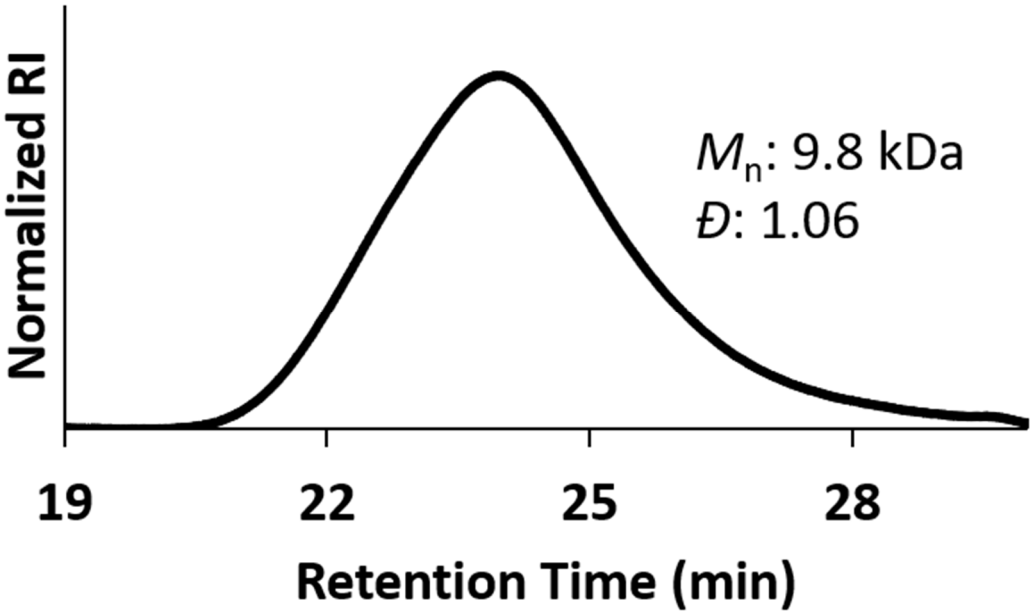

Figure 3.6. SEC chromatogram of PLA macroinitiator

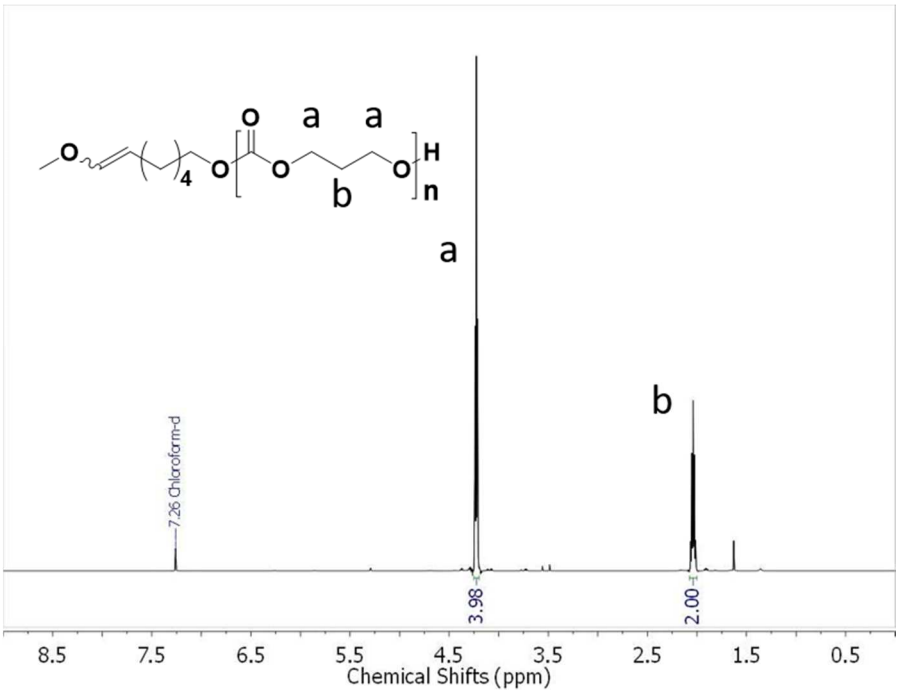

Figure 3.7. [1]H-NMR spectrum PTMC macroinitiator

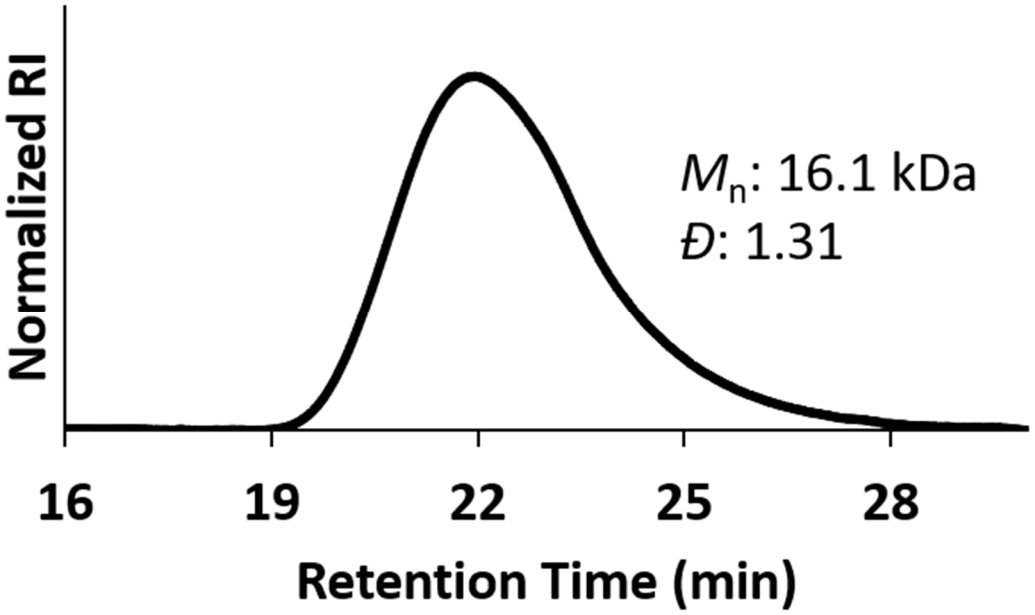

Figure 3.8. SEC chromatogram of PTMC macroinitiator

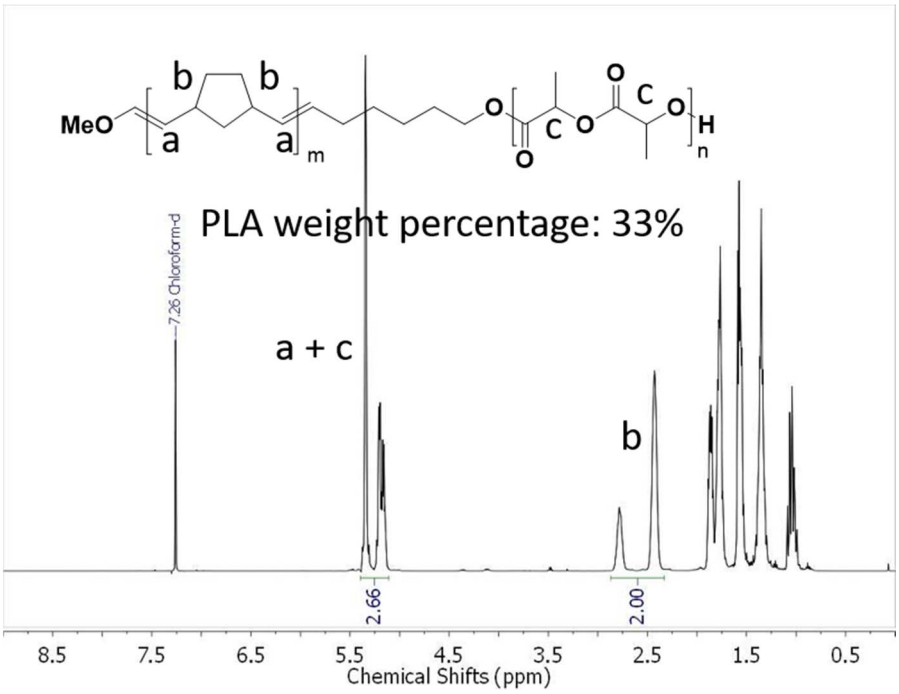

Figure 3.9. ^{1}H-NMR spectrum of PLA-*b*-PNB (entry 1 from Table 3.1)

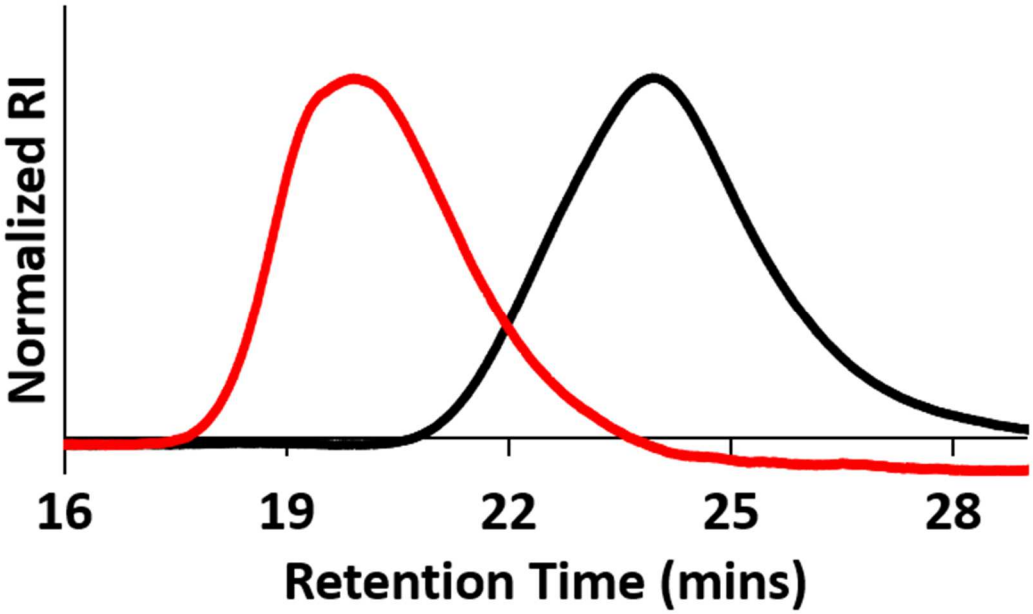

Figure 3.10. SEC chromatograms of PLA-*b*-PNB (entry 1 from Table 3.1, red line) and corresponding macroinitiator (black line)

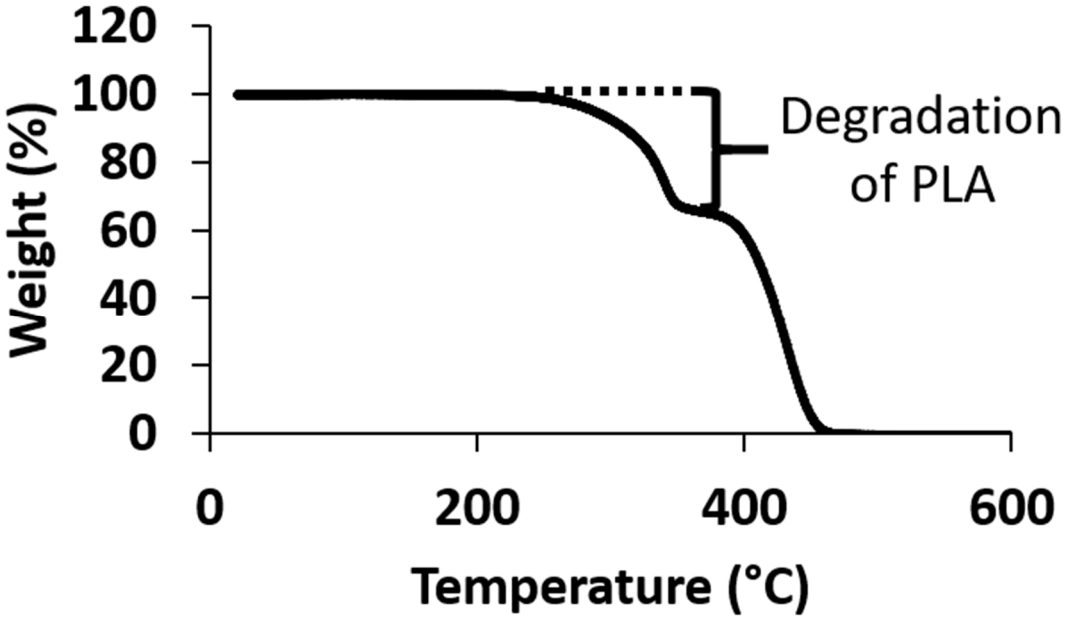

Figure 3.11. Thermogravimetric analysis of PLA-*b*-PNB (entry 1 from Table 3.1). The weight percentage of PLA block is around 33%.

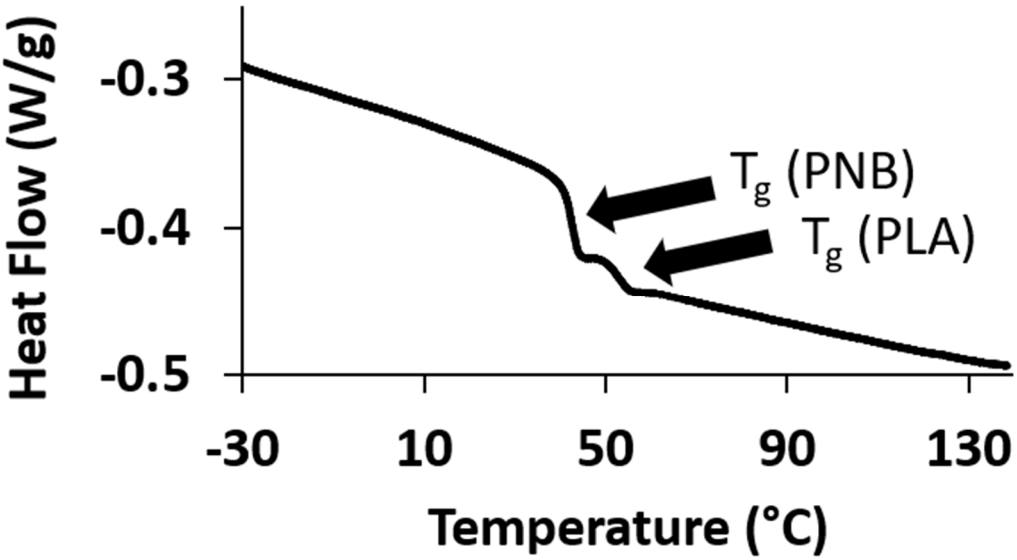

Figure 3.12. DSC (Exo up) of PLA-*b*-PNB (entry 1 from Table 3.1)

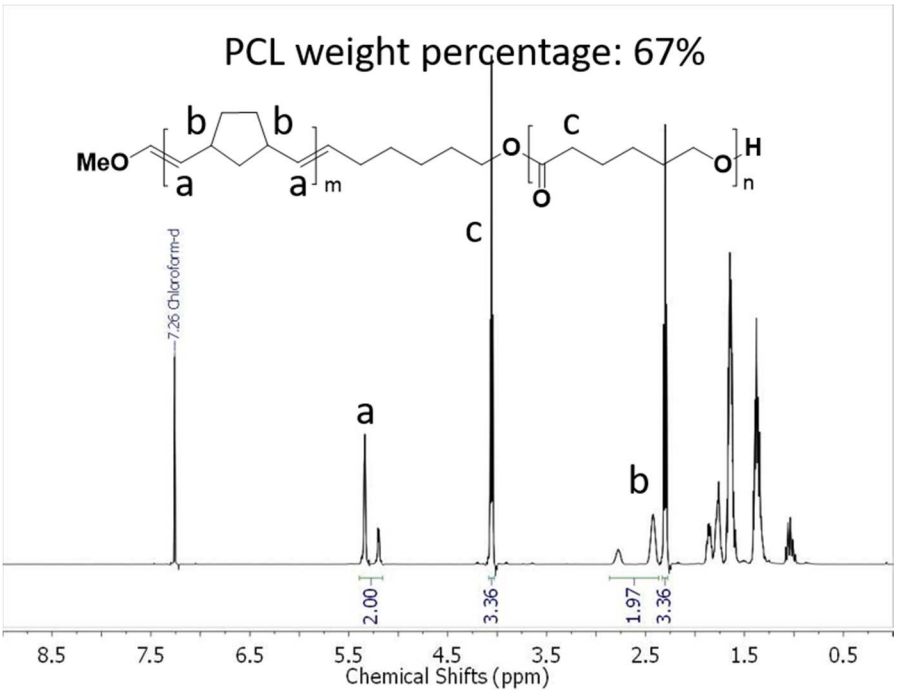

Figure 3.13. [1]H-NMR spectrum of PCL-*b*-PNB (entry 2 from Table 3.1)

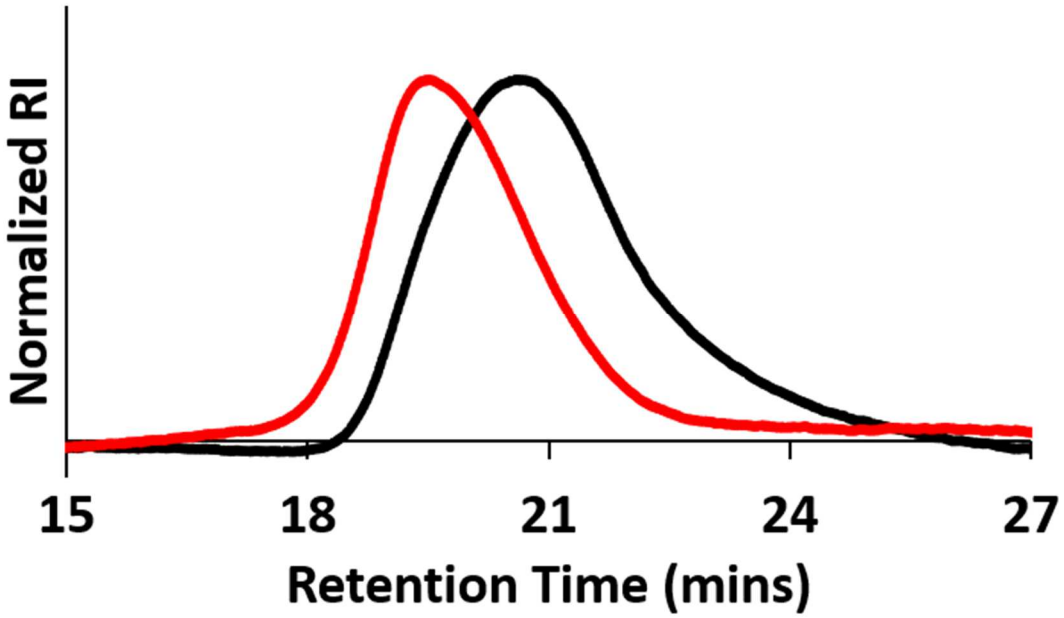

Figure 3.14. SEC chromatograms of PCL-*b*-PNB (entry 2 from Table 3.1, red line) and corresponding macroinitiator (black line)

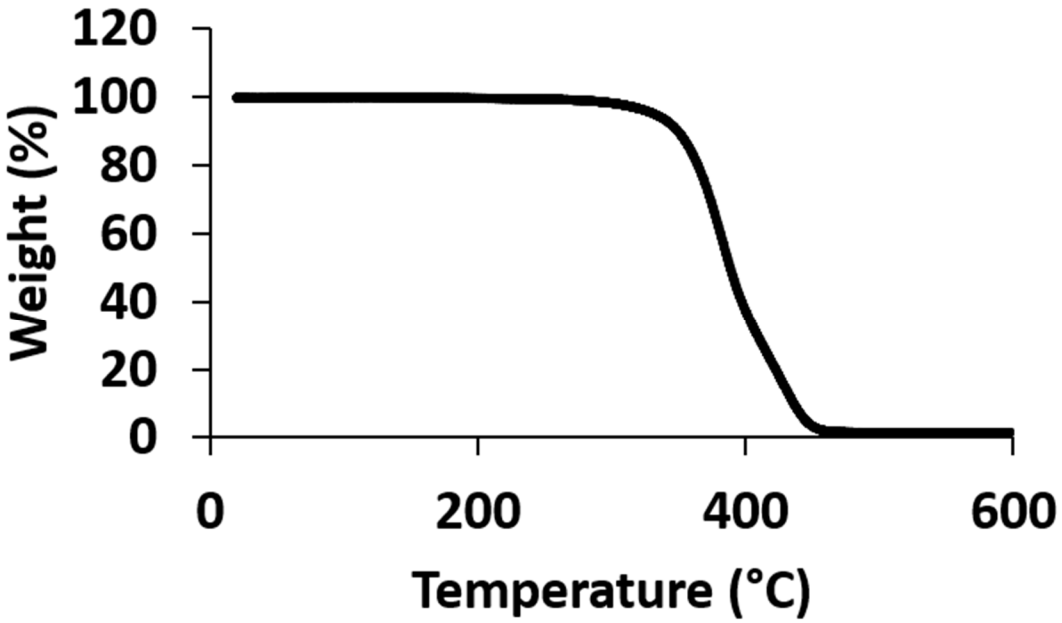

Figure 3.15. Thermogravimetric analysis of PCL-*b*-PNB (entry 2 from Table 3.1)

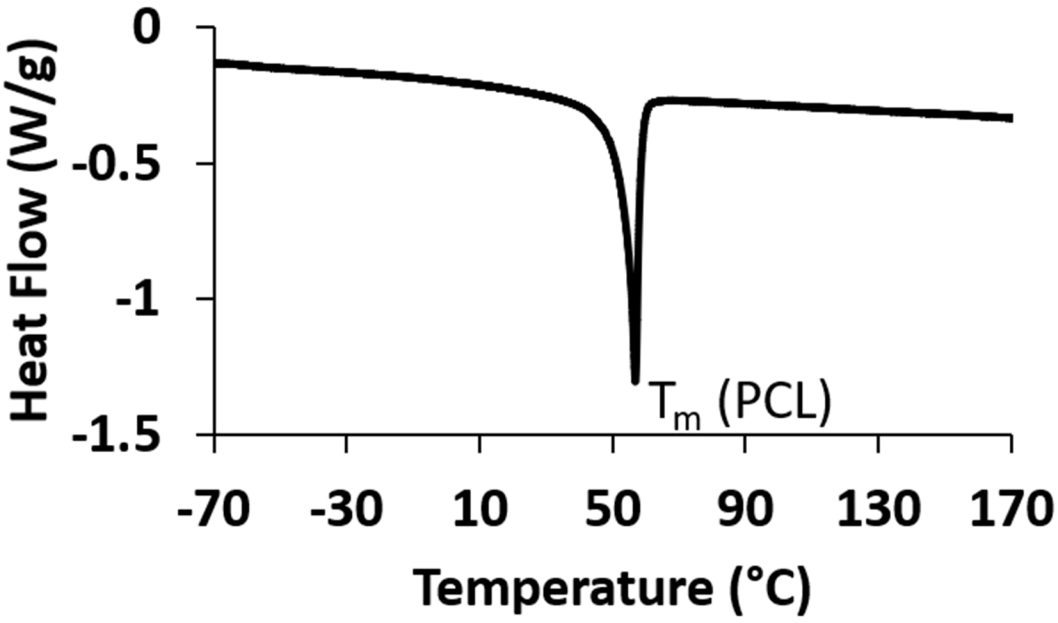

Figure 3.16. DSC (Exo up) of PCL-*b*-PNB (entry 2 from Table 3.1)

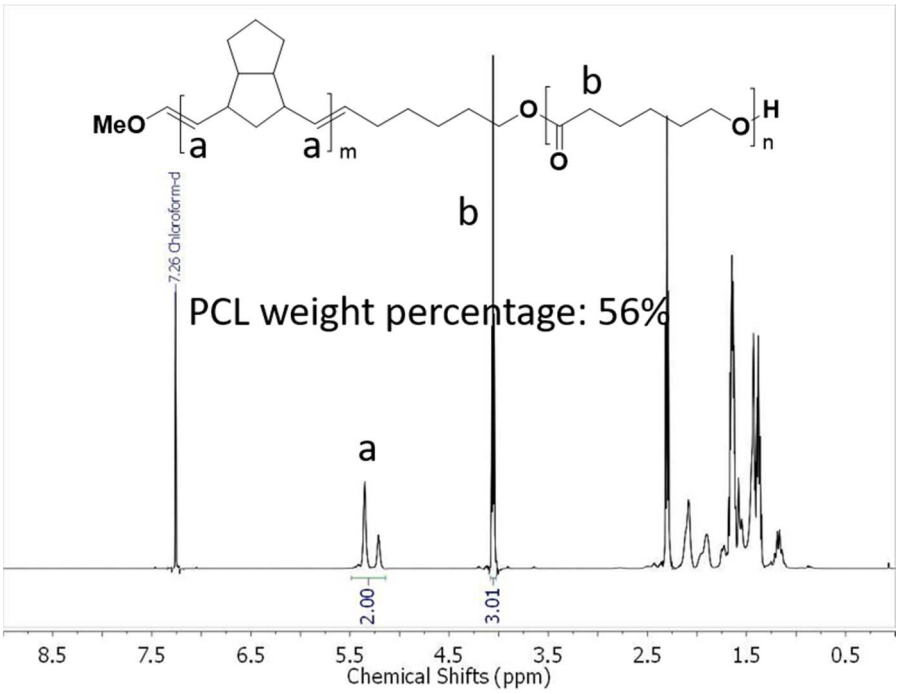

Figure 3.17. ^{1}H-NMR spectrum of PCL-*b*-PDCPD-H2 (entry 3 from Table 3.1)

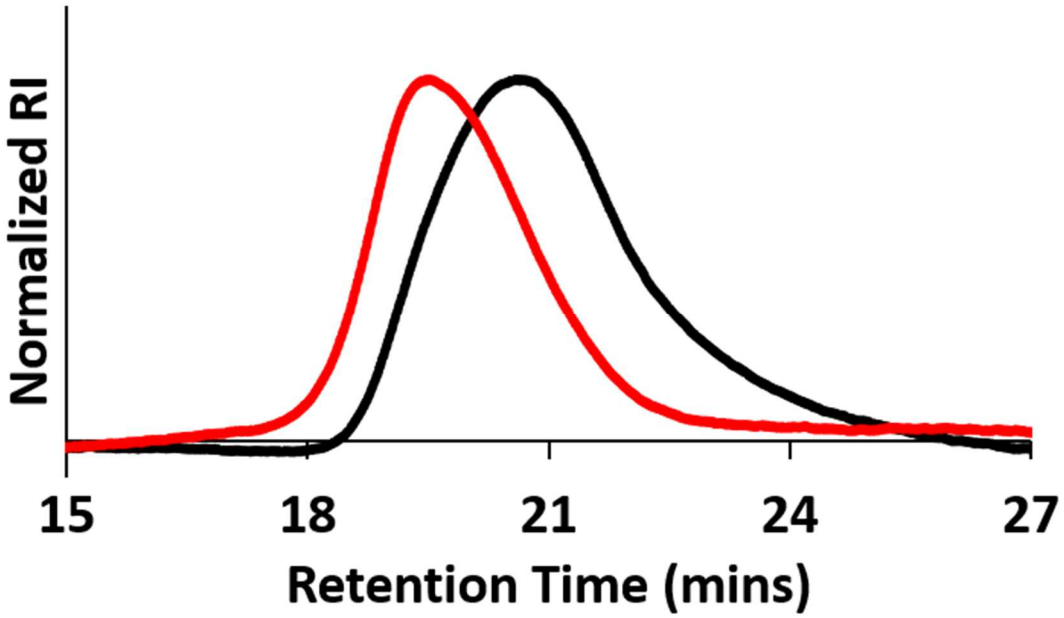

Figure 3.18. SEC chromatograms of PCL-*b*-PDCPD-H2 (entry 3 from Table 3.1, red line) and corresponding macroinitiator (black line)

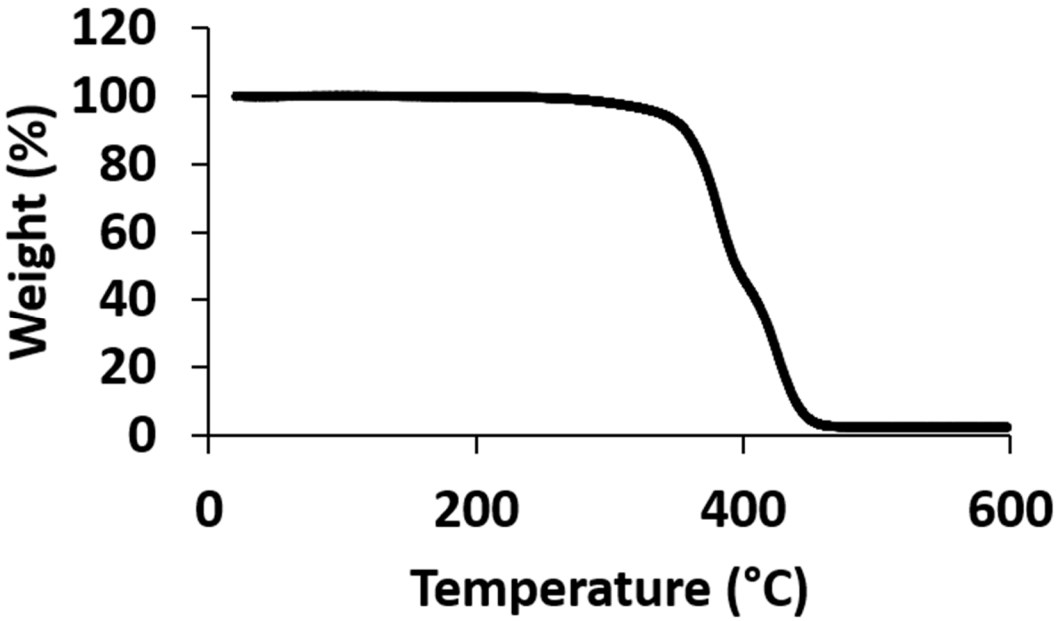

Figure 3.19. Thermogravimetric analysis of PCL-*b*-PDCPD-H2 (entry 3 from Table 3.1)

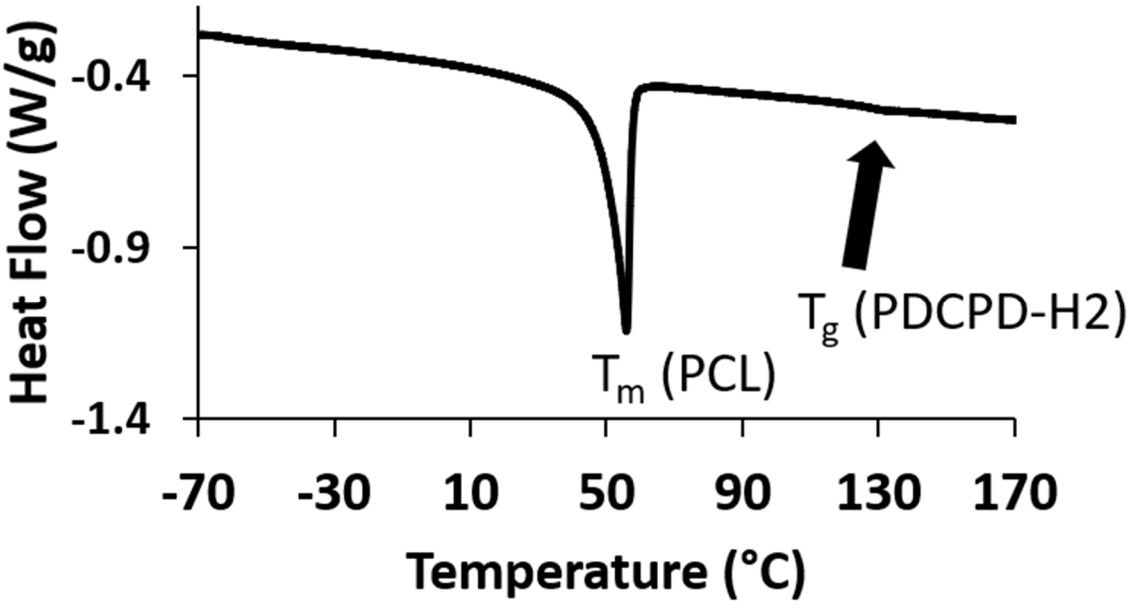

Figure 3.20. DSC (Exo up) of PCL-*b*-PDCPD-H2 (entry 3 from Table 3.1)

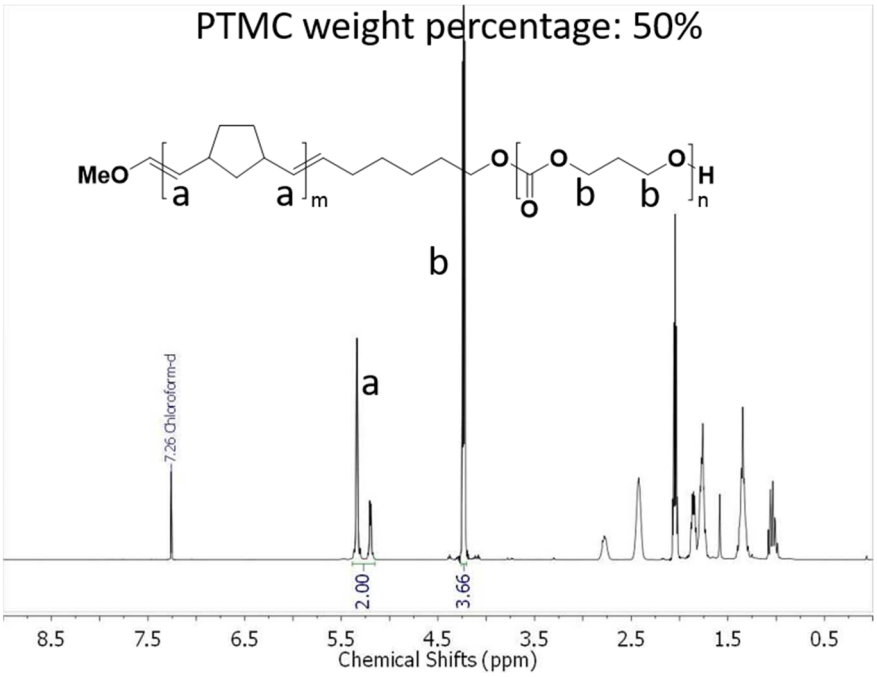

Figure 3.21. [1]H-NMR spectrum of PTMC-*b*-PNB (entry 4 from Table 3.1)

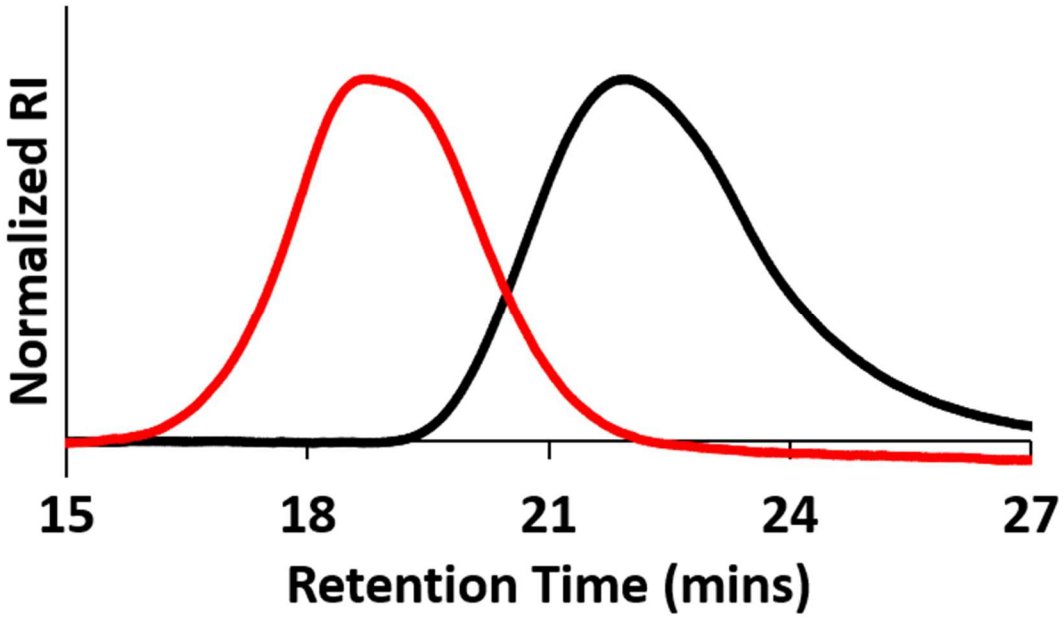

Figure 3.22. SEC chromatograms of PTMC-*b*-PNB (entry 4 from Table 3.1, red line) and corresponding macroinitiator (black line)

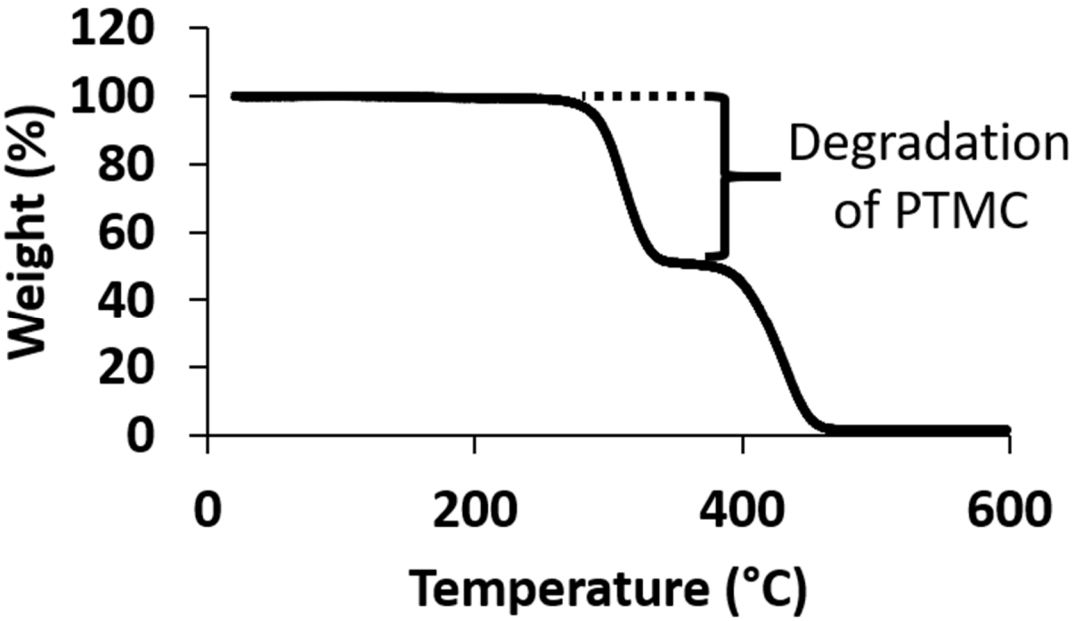

Figure 3.23. Thermogravimetric analysis of PTMC-*b*-PNB (entry 4 from Table 3.1). The weight percentage of PTMC block is around 50%.

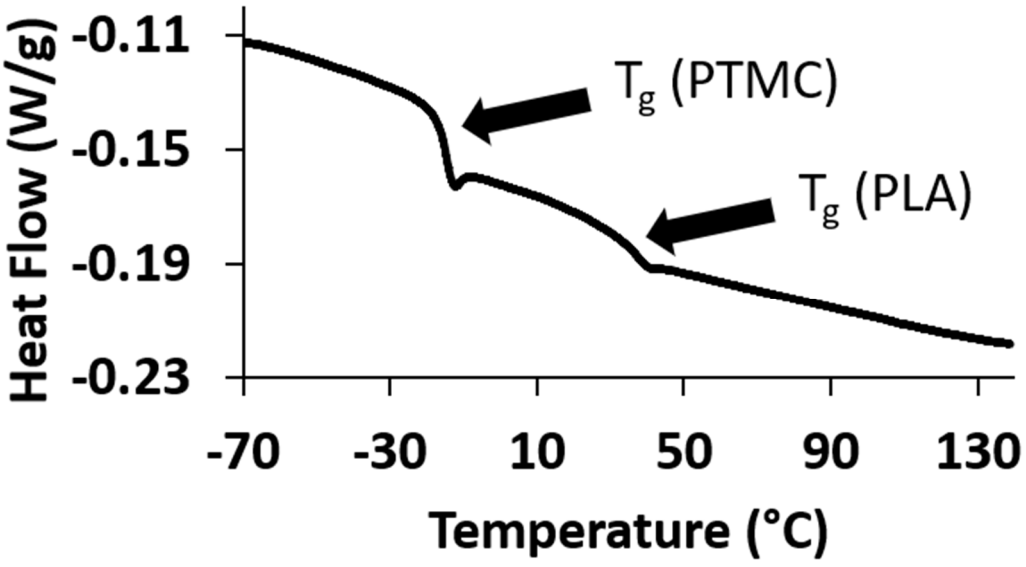

Figure 3.24. DSC (Exo up) of PTMC-*b*-PNB (entry 4 from Table 3.1)

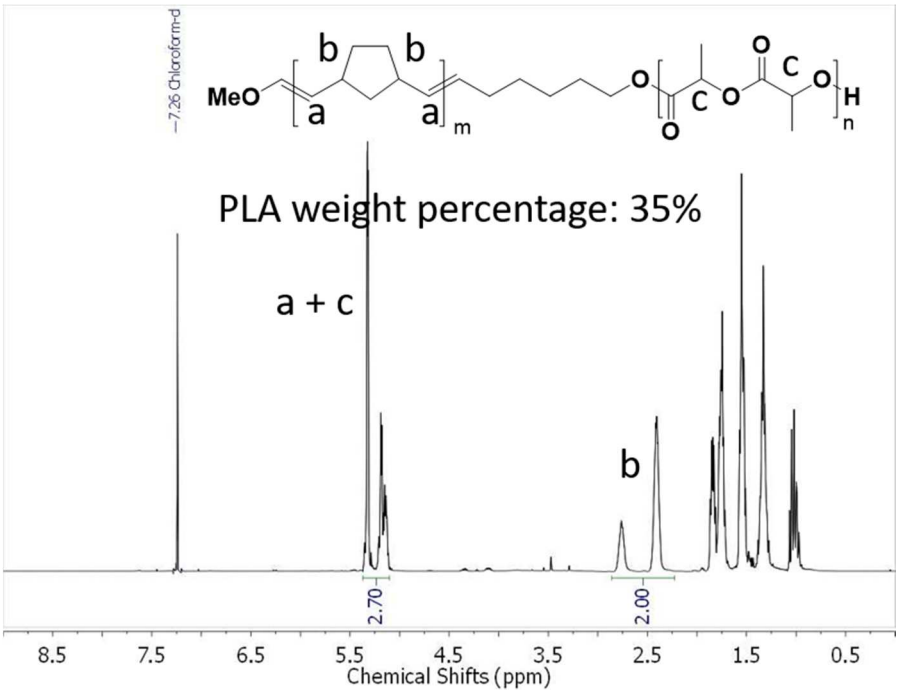

Figure 3.25. [1]H-NMR spectrum of PLA-*b*-PNB (entry 1 from Table 3.2)

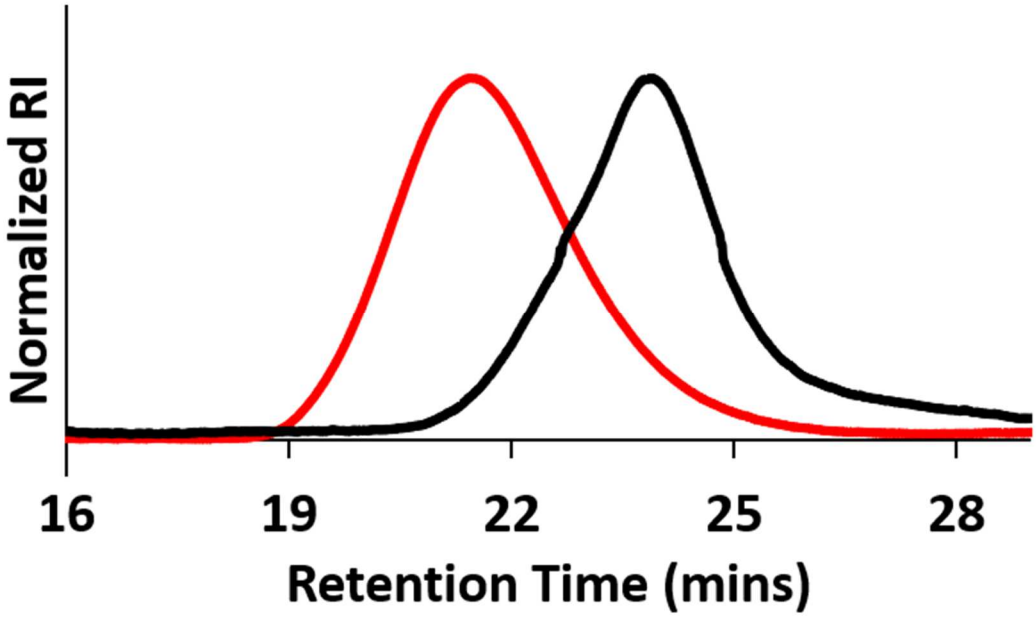

Figure 3.26. SEC chromatograms of PLA-*b*-PNB (entry 1 from Table 3.2, red line) and corresponding macroinitiators (black line)

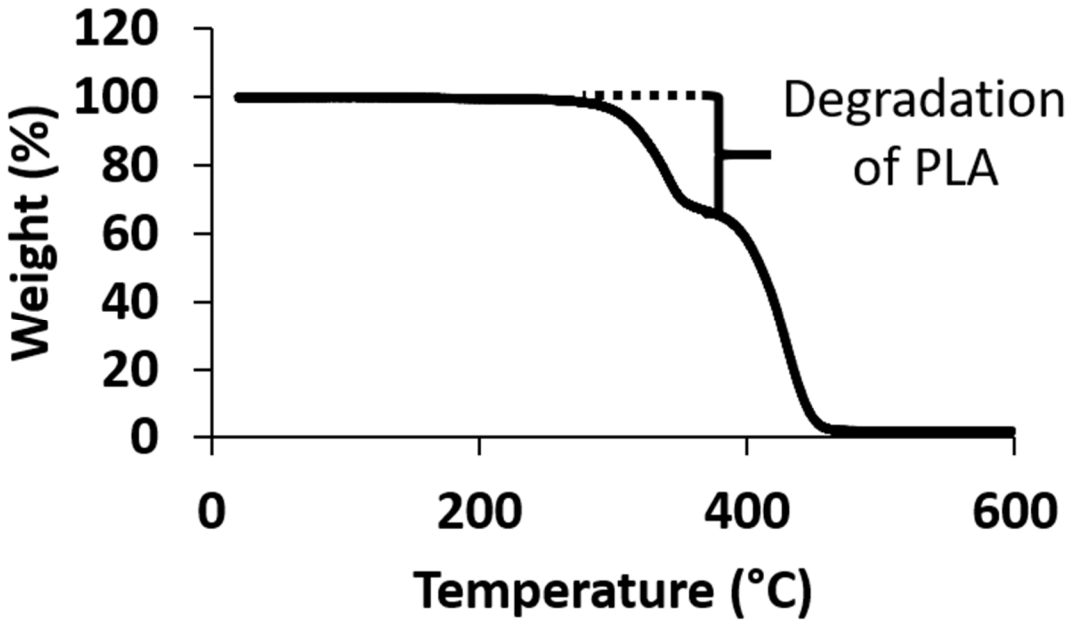

Figure 3.27. Thermogravimetric analysis of PLA-*b*-PNB (entry 1 from Table 3.2). The weight percentage of PLA block is around 34%.

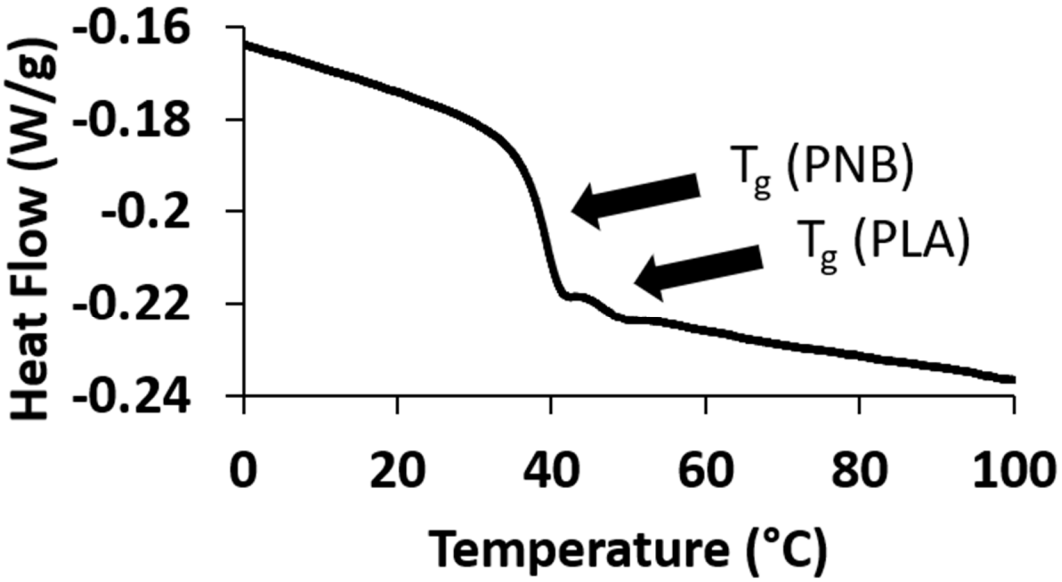

Figure 3.28. DSC (Exo up) of PLA-*b*-PNB (entry 1 from Table 3.2)

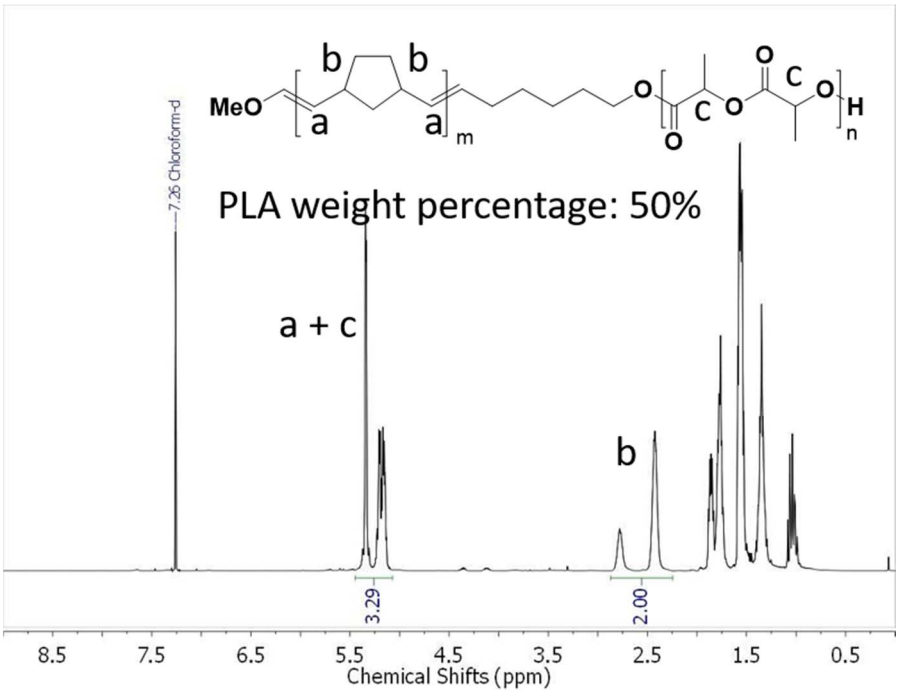

Figure 3.29. [1]H-NMR spectrum of PLA-*b*-PNB (entry 2 from Table 3.2)

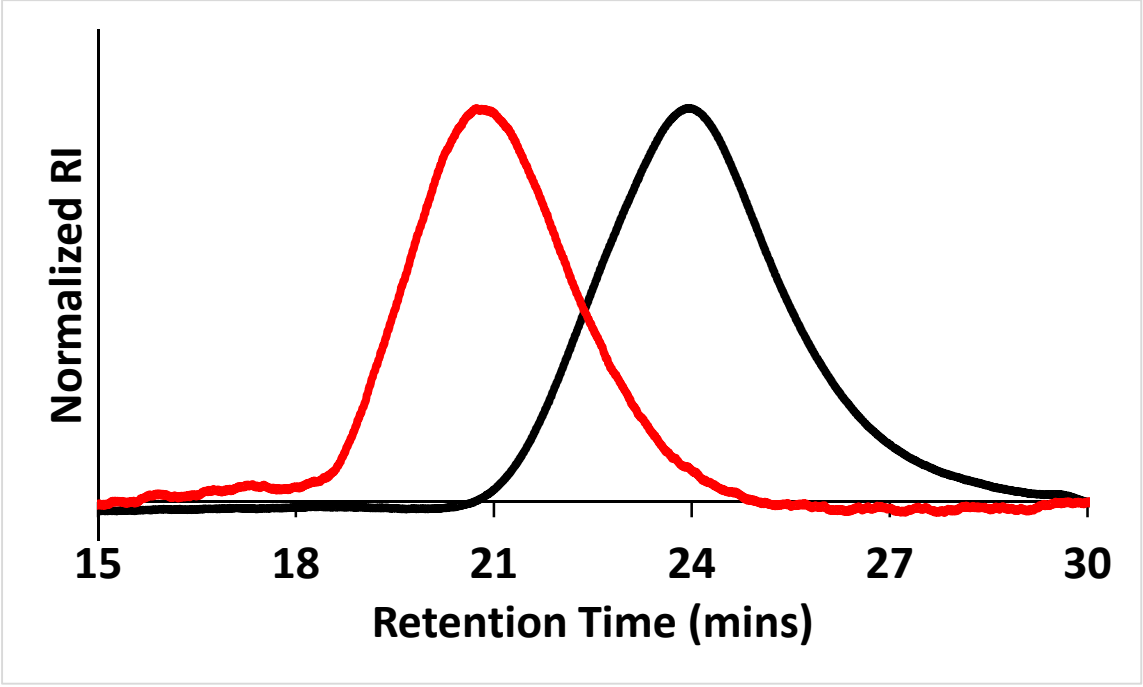

Figure 3.30 SEC chromatograms of PLA-*b*-PNB (entry 2 from Table 3.2, red line) and corresponding macroinitiator (black line)

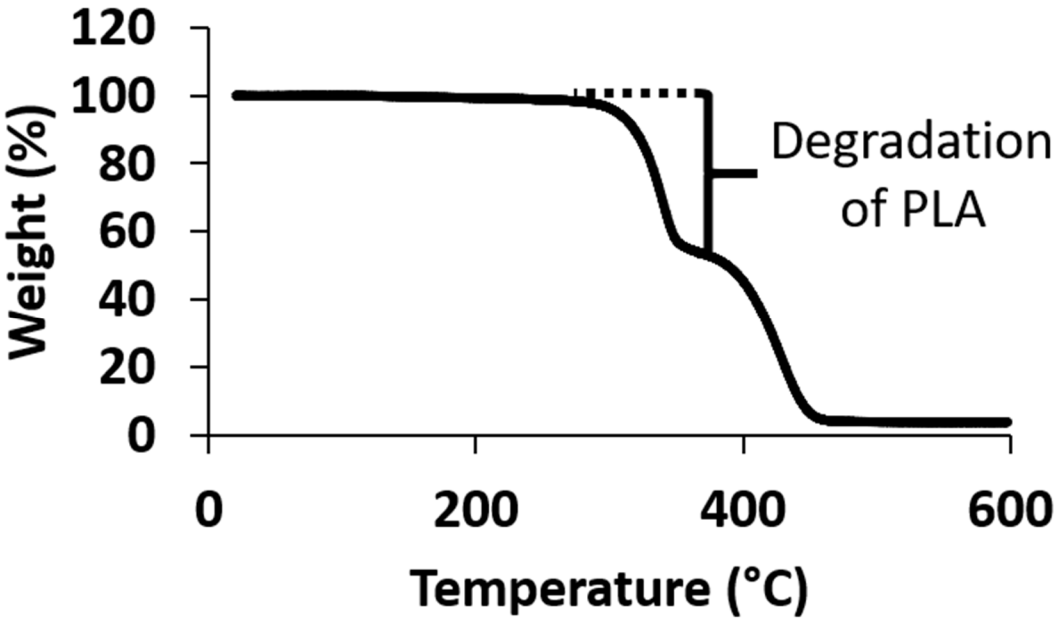

Figure 3.31 Thermogravimetric analysis of PLA-*b*-PNB (entry 2 from Table 3.2). The weight percentage of PLA block is around 47%.

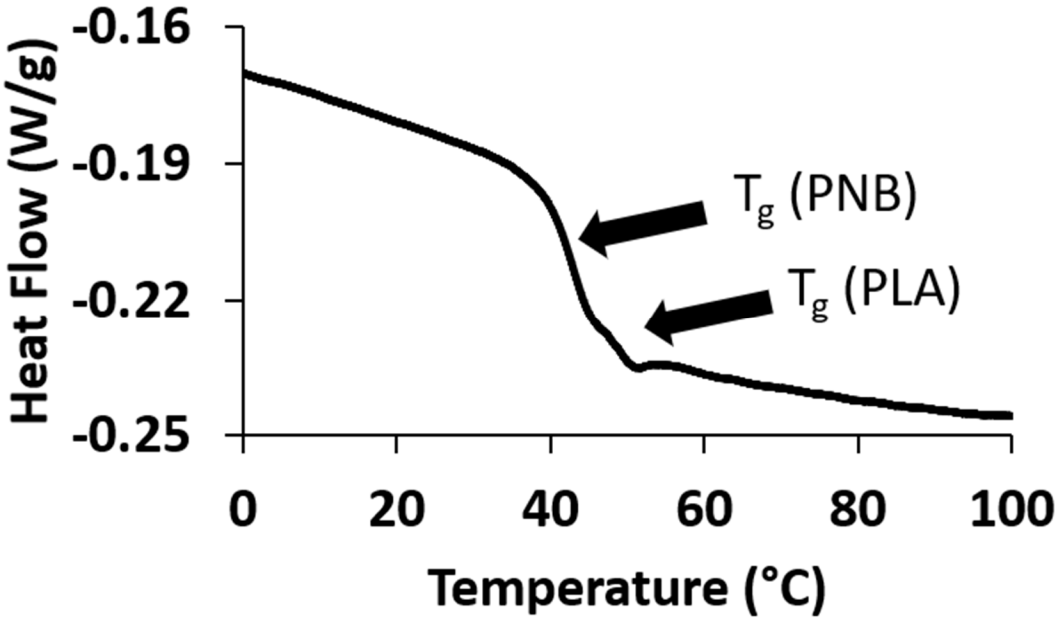

Figure 3.32 DSC (Exo up) of PLA-*b*-PNB (entry 2 from Table 3.2)

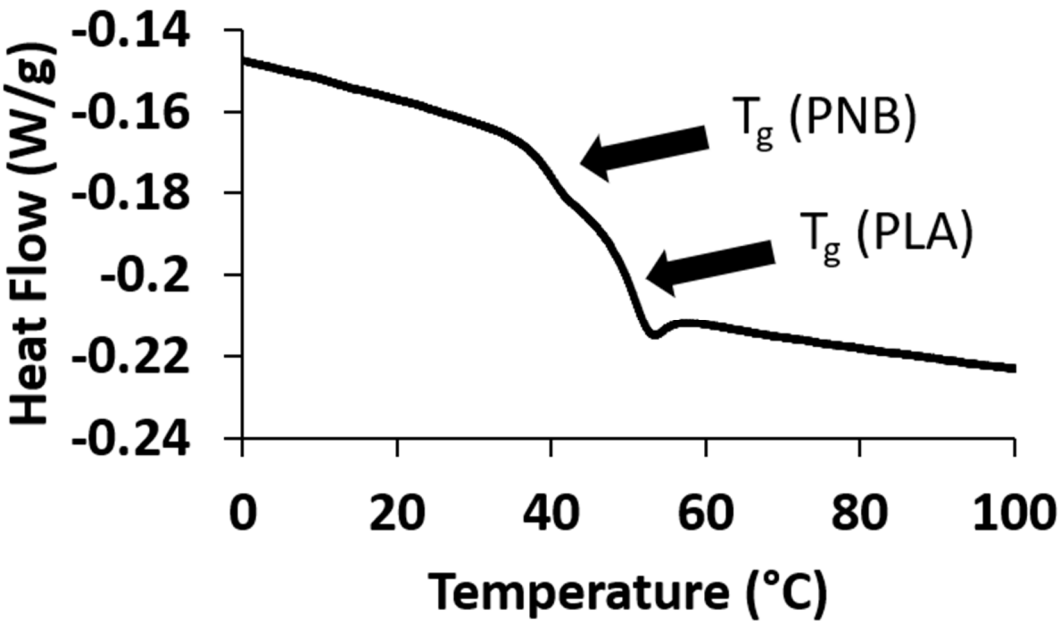

Figure 3.33 DSC (Exo up) of PLA-*b*-PNB (entry 3 from Table 3.2)

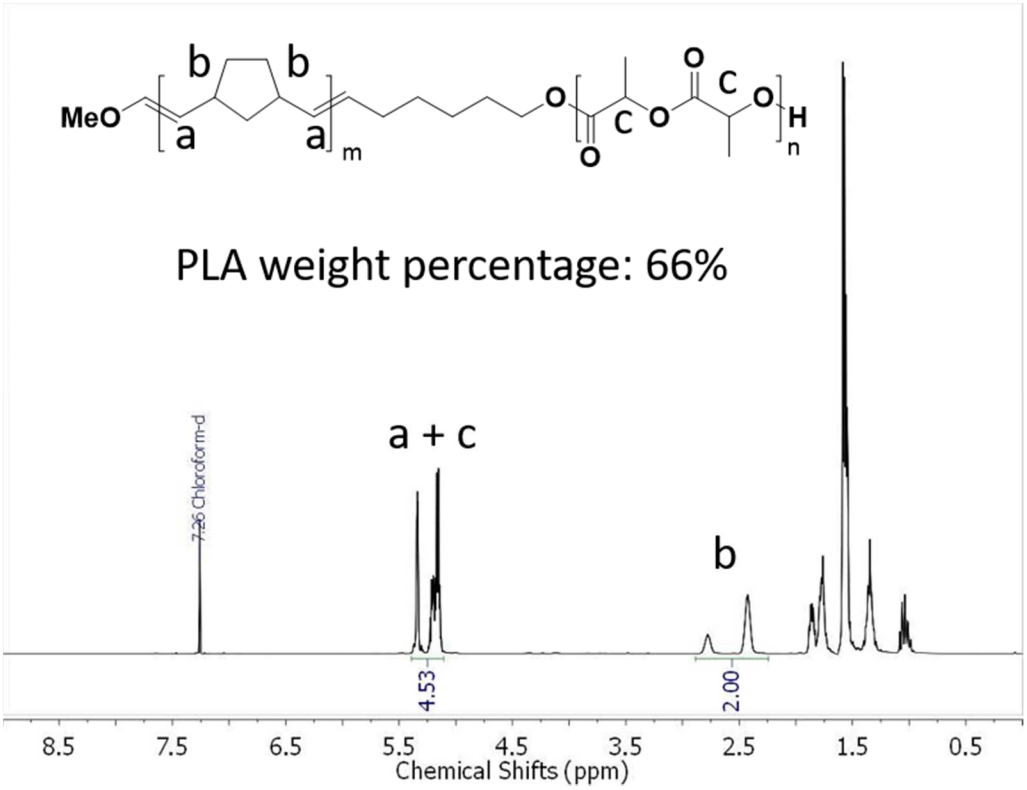

Figure 3.34. [1]H-NMR spectrum of PLA-*b*-PNB (entry 4 from Table 3.2)

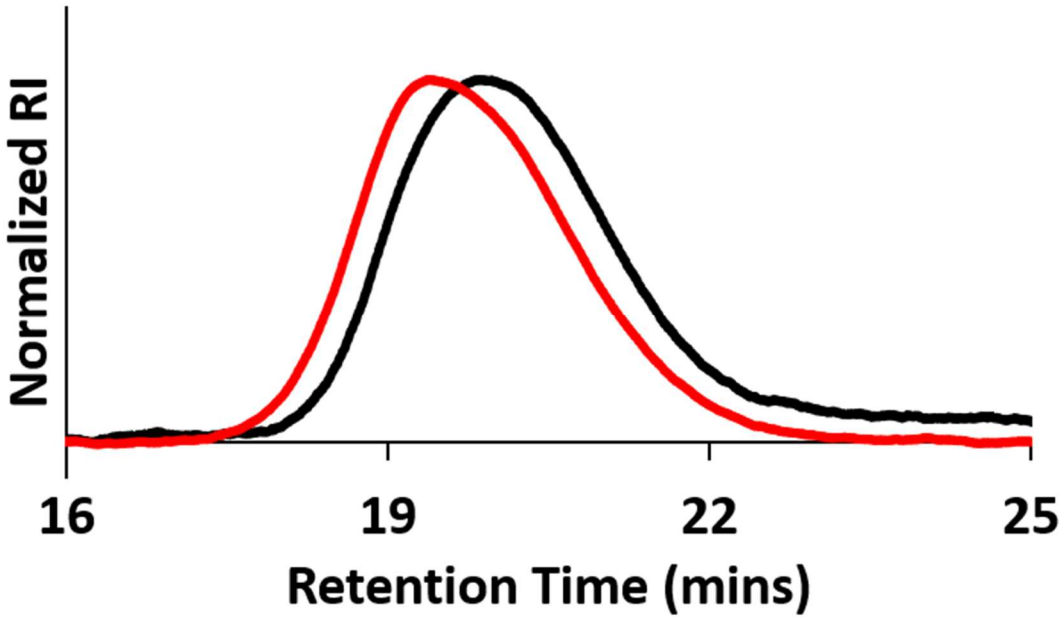

Figure 3.35. SEC chromatograms of PLA-*b*-PNB (entry 4 from Table 3.2, red line) and corresponding macroinitiator (black line)

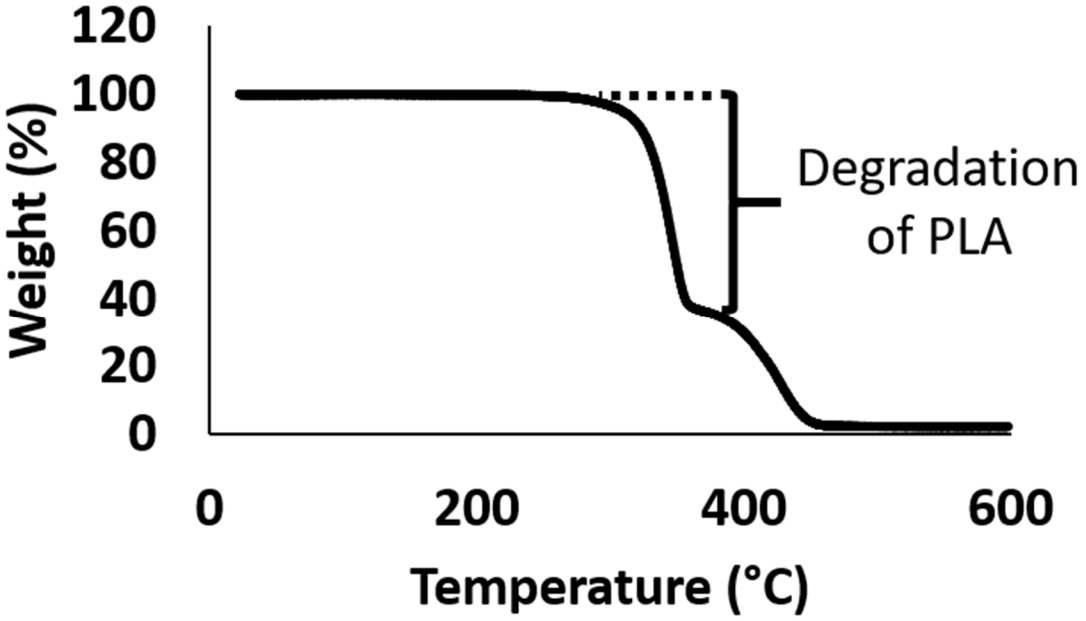

Figure 3.36. Thermogravimetric analysis of PLA-*b*-PNB (entry 4 from Table 3.2). The weight percentage of PLA block is around 64%.

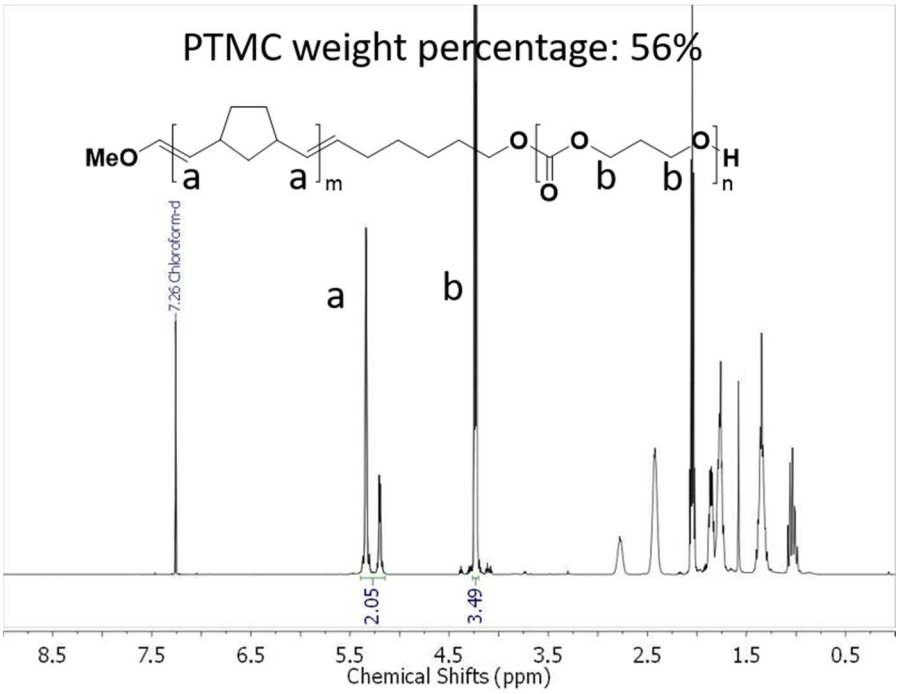

Figure 3.37. [1]H-NMR spectrum of PTMC-*b*-PNB (entry 5 from Table 3.2)

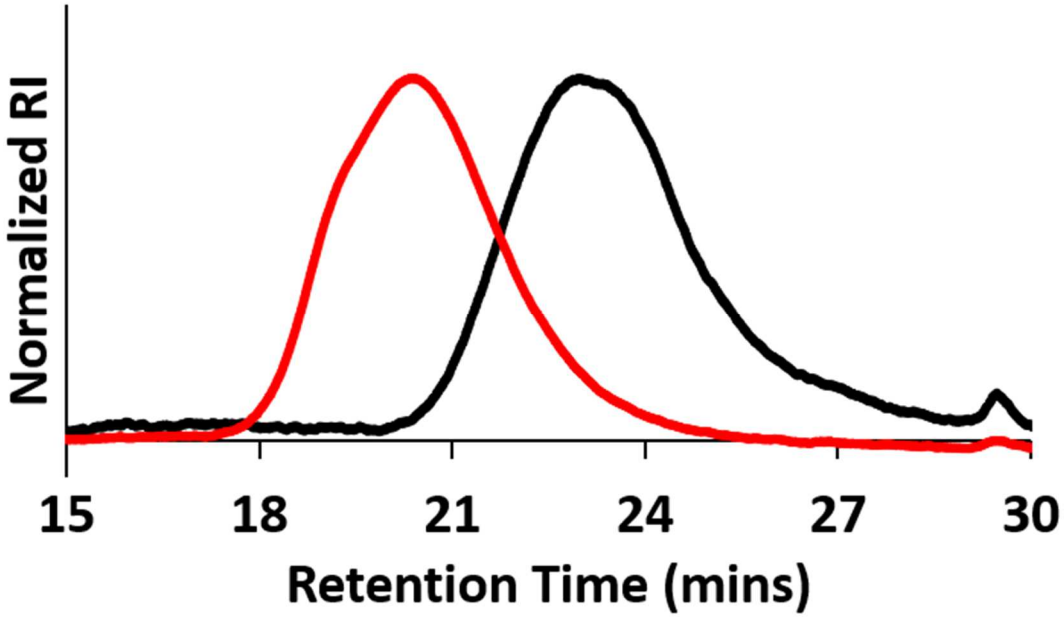

Figure 3.38. SEC chromatograms of PTMC-*b*-PNB (entry 5 from Table 3.2, red line) and corresponding macroinitiator (black line)

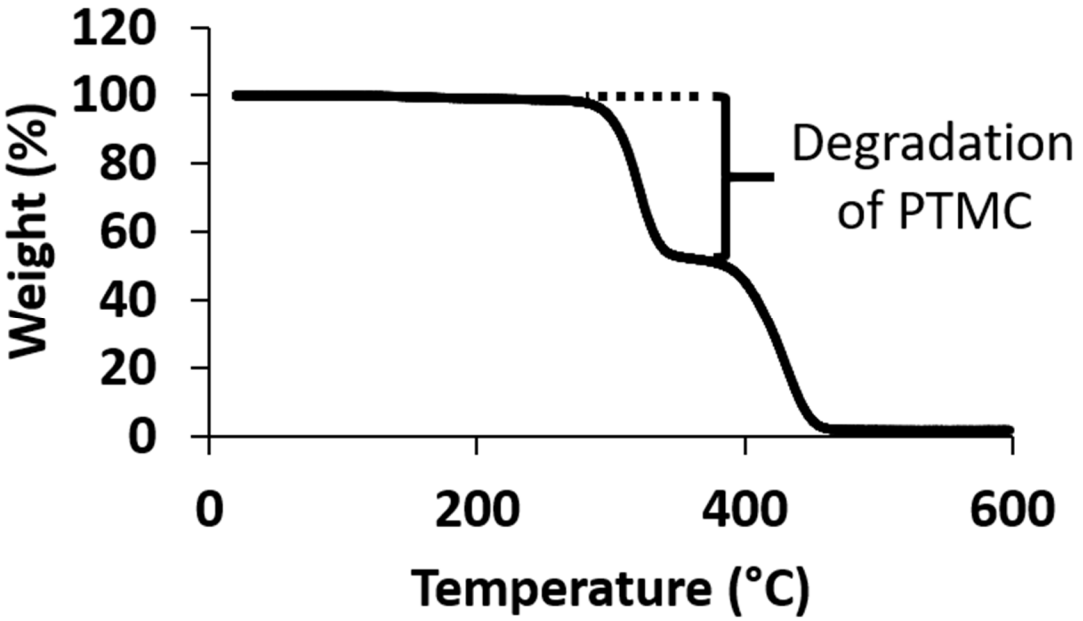

Figure 3.39. Thermogravimetric analysis of PTMC-*b*-PNB (entry 5 from Table 3.2). The weight percentage of PTMC block is around 50%.

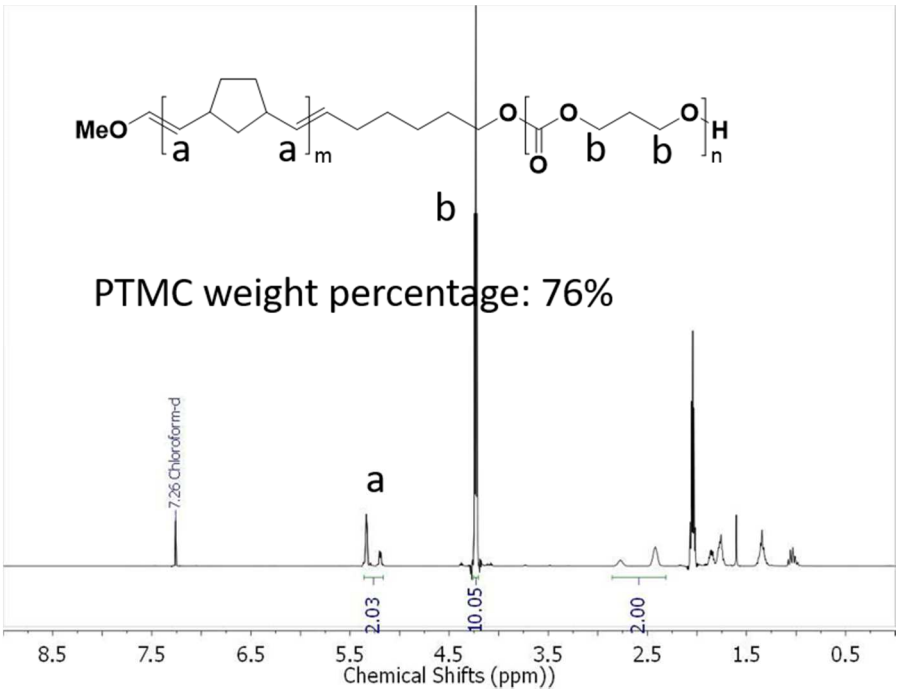

Figure 3.40. ^{1}H-NMR spectrum of PTMC-*b*-PNB (entry 6 from Table 3.2)

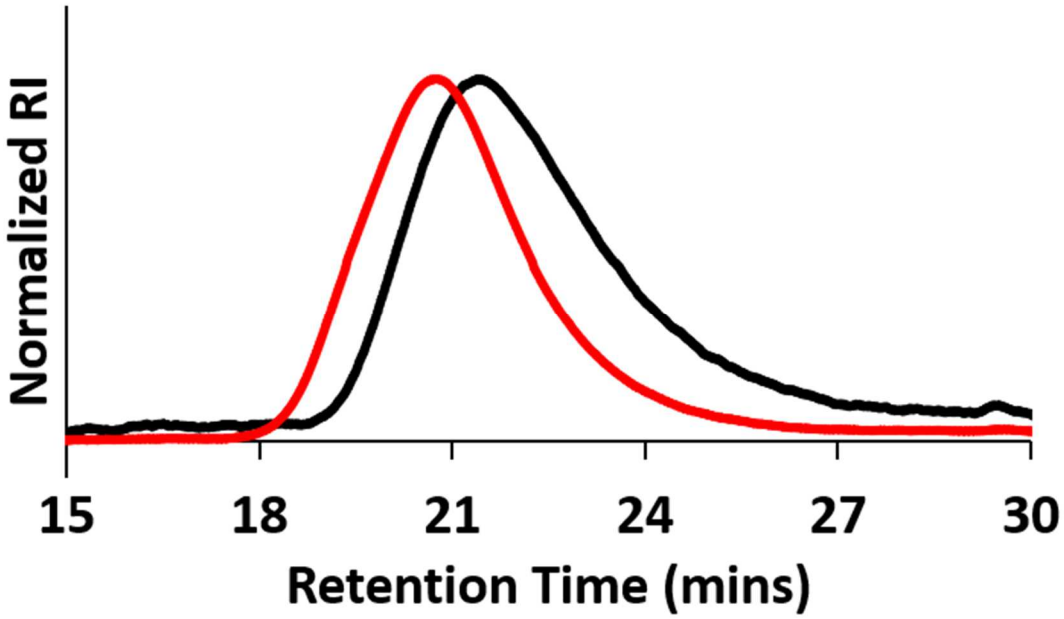

Figure 3.41. SEC chromatograms of PTMC-*b*-PNB (entry 6 from Table 3.2, red line) and corresponding macroinitiator (black line)

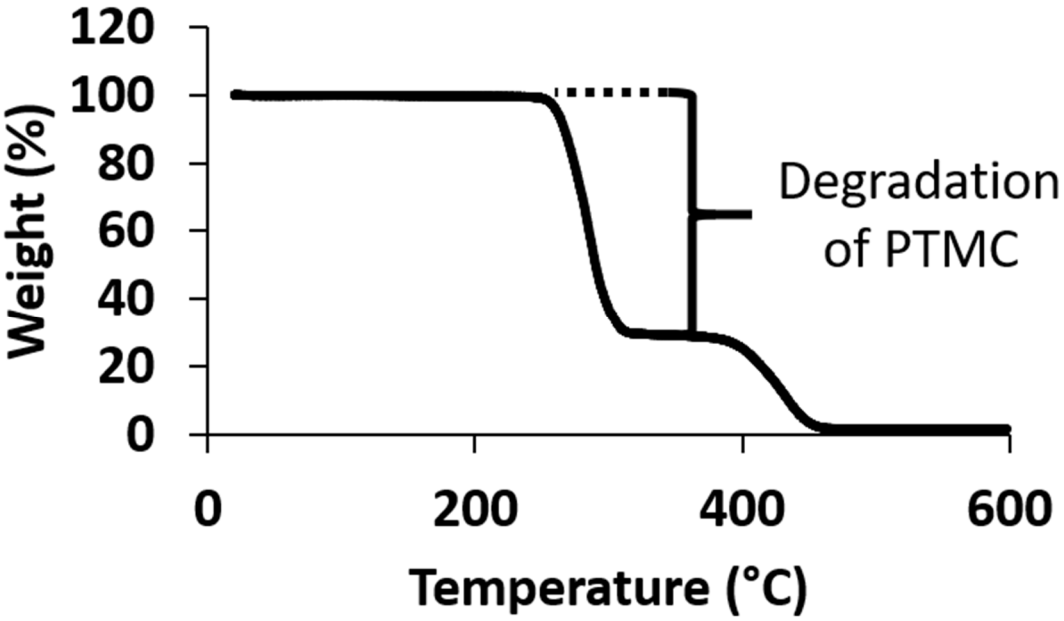

Figure 3.42. Thermogravimetric analysis of PTMC-*b*-PNB (entry 6 from Table 3.2). The weight percentage of PTMC block is around 71%.

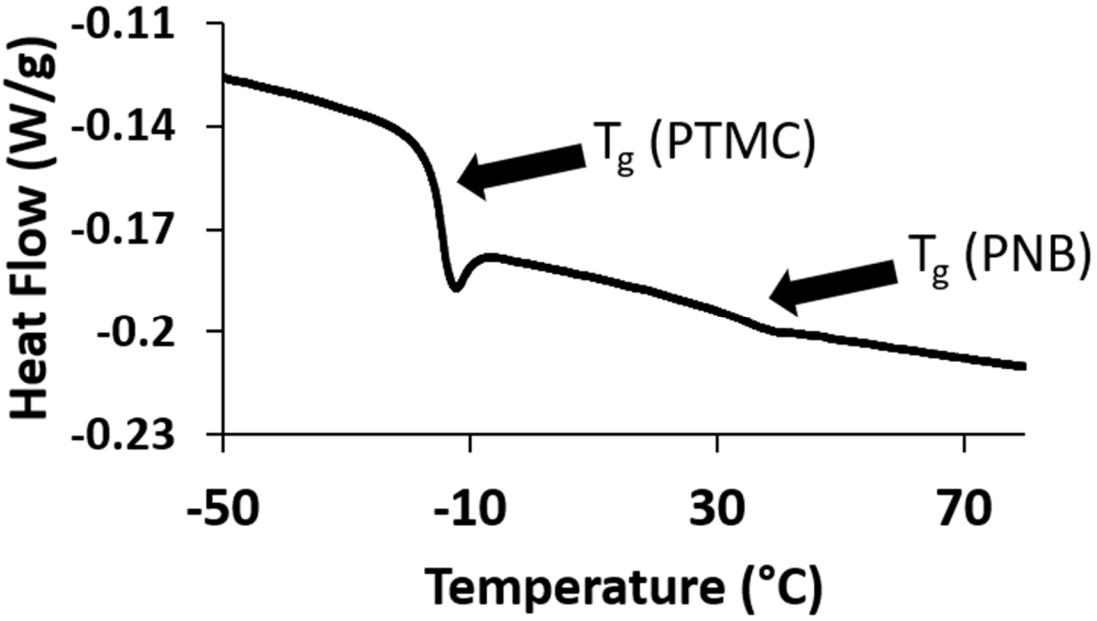

Figure 3.43 DSC (Exo up) of PTMC-*b*-PNB (entry 6 from Table 3.2)

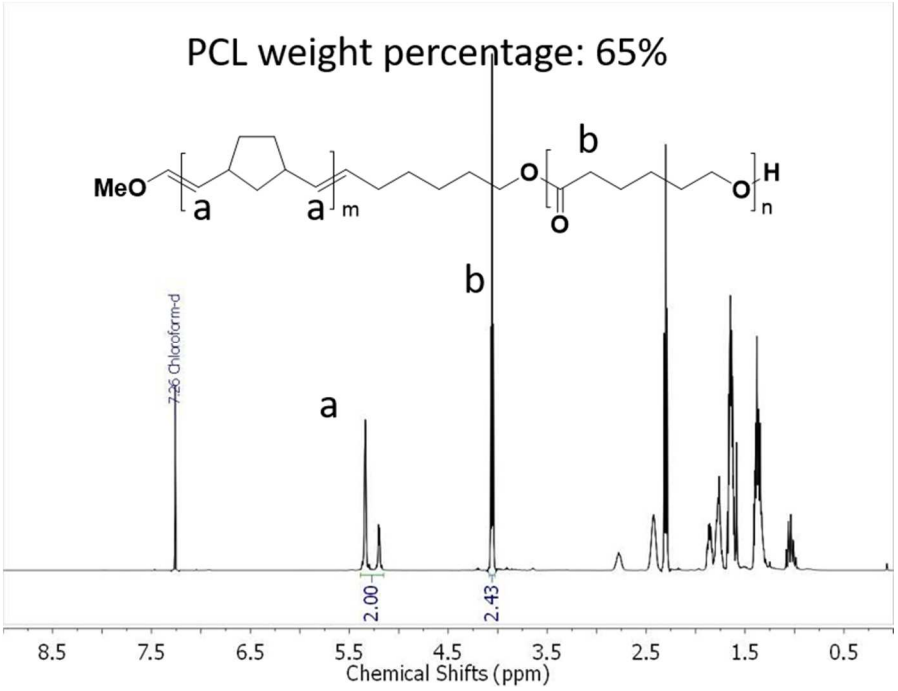

Figure 3.44 ^{1}H-NMR spectrum of PCL-*b*-PNB (entry 7 from Table 3.2)

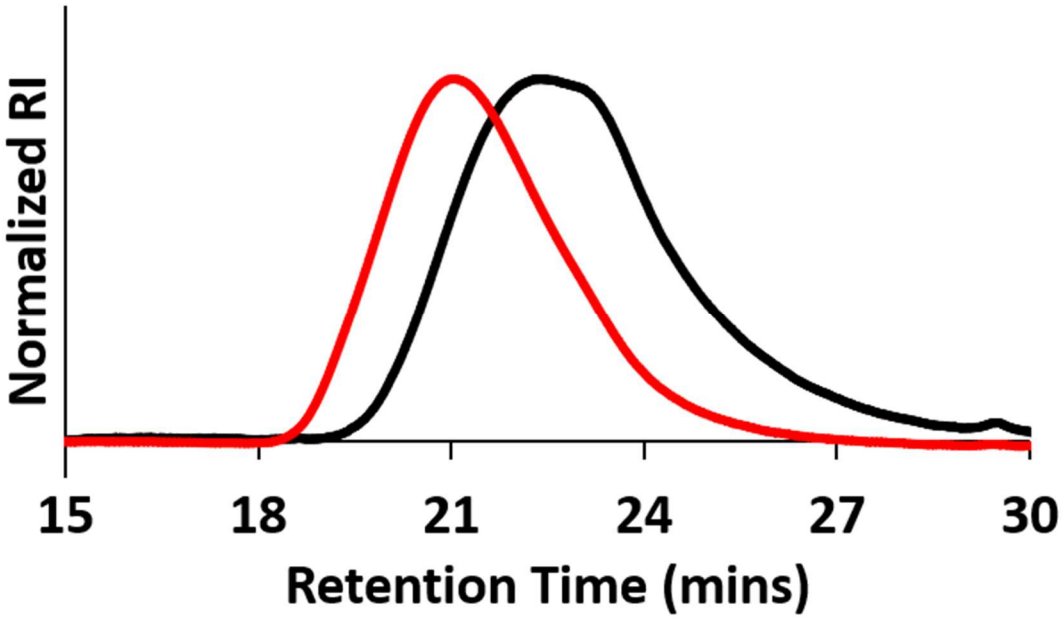

Figure 3.45. SEC chromatograms of PCL-*b*-PNB (entry 7 from Table 3.2, red line) and corresponding macroinitiator (black line)

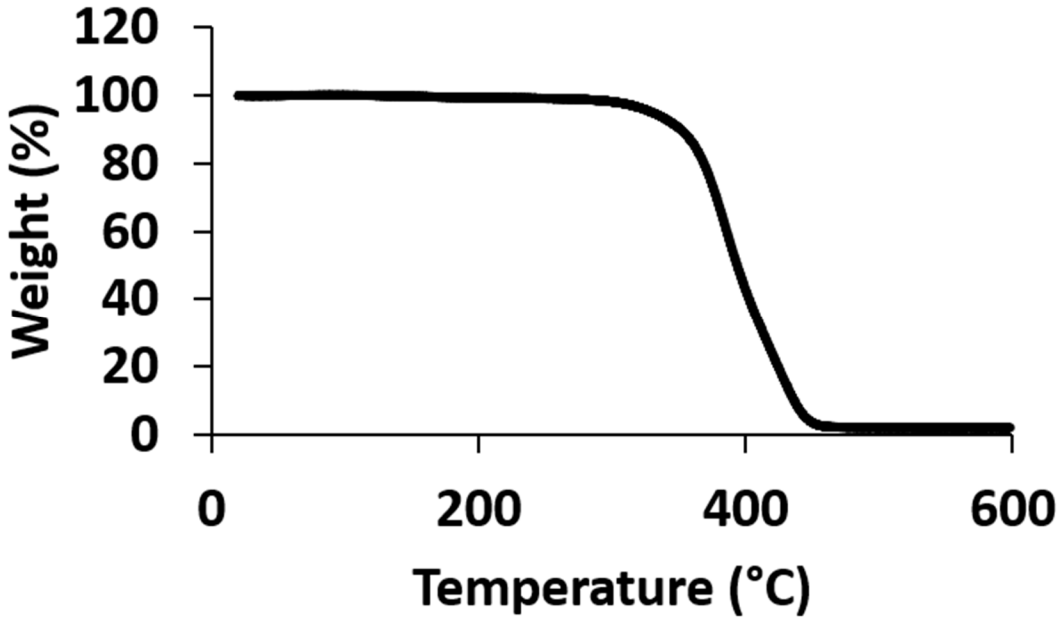

Figure 3.46. Thermogravimetric analysis of PCL-*b*-PNB (entry 7 from Table 3.2)

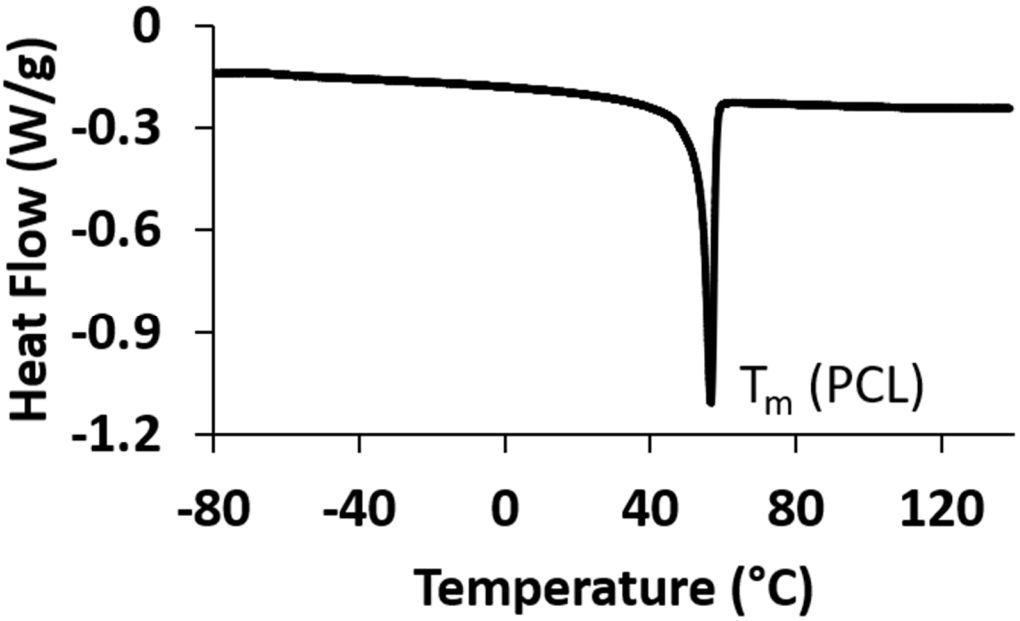

Figure 3.47. DSC (Exo up) of PCL-*b*-PNB (entry 7 from Table 3.2)

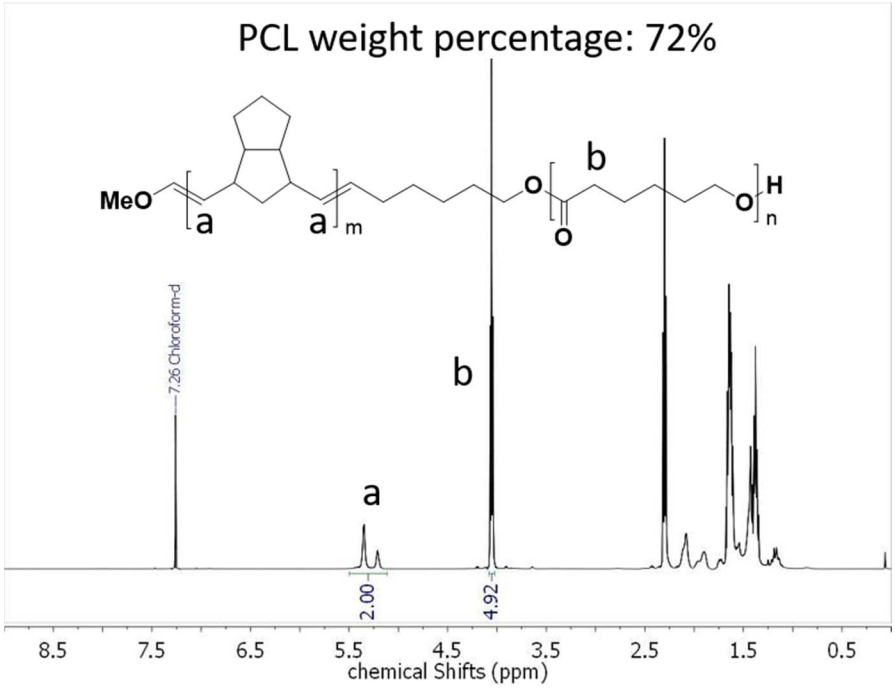

Figure 3.48. [1]H-NMR spectrum of PCL-b-PDCPD-H2 (entry 8 from Table 3.2)

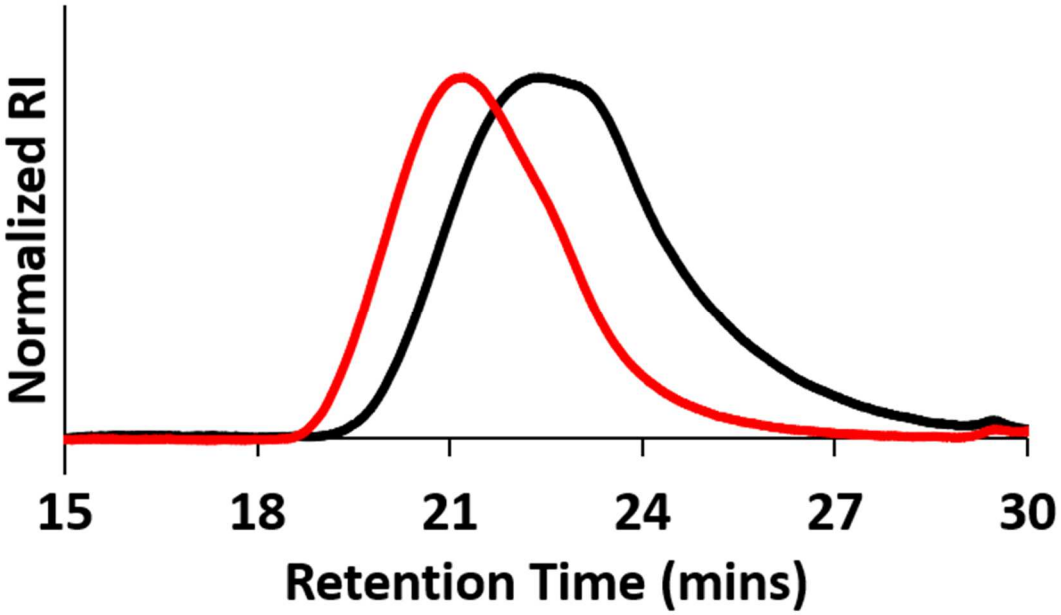

Figure 3.49. SEC chromatograms of PCL-b-PDCPD-H2 (entry 8 from Table 3.2, red line) and corresponding macroinitiator (black line)

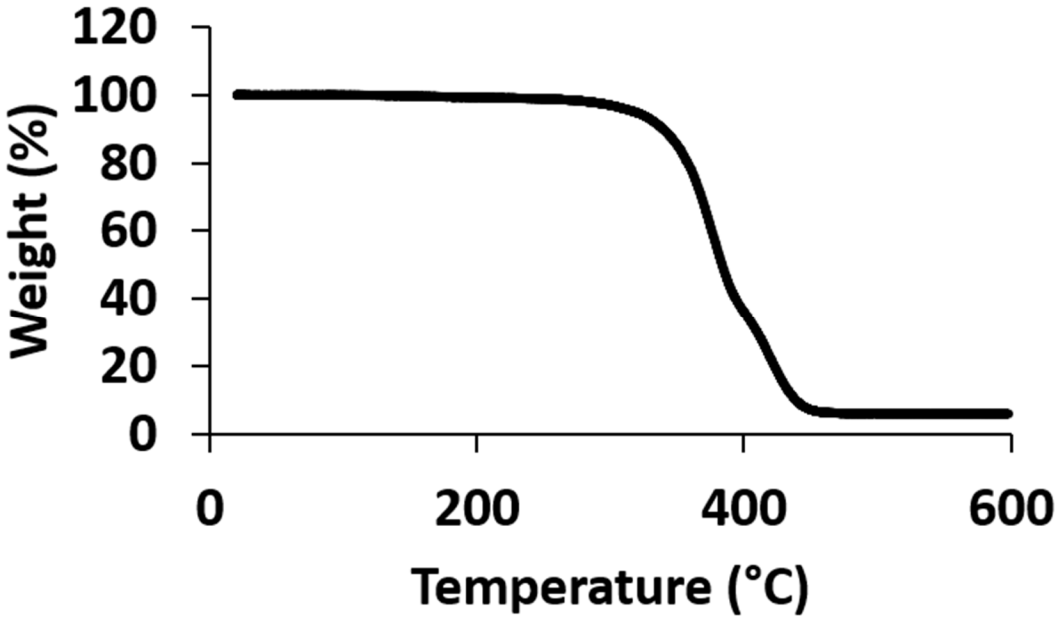

Figure 3.50. Thermogravimetric analysis of PCL-b-PDCPD-H2 (entry 8 from Table 3.2)

Notes and References for Chapter 3

[1] Bates, C. M.; Bates, F. S. *Macromolecules*, **2017**, *50*, 3.
[2] Zhang, J.; Schneiderman, D. K.; Li, T.; Hillmyer, M. A.; Bates,F.S. *Macromolecules*, **2016**, *49*, 9108.
[3] Bates, C. M.; Maher, M. J.; Janes, D. W.; Ellison, C. J.; Willson, C. G. *Macromolecules*, **2014**, *47*, 2.
[4] Elsabahy, M.; Wooley, K. L. *Chem. Soc. Rev.*, **2012**, *41*, 2545.
[5] Opsteen, J. A.; Hest, J. C. M. v. *Chem. Commun.*, **2005**, 57.
[6] Agut, W.; Taton, D.; and Lecommandoux, S. *Macromolecules*, **2007**, *40*, 5653.
[7] Durmaz, H.; Dag, A.; Altintas, O.; Ergodan, T.; Hizal, G.; Tunca, U. *Macromolecules*, **2007**, *40*, 191.
[8] Lin, W.; Fu, Q.; Zhang, Y.; Huang, J. *Macromolecules*, **2008**, *41*, 4127.
[9] Notestein, J. M.; Lee, L.-B. W.; Register, R. A. *Macromolecules*, **2002**, *35*, 1985.
[10] Ouchi, M.; Sawamoto, M. *Macromolecules*, **2017**, *50*, 2603.
[11] Perrier, S. *Macromolecules*, **2017**, *50*, 7433.
[12] Bielawski, C. W.; Grubbs, R. H. *Prog. Polym. Sci.*, **2007**, *32*, 1.
[13] Szwarc, M.; *J. Polym. Sci., Part A: Polym. Chem.*, **1998**, *36*, 9.
[14] Yagci, Y.; Tasdelen, M. A. *Prog. Polym. Sci.*, **2006**, *31*, 1133.
[15] Guo, X.; Choi, B.; Feng, A.; and Thang, S. H. *Macromol. Rapid Commun.*, **2018**, *39*, 1800479.
[16] Altintas, O.; Yilmaz, I.; Hizal, G.; Tunca, U. *J. Polym. Sci., Part A: Polym. Chem.*, **2006**, *44*, 3242.
[17] St Thomas, C.; Guerrero-Santos, R.; D'Agosto, F. *Polym. Chem.*, **2015**, *6*, 5405.
[18] Chagneux, N.; Trimaille, T.; Rollet, M.; Beaudoin, E.; Gerard, P.; Bertin, D.; Gigmes, D. *Macromolecules*, **2009**, *42*, 9435.
[19] Jung, H.; Brummelhuis, N. t.; Yang, S. K.; Weck, M. *Polym. Chem.*, **2013**, *4*, 2837.
[20] Freudensprung, I.; Klapper, M.; Mullen, K. *Macromol. Rapid Commun.*, **2016**, *37*, 209.
[21] Theriot, J. C.; Miyake, G. M.; Boyer, C. A. *ACS Macro Lett.*, **2018**, *7*, 662.
[22] Fu, C.; Xu, J.; Kokotovic, M.; Boyer, C. *ACS Macro. Lett.*, **2016**, *5*, 444.
[23] Aydogan, C.; Kutahya, C.; Allushi, A.; Yilmaz, G.; Yagci, Y. *Polym. Chem.*, **2017**, *8*, 2899.
[24] Ogawa, K. A.; Goetz, A. E.; Boydston, A. J. *J. Am. Chem. Soc.*, **2015**, *137*, 1400.
[25] Goetz, A. E.; Boydston, A. J. *J. Am. Chem. Soc.*, **2015**, *137*, 7572.
[26] Pascual, L. M. M.; Dunford, D. G.; Goetz, A. E.; Ogawa, K. A.; Boydston, A. J. *Synlett*, **2016**, *27*, 759.
[27] Goetz, A. E.; Pascual, L. M. M.; Dunford, D. G.; Ogawa, K. A.; Knorr, Jr., D. B.; Boydston, A. J. *ACS Macro Lett.*, **2016**, *5*, 579.
[28] Pascual, L. M. M.; Goetz, A. E.; Roehrich, A. M.; Boydston, A. J. *Macromol. Rapid Commun.*, **2017**, *38*, 1600766.
[29] Lu, P.; Alrashdi, N. M.; Boydston, A. J. *J. Polym. Sci., Part A: Polym. Chem.*, **2017**, *55*, 2977.
[30] Kamber, N. E.; Jeong, W.; Waymouth, R. M.; Pratt, R. C.; Lohmeijer, B. G. G.; Hedrick, J. L. *Chem. Rev.*, **2007**, *107*, 5813.
[31] Kiesewetter, M. K.; Shin, E. J.; Hedrick, J. L.; Waymouth, R. M. *Macromolecules*, **2010**, *43*, 2093.
[32] Sardon, H.; Pascual, A.; Mecerreyes, D.; Taton, D.; Cramail, H.; Hedrick, J. L. *Macromolecules*, **2015**, *48*, 3153.
[33] Hu, S.; Zhao, J.; Zhang, G.; Schlaad, H. *Prog. Polym. Sci.*, **2017**, *74*, 34.
[34] Sutterer, A.; Moeller, K. D. *J. Am. Chem. Soc.*, **2000**, *122*, 5636.

[35] Moeller, K. D. *Synlett*, **2009**, *8*, 1208.
[36] Moeller, K. D. *Chem. Rev.*, **2018**, *118*, 4817.
[37] Liu, B.; Duan, S.; Sutterer, A. C.; Moeller, K. D. *J. Am. Chem. Soc.*, **2002**, *124*, 10101.
[38] Campbell, J. M.; Xu, H.-C.; Moeller, K. D. *J. Am. Chem. Soc.*, **2012**, *134*, 18338.
[39] Nyce, G. W.; Glauser, T.; Connor, E. F.; Mock, A.; Waymouth, R. M.; Hedrick, J. L. *J. Am. Chem. Soc.*, **2003**, *125*, 3046.
[40] Nederberg, F.; Lohmeijer, B. G. G.; Leibfarth, F.; Pratt, R. C.; Choi, J.; Dove, A. P.; Waymouth, R. M.; Hedrick, J. L. *Biomacromolecules*, **2007**, *8*, 153.
[41] Lohmeijer, B. G. G.; Pratt, R. C.; Leibfarth, F.; Logan, J. W.; Long, D. A.; Dove, A. P.; Nederberg, F.; Choi, J.; Wade, C.; Waymouth, R. M.; Hedrick, J. L. *Macromolecules*, **2006**, *39*, 8574.
[42] Zhu, L.; Chen, Y.; Zhang, A.; Calhoun, B. H.; Chun, M.; Quirk, R. P.; Cheng, S. Z. D.; Hsiao, B. S.; Yeh, F.; Hashimoto, T. *Phys. Rev. B.*, **1999**, *60*, 10022.
[43] Martiny, M.; Steckhan, E.; Esch, T. *Chem. Ber.*, **1993**, *126*, 1671.
[44] Hintermann, L. *Beilstein J. Org. Chem.*, 2007, **3**, No. 22.
[45] Oertel, A. M.; Ritleng, V.; Burr, L.; Chetcuti, M. J. *Organometallics*, **2011**, *30*, 6685.
[46] Huang, Y.; Moeller, K. D. *Tetrahedron*, **2006**, *62*, 6536.

Chapter 4. Expanding Monomer Scopes of Organic Photoredox-Mediated Ring-Opening Metathesis Polymerization (*o*-ROMP)

Section 1: Introduction

4.1.a o-ROMP of Dicyclopentadiene-Related Monomers

The development of well-defined metal catalysts has transformed traditional ROMP into an extraordinary polymerization technique with remarkable functional group tolerance and monomer scope.[1] Since our *o*-ROMP experiments had thus far only focused on norbornene **1**, we decided to prepare polymers with more complex functionality.[2] We started our examination by testing dicyclopentadiene (DCPD) and related monomers.[3] When polymerized within metal-based ROMP catalysts, *endo*-DCPD **2a** affords cross-linked thermoset materials with excellent properties, that can be used in applications such as vehicle body panels and wind turbine blades.[4] However, the nature of the cross-linking process generally traps the metal catalysts inside the bulk material, resulting in limited lifetime from deleterious side reactions. We questioned if our *o*-ROMP method could allow for the preparation of cross-linked polyDCPD without metal contamination.

Monomer **2a** was then subjected to our previous reported *o*-ROMP condition with **OPC 13** as photoredox mediator and ethyl propenyl ether (**EPE**) as organic initiator. Although there was no sign of cross-linking, we were able to synthesize a linear polyDCPD (M_n = 3.8 kDa; $Đ$ = 1.1) with monomer conversion around 15%. Because of their great solubility and pendant olefin moieties, these linear polyDCPD were subjected to thiol-ene reaction conditions to afford cross-linked materials under fully metal-free protocols. We attempted to optimize this polymerization to achieve higher monomer conversion (Table 4), however, the variation of monomer concentration and pyrylium salts loading resulted in no significant change in conversion. Decreasing

polymerization temperature and initial ratio of monomer to initiator gave a slight improvement in conversion. ^{1}H-NMR revealed that multiple enol ether species at the polymer chain ends, possibly from deleterious side reactions of the vinyl ether radical cations, thus limiting monomer conversion.[5]

Table 4.1. Attempted optimization on *o*-ROMP of *endo*-DCPD **2a**

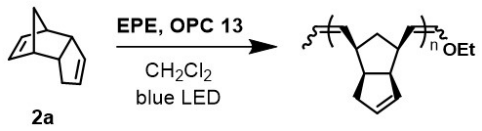

2a

[**2a**]$_0$: [EPE]$_0$: [**OPC 13**]$_0$[a]	[**2a**]$_0$ (M)[b]	temp (^{o}C)	conversion[c] (%)
100 : 1 : 0.07	2.25	23	13
100 : 1 : 0.07	1.75	23	15
100 : 1 : 0.07	2.80	23	13
102 : 1 : 0.25	1.75	23	15
100 : 1 : 0.07	1.75	4	19
51 : 1 : 0.07	1.76	23	20

[a]Initial molar ration of **2a**, **EPE** and **OPC 13**. [b]Initial concentration of **2a**. [c]Conversion of **2a**, as determined by ^{1}H-NMR analysis.

We next investigated whether the presence of monomer **2a** was detrimental to the *o*-ROMP of monomer **1**. The copolymerization between **2a** and **1** was set up using feed ratio of monomers (**2a** + **1**) to initiator **EPE** of 100 : 1. Figure 4.1 shows good correlation of *endo*-DCPD **2a** loading to the composition and M_n of the final polymer. We realized that the amount of incorporation of **2a** increases with increasing initial loading, although the amount of *endo*-DCPD content is less than the theoretical value based on the feed ratio. As we expected, higher initial loading of **2a** led to a significant decrease in both monomer conversion and M_n of final polymer. Since moderate conversion (~ 50 – 60 %) of **2a** was achieved at low loading, we concluded that the decreased

reactivity of the monomer was not responsible for low conversions of **5a** during *o*-ROMP homopolymerization.

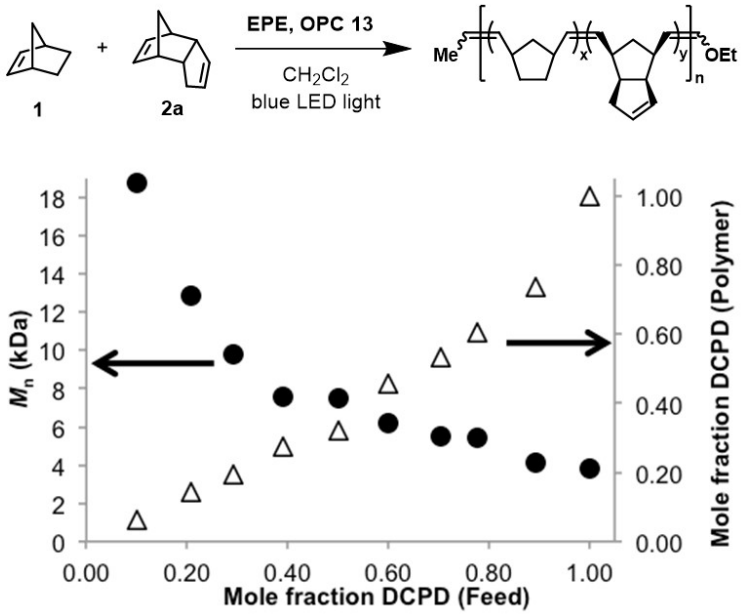

Figure 4.1. Plot of M_n (black dot) and DCPD incorporated into final polymer (white triangle) vs DCPD loaded for DCPD/NB copolymerization.

To better rationalize the low conversion of *endo*-DCPD, we examined two potential explanations (Figure 4.2). The first scenario hypothesizes that the steric bulk of the additional cyclopentene ring in monomer **2a** might attenuate the rate of new monomer incorporation. The second hypothesis is that, the proximity of the pendant cyclopentene to the propagating radical cation might create problems, since the intramolecular reactivity of neighboring olefins with radical cation intermediates is well-documented. To probe these two possible pathways, we prepared monomers **2b-d** to compare their *o*-ROMP performance with **2a**. While monomers **2b** and **2d** avoid the possibility of any undesired intramolecular reactivity with the extra olefin, monomer **2c** would be expected to perform well if the problem was strictly sterics in nature.

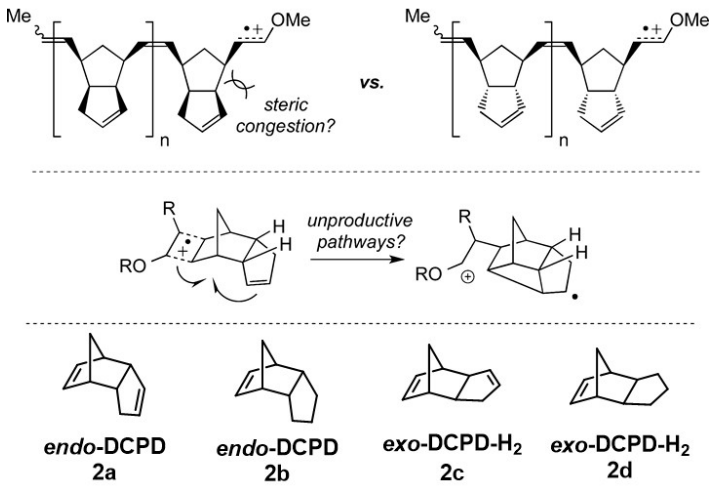

Figure 4.2. Potential reasons for decreased DCPD conversion and scope of monomers examined.

Monomers **2a-d** underwent *o*-ROMP to varying degrees under our previously reported conditions (Figure 4.3). Similar to what was observed for *endo*-DCPD monomer **2a**, *exo*-DCPD monomer **2c** was found to perform poorly with 20% conversion. However, for dihydroDCPD monomers **2b** (55% conversion) and **2d** (>90% conversion), these *o*-ROMP reactions performed significantly better. The results from monomer **2d** was actually comparable to previous *o*-ROMP of norbornene **1**. These results suggested to us that the poor performance of monomers **2a** and **2c** most likely arises from the pendant cyclopentene structures, since the steric impedance in monomer **2b** did not diminish its reactivity. To further investigate the poor monomer conversion of DCPD, we performed *o*-ROMP of **1** in the presence of cyclopentene, which afforded similar conversion to control experiments with no additives. Also, cyclopentene proved to be unreactive in homopolymerization or in stoichiometric reactions with **2a**. Taken together, these control experiments confirmed that the intramolecular nature of the side reaction between pendant cyclopentene groups and propagating radical cation chain end is hindering conversion.

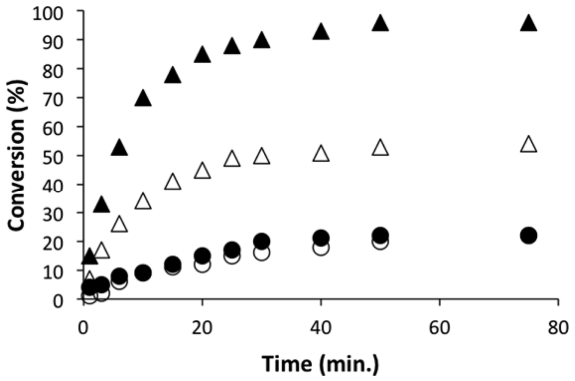

Figure 4.3. Plot of conversion vs time for monomers **2a** (white dot), **2b** (white circle), **2c** (black dot) and **2d** (black triangle).

4.1.b o-ROMP of Monomers with Protected Alcohols

To further expand the monomer scope of *o*-ROMP, we became interested in exploring the functional group tolerance for this new method so that we could identify functionalized monomers compatible with our methodology.[6] For simply testing the functional group compatibility within *o*-ROMP, we studied the effect of small molecule additives on the polymerization of monomer **1** using our previously reported photoredox conditions. Feed ratio of these additives was varied from 1 to 100 vs vinyl ether initiator to mimic stoichiometric conditions with initiator and monomer, respectively. Given the high reactivity of radical cation intermediates, we initially were concerned about polar functional groups.[7] However, the results from additive study, as summarized in Table 4.2, were quite encouraging. The difference in monomer conversion for the series of added alcohols was ascribed to their relative nucleophilicity, since tert-butanol with the highest steric hindrance resulted in the best *o*-ROMP performance. For those less nucleophilic additives, such as electron-deficient hexafluroisopropanol (HFIP) and sterically hindered methyl-tertbutyl-ether (MTBE), there was little impact on norbornene conversion even at 100 equivalents relative to initiator. Moreover, the observed moderate conversion of **1** in the presence of small amounts of water (1 : 1 with initiator, 310 ppm by wt) encouraged us to explore the *o*-ROMP efficiency outside

glovebox. The procedure of photoredox mediated *o*-ROMP was greatly simplified after we observed excellent conversion from reactions set up under ambient conditions.

Table 4.2. Effect of additives on *o*-ROMP of norbornene **1**

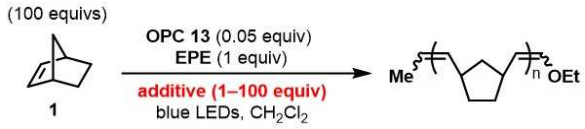

Additive	Equivalents[a]	Conversion[b] (%)
none	-	80
H2O	1	53
MeOH	1	40
i-PrOH	1	68
t-BuOH	1	80
t-BuOH	100	0
HFIP	100	72
MTBE	100	78

[a]Relative to vinyl ether initiator. [b]Conversion of **1**, as determined by ^{1}H-NMR analysis.

After observing tolerance toward alcohols and ethers, we started to investigate monomers with similar functionality (Table 4.3). We initially targeted norbornenes **3** and **4** functionalized with unprotected alcohols; however, they unsurprisingly precluded any polymerization. We then prepared a series of norbornene derivatives with protected alcohols (**5a-d**). Among these monomers, only the tertbutyldimethylsilyl (TBS) group, **5d,** resulted in successful homopolymerization with 50% conversion. We also investigated the copolymerization ability of those functional norbornene derivatives when they were loaded in a 1 : 3 feed ratio relative to norbornene. Each monomer underwent successful copolymerization with **1** though conversions and incorporation varied with **5d** showing the best *o*-ROMP compatibility. We also prepared

monomers **5e-g** to investigate the tolerance of MF-ROMP toward other functional groups. Neither **5e** nor **5f** showed any homopolymerization but copolymerized with **1** to low conversion and incorporation. **5g** surprisingly homopolymerized but did not inhibit or react in copolymerization with **1,** which was determined to be due to the much more rapid polymerization of **1** compared to **5g**. In addition to demonstrating several new monomers that perform well for *o*-ROMP, these investigations also provide insight into mechanistic considerations for future monomer design.

Table 4.3. Results of copolymerization between norbornene and functional monomers

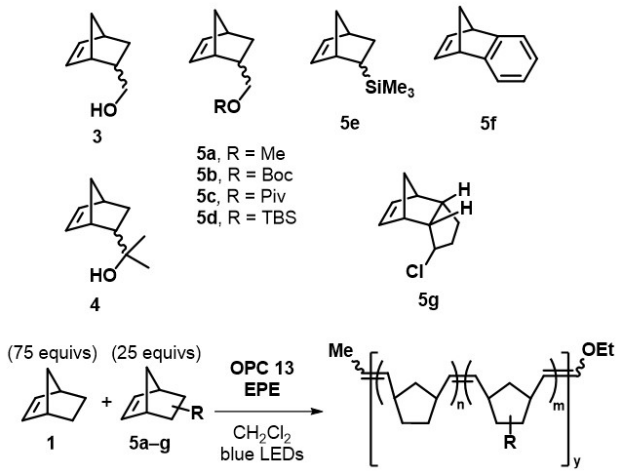

Co-monomer	conversion[a] (%)	1 : 8[b] (polymer)	Mw[c] (kDa)	*Đ*
5a	77 (34)	82 : 18	20.3	1.4
5b	70 (30)	88 : 12	95.0	3.7
5c	74 (55)	89 : 11	37.2	2.2
5d	78 (71)	80 : 20	27.0	1.5
5e	47 (9)	90 : 10	5.3	1.3
5f	34 (19)	74 : 26	7.9	1.2
5g	87 wrt **1**	100 : 0	24.0	1.5

[a]Determined by ^{1}H-NMR analysis of a reaction aliquot. Yield in parentheses after isolation of polymer.[b]Determined by ^{1}H-NMR spectroscopy of isolated polymer. [c]Weight-average molecular weight determined by GPC using MALLS. Dispersities (*Đ*) determined by GPC.

4.1.c Plausible Future Direction of Expanding o-ROMP Monomer Scope

Although there are several different kinds of functional monomer can undergo either homopolymerization or random copolymerization with norbornene, the most successful monomer family is still protected alcohol. However, if we want to utilize the potential of these functional polymer which contain protected alcohol, one more deprotection step, either heating or fluoride assisted silyl deprotection, will be required to free these alcohols.

To avoid such deprotection steps and in the meantime, facilitate the synthesis of functional materials, we think there are two requirements that future functional *o*-ROMP monomer should fulfill at least one of them: 1) the functional group should be orthogonal to *o*-ROMP condition; 2) the functional group should be post-polymerization modifiable. The orthogonality of monomer's functional group will exclude the necessity of protecting group. And after being incorporated into final polymer, desired monomer should also provide functional groups that can undergo further transformation to access materials with tailored properties.

Section 2: Results and Discussion

4.2.a Effect of Additives on o-ROMP

To realize potential post-polymerization modifications, we turned our attention towards three different functional groups, which are acrylates, maleimides and epoxides. It has been reported that all of those functional groups are vulnerable to nucleophilic attack under basic conditions.[8] While acylates and maleimides undergo nucleophilic additions with various thiols, assorted primary amines can force the ring-opening of epoxides (Scheme 4.1). Both reactions have been examined as great candidates to perform post-polymerization modifications due to the broad scope of commercially available functional thiols and amines. For acrylates, besides attacking by

nucleophiles, this specific functional group could also be photo-polymerized through radical pathway if photoinitiators are present. Similar photomediated pathway are also well documented for epoxides.

Scheme 4.1 Select post-polymerization modification through acrylate, maleimide and epoxide

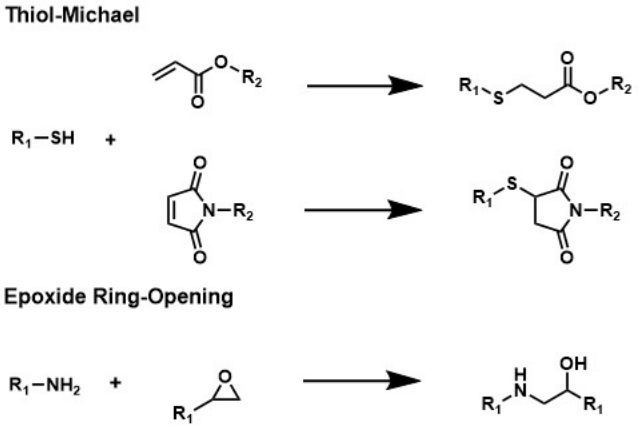

As a simple method to explore functional group compatibility with *o*-ROMP conditions, we initially examined the effect of small-molecule additives on the polymerization of norbornenes using our previously reported photoredox conditions (Table 4.4). To closely resembles homo- or copolymerization with functionalized monomers, we examined one feed ratio for the additives: a 1 : 1 molar ratio relative to monomer. Methyl acrylates were selected as additives for testing *o*-ROMP tolerance of acrylate groups, which afforded high conversion under optimized condition. However, with very similar structures, methyl methacrylates seemed to be detrimental to *o*-ROMP. This intricate structural effect was also observed in epoxide related additives. While the addition of either 1,2-epoxide butane or epichlorohydrin still resulted in decent *o*-ROMP conversion, adding disubstituted epoxide, such as cyclohexene oxide, dramatically halted this polymerization. Since the reactive intermediate of *o*-ROMP is considered as electrophilic radical cation species, it is plausible that the distinction in reactivities of similar additives result from their different nucleophilicities.

Table 4.4 Effect of Additives on Polymerization of 1 to Polynorbornene

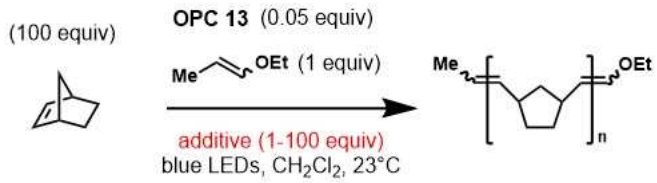

additive	equivalents[a]	purification	conversion (%)[b]
none	N/A	N/A	90
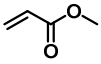	100	Yes[c]	74
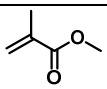	100	Yes[c]	39
	100	Yes[d]	68
	100	Yes[d]	67
	100	Yes[d]	12
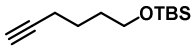	100	Yes[e]	20
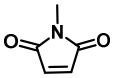	100	No	78

[a]Relative to enol ether initiator. [b]Determined using 1H-NMR spectroscopy by comparison of monomer and polymer peaks. [c]Purified by filtering through neutral alumna plug and drying over molecular sieves. [d]Purified by drying over molecular sieves. [e]Purified by flash chromatography. PMP = p-methoxyphenyl. All reaction times = 90 min.

We also examined the effect of additives, which incorporate alkyne and maleimide, on the performance of *o*-ROMP. Although terminal alkynes are well-known for participating in Cu-catalyzed "Click Chemistry", it turned out that this specific functional group is detrimental to *o*-ROMP. On the other hand, maleimides still afforded high *o*-ROMP conversion with the same feed ratio. However, the ^{1}H-NMR spectrum of precipitated polymer demonstrated that maleimides would react with the backbone of polynorbornene under *o*-ROMP conditions.

4.2.b o-ROMP of Monomers with Expanded Functionalities

Table 4.5 Copolymerization of **6** and *o*-ROMP benchmark monomers **1** or **2d**

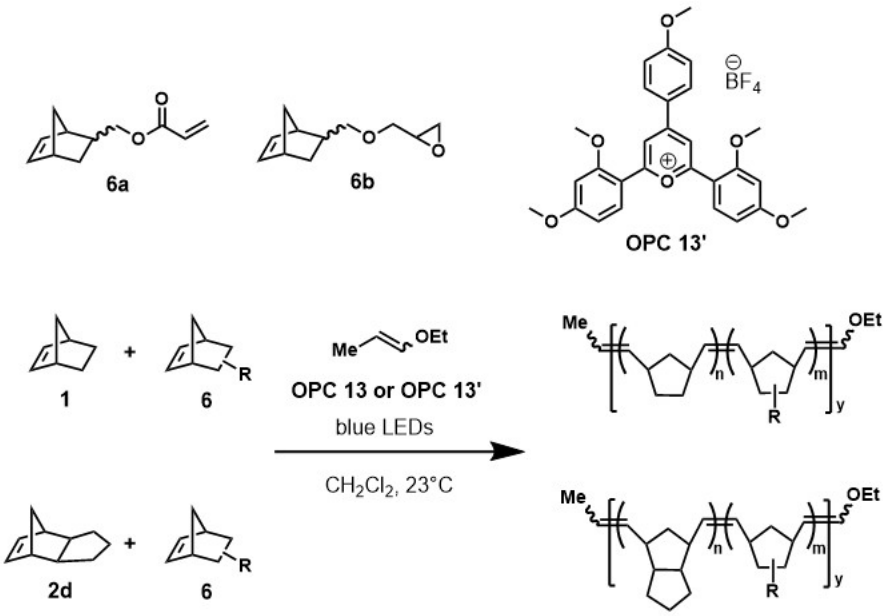

entry	Feed ratio	conversion (isolated yield)[a]	Polymer composition[b]	M_w (kDa)[c]	$Đ$[c]
1	75 (**1**) : 25 (**6a**)	48% (20%)	92 (**1**) : 8 (**6a**)	12.3	1.9
2	90 (**1**) : 10 (**6a**)	68% (50%)	97 (**1**) : 3 (**6a**)	16.2	1.9
3	75 (**2d**) : 25 (**6a**)	40% (25%)	93 (**2d**) : 7 (**6a**)	10.1	1.8
4	75 (**1**) : 25 (**6b**)	39% (20%)	89 (**1**) : 11 (**6b**)	7.8	1.5
5	90 (**1**) : 10 (**6b**)	50% (23%)	95 (**1**) : 5 (**6b**)	9.6	1.4
6	75 (**2d**) : 25 (**6b**)	40% (30%)	92 (**2d**) : 8 (**6b**)	8.4	1.4

[a]Determined by ^{1}H-NMR spectroscopy of a reaction aliquot. Yield in parentheses after isolation of polymer. [b]Determined by ^{1}H-NMR spectroscopy of isolated polymer. [c]Weight-average molecular weight determined by gel-permeation chromatography with in-line multiangle laser-light scattering detection. Molecular weight dispersity ($Đ$) = M_w/M_n. All reaction = 90 mins.

Since we have identified some level of tolerance toward both acrylates and epoxides with *o*-ROMP conditions, we prepared corresponding monomers to inspect their *o*-ROMP performance (Table 4.5). Unfortunately, homopolymerization of neither **6a** nor **6b** led to any detectable polymer. However, both monomers were found to undergo successful copolymerization with previously reported benchmark *o*-ROMP monomers. Based on ^{1}H-NMR spectrum of precipitated copolymers, the incorporation of those functional monomers didn't match the feed ratio that was used. While **6a** led to bimodal molecular weight distributions, partial gelation was observed during

copolymerization when **6b** was chosen as comonomer. Although the bimodality was not remedied for **6a**, the partial gelation happening to **6b** was never observed after switching to a less electrophilic **OPC 13'**. So, we hypothesized that partial gelation was due to nucleophilic attack of epoxide side chain in **6b** toward electrophilic **OPC 13**, which triggered following ring opening polymerization of epoxide. When **6a** and **6b** were loaded in a 1:3 feed ratio relative to **1**, the highest incorporation ratio was realized with monomer **6b** (11mol%). The incorporation ratio of these two monomers was not improved when comonomer (from **1** to **2d**) and solvent (from CH_2Cl_2 to $CHCl_3$) was changed. As the additive study has proved that both acrylates and epoxides should be compatible with *o*-ROMP, the poor performance of 6a and 6b is attributed to the fast quench of reactive radical cation chain ends through intramolecular pathway.

Scheme 4.2 Photo-crosslink of Functional *o*-ROMP copolymer

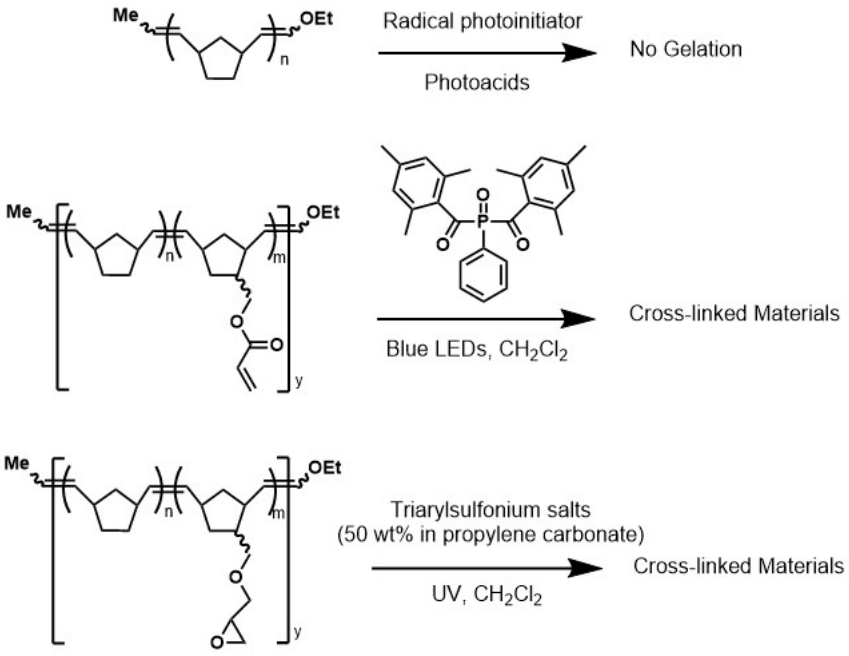

As we were not able to control the polymer composition by manipulating the feed ratio, we didn't pursue the further employment of those functional polymers as platforms for post-polymerization modification. But we turned to investigate their cross-linking reaction as to prove

the existence of those acrylates and epoxides (Scheme 4.2). It is noteworthy that nude polynorbornene does not gel when using conventional photoradical or photoacid generators. On the other hand, those functional copolymers with pendant acrylate or epoxide groups successfully underwent full gelation in minutes. In the future, the synthesis of corresponding functional oligomers (DP < 6) will be interesting since those oil-like liquids might have potential applications as photoresins for additive manufacturing.

4.2.c o-ROMP of Functional Monomers with Long Alkyl Linker

To outcompete the hypothesized intramolecular pathway, we sought to prepare functional monomers with tethered long alkyl linker (Table 4.6). The first monomer we tried was a norbornene derivative **7a** with pendant alkyl ester groups. The synthesis of **7a** has been reported in previous literature, which features the integration of starting materials from both petrochemical and biomass source. After the initial test, we realized that **7a** could undergo *o*-ROMP homopolymerization with up to 30% conversion. This performance is quite encouraging since the conversion of **1** in its homopolymerization actually decreased from 90% to 53% when ethyl acetate was used as additive (the same equivalents as **1**) in *o*-ROMP. However, we were not able to isolate homopolymer of **7a** from the reaction mixture.

We then looked at *o*-ROMP copolymerization between **1** and **7a**. Without significant decrease in conversion and isolated yield, we found that **7a** could be successfully incorporated into copolymer with high loading. This is the first time that we can make *o*-ROMP polymer with carboxylic acid derivative. In each cases, the amount of the ethyl ester-containing monomer incorporated into the polymer chain was approximately 1-2 % less than the feed ratio. This enabled us to manipulate the glass transition temperature (T_g) of the resulted copolymer with fine tuning

the feed ratio of starting materials. Based on these preliminary data, we prepared monomers **7b** and **7c**, which could be viewed as derivatives of **6a** and **6b**. Although the incorporation ratio of those two functional monomers are not as high as that of **7a**, the results are much better compared to the performance of either **6a** or **6b**.

Table 4.6 Copolymerization of **7** and *o*-ROMP benchmark monomer **1**

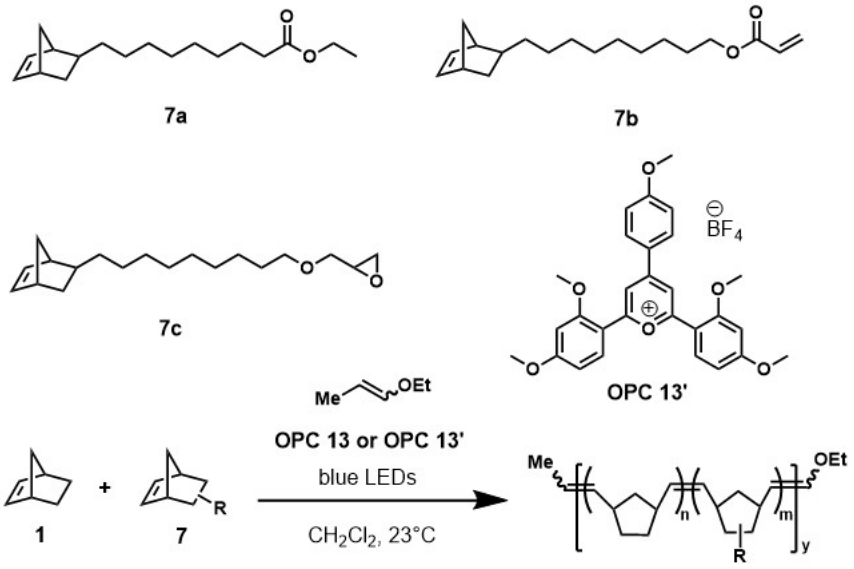

entry	Feed ratio	conversion (isolated yield)[a]	Polymer composition[b]	M_w (kDa)[c]	$Đ$
1	75 (**1**) : 25 (**7a**)	60% (40%)	77 (**1**) : 23 (**7a**)	16.4	1.2
2	90 (**1**) : 10 (**7a**)	73% (60%)	91 (**1**) : 9 (**7a**)	12.9	1.3
3	80 (**1**) : 20 (**7b**)	60% (15%)	85 (**1**) : 15 (**7b**)	N/A	N/A
4	80 (**1**) : 20 (**7c**)	50% (18%)	82 (**1**) : 18 (**7c**)	N/A	N/A
5	90 (**1**) : 10 (**7c**)	55% (23%)	92 (**1**) : 8 (**7c**)	9.7	1.2

[a]Determined by ^{1}H-NMR spectroscopy of a reaction aliquot. Yield in parentheses after isolation of polymer. [b]Determined by ^{1}H-NMR spectroscopy of isolated polymer. [c]Weight-average molecular weight determined by gel-permeation chromatography with in-line multiangle laser-light scattering detection. Molecular weight dispersity ($Đ$) = M_w/M_n. All reaction = 90 mins.

We also tried extending the benefit of long alkyl linker to other type of functional monomers, such as inimer **7d**, which integrate both initiation sites and repeating units. In previous experiments, the addition of inimer without alkyl linker resulted in extremely low *o*-ROMP conversion (< 10 mol%). On the other hand, inimer **8** successfully copolymerized with either **1** or

2d, affording much higher conversion (>65 mol%). However, we did observe slight insoluble materials at the surface of reaction vessels, which was attributed to the homopolymerization of vinyl ether moieties. In future, if we can find out a way to suppress this side reaction from happening, inimer **8** could be used to make o-ROMP polymer with highly branched topology.

Scheme 4.3 Copolymerization of **8** and *o*-ROMP benchmark monomers **1** and **2d**

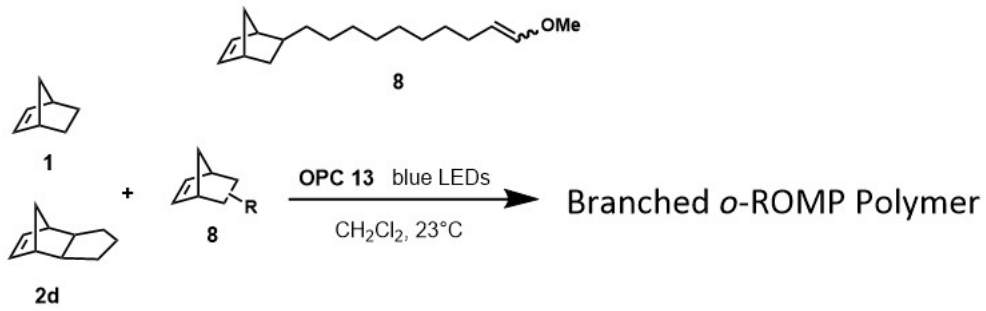

Section 3: Conclusions

In conclusion, we successfully demonstrate the *o*-ROMP of functional monomers with expanded functionality beyond simple protected alcohols. The direct installation of acrylate and epoxide groups diminish time-consuming deprotection steps, which facilitate the preparation of functional *o*-ROMP polymers suitable for potential downstream applications. To circumvent the relatively low incorporation ratio of those functional monomers, we engineered structure of monomers by moving functional groups away from the repeating units. The *o*-ROMP performances of these functional monomers with long alkyl side chains were much better since each monomer could be successfully incorporated into copolymer with high loading. We also extended this strategy to the preparation of unique *o*-ROMP inimer, which would potentially afford polymer with branched architecture.

Section 4: Experimental

General Consideration. Dichloromethane (CH_2Cl_2), tetrahydrofuran (THF) were obtained from a solvent purification system. For MF-ROMP procedure, CH_2Cl_2 was dried over 4Å molecular sieves before use. Norbornene **1** was sublimed prior to use. Triethyl amine (Et_3N) was distilled over CaH_2 and stored under inert atmosphere. The pyrylium tetrafluoroborates **OPC 13** and **OPC 13'** were prepared according to literature procedure. Monomers **2d**, **6a**, **6b** and **7a** were prepared with modified procedure as previously described in literature. All other reagents and solvents were obtained from commercial sources and used as received unless otherwise noted. All polymerizations were carried out in standard borosilicate glass vials with magnetic stirring. Irradiation of photochemical reactions was done using a 2W Miracle Blue LED indoor gardening bulb purchased from Amazon. ^1H and ^{13}C NMR spectra were recorded on Bruker AVance 300 MHz or 500 MHz spectrometers. Chemical shifts are reported in delta (δ) units, expressed in parts per million (ppm) downfield from tetramethylsilane using the residual protio-solvent as an internal standard (CDCl3, ^1H: 7.26 ppm and ^{13}C: 77.0 ppm). Data are reported as follows: chemical shift, multiplicity (s = singlet, d = doublet, dd = doublet of doublet, dt = doublet of triplets, q = quartet, m = multiplet, br = broad peak), coupling constants (Hz) and integration. Gel Permeation Chromatography (GPC) was performed using a GPC setup consisting of: an Agilent pump, 3 in-line columns, and Wyatt light scattering and refractive index detectors with THF as the mobile phase. Number average molecular weight (M_n) and weight average molecular weight (M_w) were calculated from refractive index data and light scattering, respectively, using Astra software from Wyatt Technology Corp. Differential Scanning Calorimetry (DSC) was performed on a TA DSC Q250 calorimeter under nitrogen. Heat flow as watts from the second heating was recorded and reported after normalizing by mass of the sample (W/g).

Scheme 4.4 Preparation of Select Functional *o*-ROMP Monomers

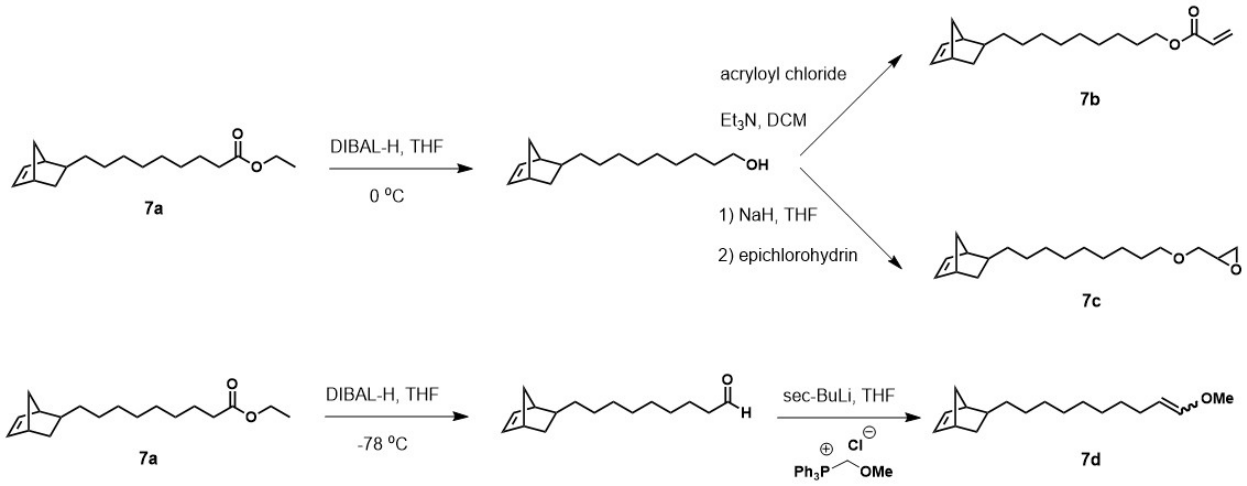

*Preparation of Monomer **7b***

To a solution of **7a** (3.0 g, 10.8 mmol) in THF (30 ml) at 0 ºC was added a solution of DIBAL-H in hexane (23 ml, 1M, 23 mmol). The reaction mixture was stirred for 90 mins and then CH_3OH was added to the mixture. Celite was added to the solution afterwards and the suspension was stirred overnight. Finally, the suspension was filtered through a Celite plug and the filtrate was concentrated to afford an oil-like compound. The crude product was carried on for next step without further purification.

To a solution of intermediate alcohol (935.2 mg, 4.0 mmol) in CH_2Cl_2 (20 ml) at 0 ºC was added Et_3N (0.84 ml, 6 mmol) and acryloyl chloride (0.36 ml, 4.4 mmol). The reaction mixture was stirred for 90 mins. Then the solution was concentrated, and the crude product was dissolved into diethyl ether. The ether solution was washed with saturated $NaHCO_3$ and saturated Brine solution. The organic phase was collected and dried with Na_2SO_4. Purification of the desired product by flash chromatography (1:9, ethyl acetate:hexane eluent) provided 1.0 g (88% yield) of monomer **7b**. ^{1}H-NMR: δ = 6.40-6.36 (dd, 1H) 6.13-6.08 (dd, 1H) 6.09-5.88 (dd, 2H) 5.80-5.78 (dd, 1H)

4.13 (t, 2H) 2.81-2.48 (br, 2H) 1.99-1.89 (br, 1H) 1.83-1.78 (br, 1H) 1.68-1.62 (br, 2H) 1.41-1.15 (br, 15H), 1.10-0.95 (br, 2H)

*Preparation of Monomer **7c***

To a suspension of NaH (1.1 g, 60 wt%, 27 mmol) in THF (50 ml) at 0 ºC was added intermediate alcohol (2.1 g, 9 mmol). The suspension was stirred for 45 mins. Then 18-crown-6 (238 mg, 0.9 mmol) and epichlorohydrin (2.1 ml, 27 mmol) were added to the mixture. The solution was stirred for 16 hours at room temperature until the reaction was quenched by adding deionized water. The solution was diluted with ether and the ether solution was washed with saturated Brine solution. The organic phase was collected and dried with Na_2SO_4. Purification of the desired product by flash chromatography (1:10, ethyl acetate:hexane eluent) provided 2.1 g (84% yield) of monomer **7c**. ^{1}H NMR (300 MHz, $CDCl_3$) δ = 6.09-5.88 (dd, 2H) 3.70-3.12 (br, 5H) 2.79-2.48 (br, 4H) 1.98-1.92 (br, 1H) 1.83-1.78 (br, 1H) 1.60-1.54 (br, 2H), 1.37-1.18 (br, 15H) 1.08-0.97 (br, 2H)

*Preparation of Monomer **7d***

To a solution of **7a** (3.5 g, 12.6 mmol) in THF (40 ml) at -78 ºC was added a solution of DIBAL-H in hexane (16 ml, 1M, 16 mmol). The reaction mixture was stirred for 90 mins and then CH_3OH was added to the mixture. Celite was added to the solution afterwards and the suspension was stirred overnight. Finally, the suspension was filtered through a Celite plug and the filtrate was concentrated to afford an oil-like compound. Purification of the desired product by flash chromatography (1:20, ethyl acetate:hexane eluent) provided 1.7 g (60% yield) of intermediate aldehyde.

A solution of sec-BuLi (12 ml, 1.4 M, 16.9 mmol) was slowly added to a solution of (methoxymethyl)triphenylphosphonium chloride (5.8 g, 16.9 mmol) in 30 ml of THF. After stirring the red solution for 45 mins, a solution of the intermediate aldehyde (11.3 mmol) in 5 ml of THF was slowly added and allowed to stir for an additional 3 hours. The solvent was removed under vacuum and the residue was diluted with hexanes. The organic layer was washed with water and dried over Na_2SO_4. The solvent was removed under reduced pressure and the resulting residue was purified by filtering through a plug of silica with diethyl ether as the eluent. ^{1}H NMR (300 MHz, $CDCl_3$) δ = 6.28-5.86 (br, 3H) 4.75-4.30 (br, 1H) 3.54-3.47 (d, 3H) 2.75-2.49 (br, 2H) 2.03-1.94 (br, 2H) 1.92-1.88 (br, 1H) 1.85-1.80 (br, 1H) 1.36-1.20 (br, 12H), 1.10-0.95 (br, 2H)

^{1}H-NMR and GPC Data

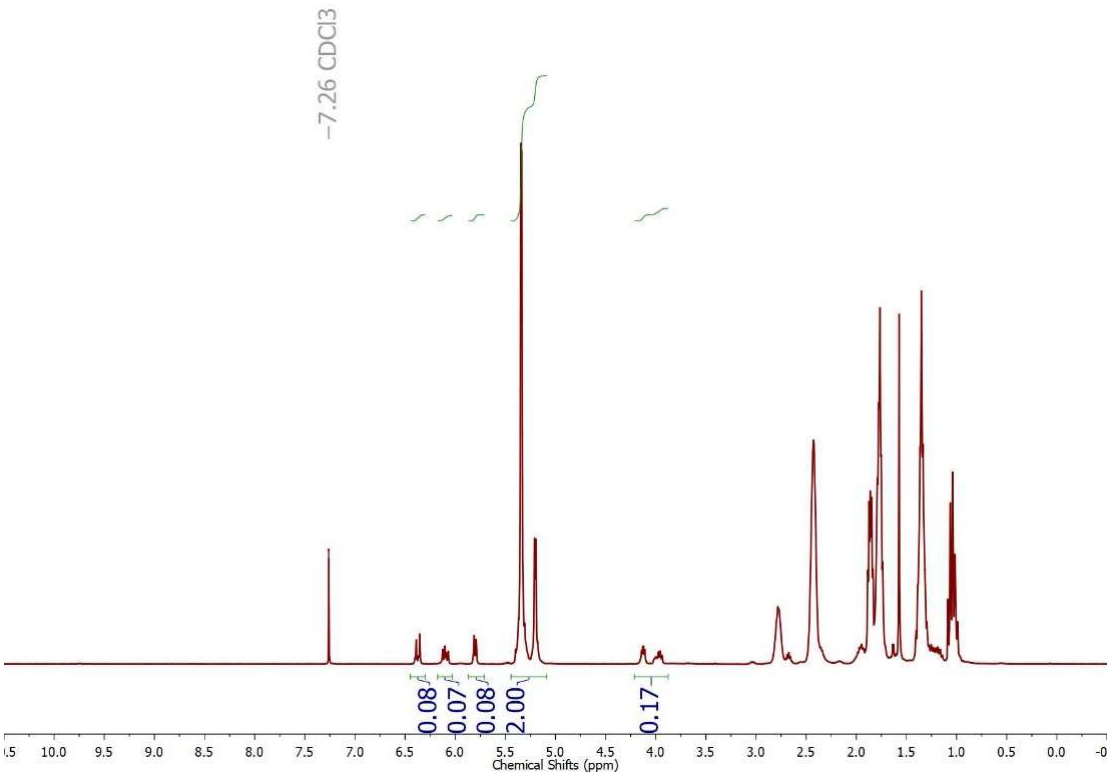

Figure 4.4 ^{1}H-NMR spectrum of copolymer from entry 1 in Table 4.5

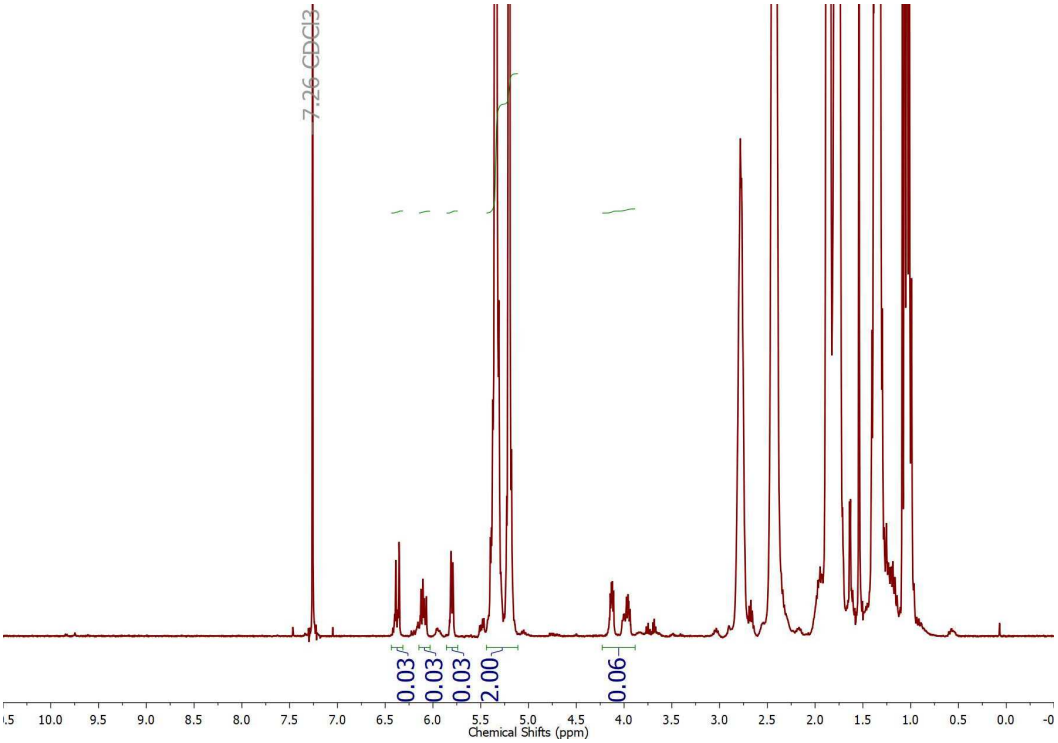

Figure 4.5 ^{1}H-NMR spectrum of copolymer from entry 2 in Table 4.5

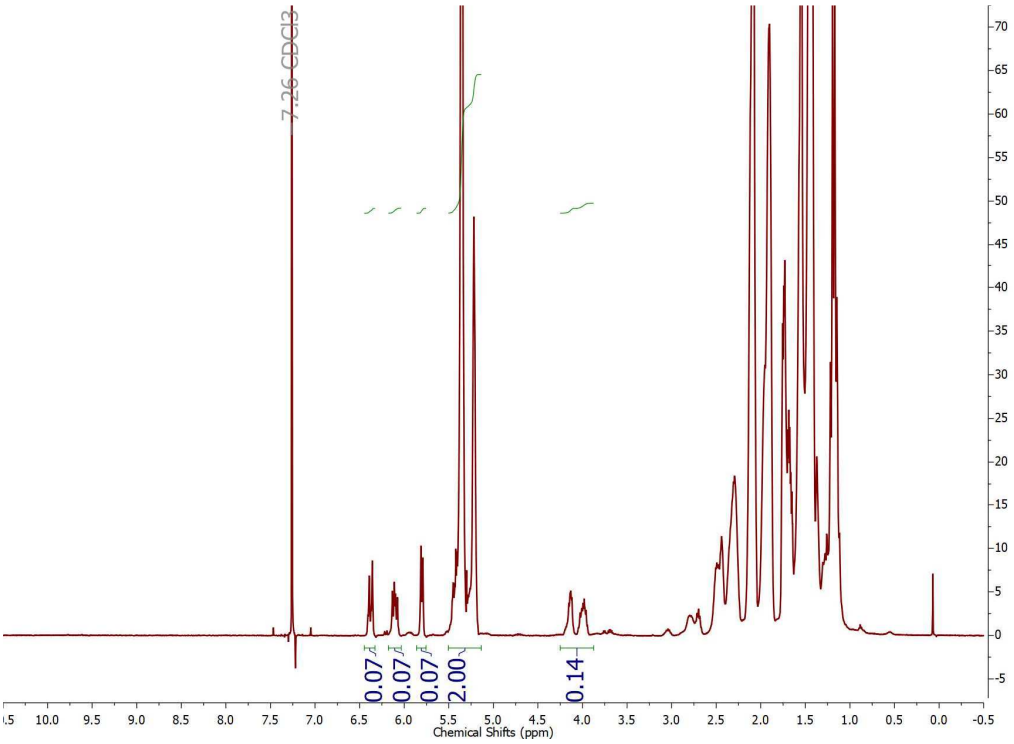

Figure 4.6 ^{1}H-NMR spectrum of copolymer from entry 3 in Table 4.5

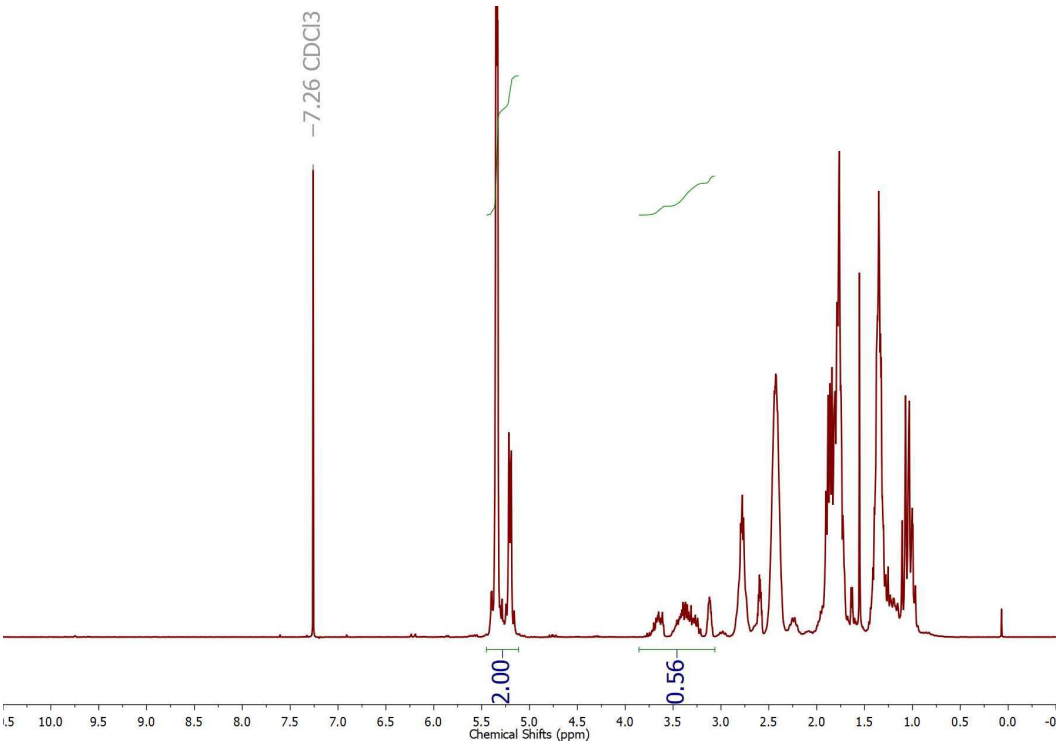

Figure 4.7 ^{1}H-NMR spectrum of copolymer from entry 4 in Table 4.5

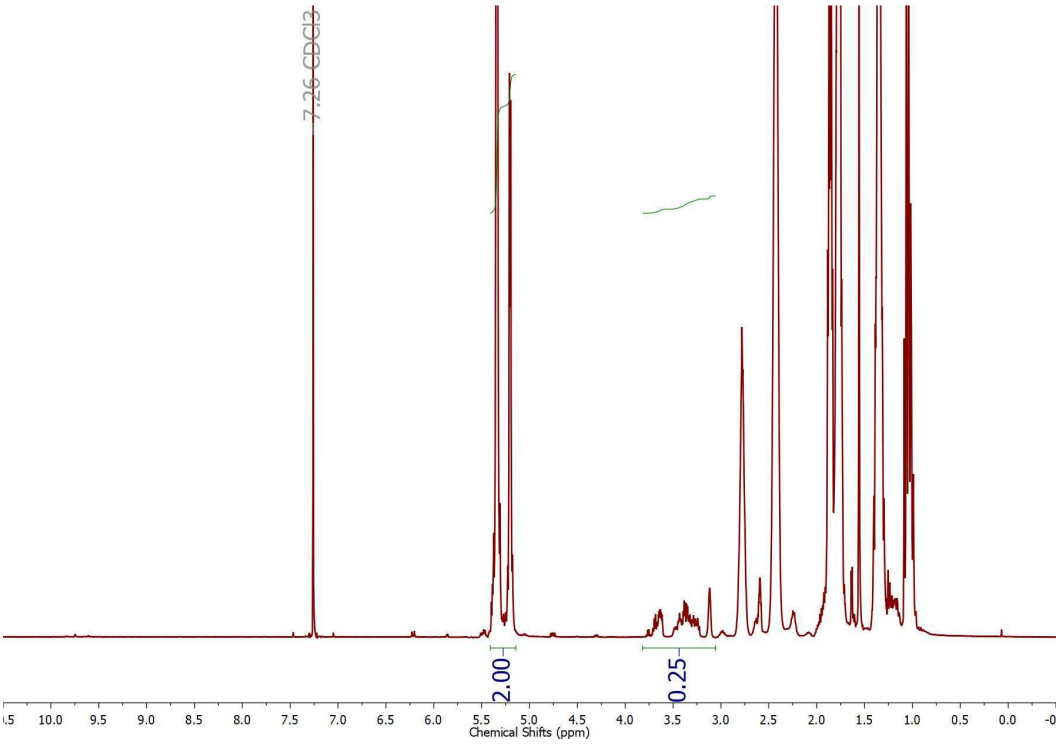

Figure 4.8 ^{1}H-NMR spectrum of copolymer from entry 5 in Table 4.5

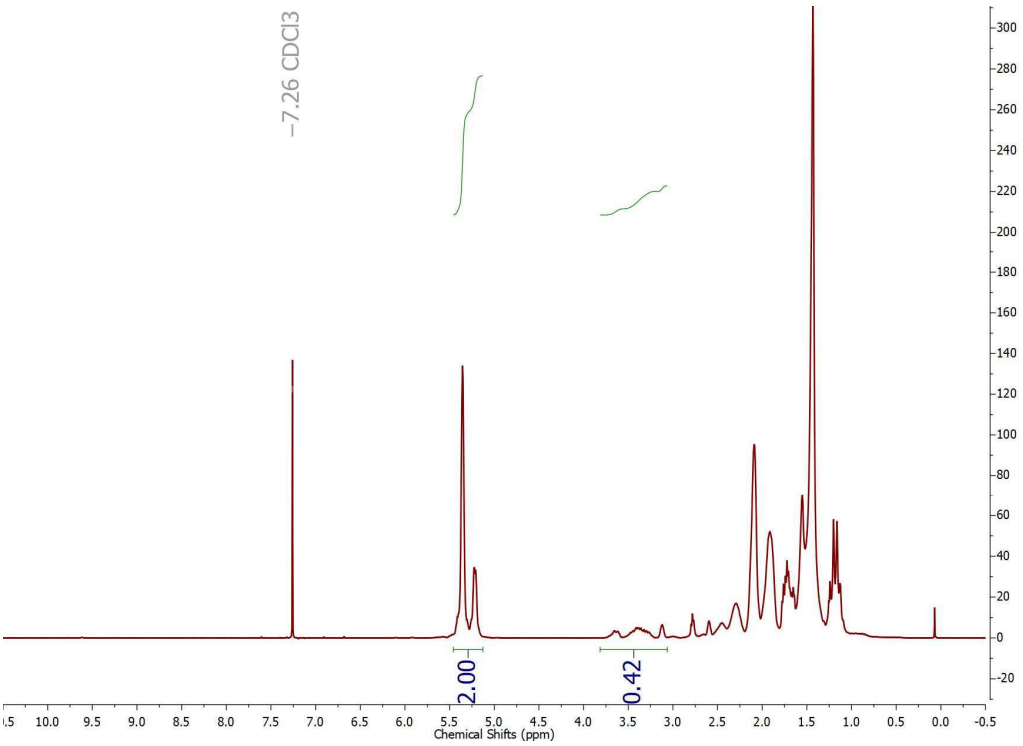

Figure 4.9 [1]H-NMR spectrum of copolymer from entry 6 in Table 4.5

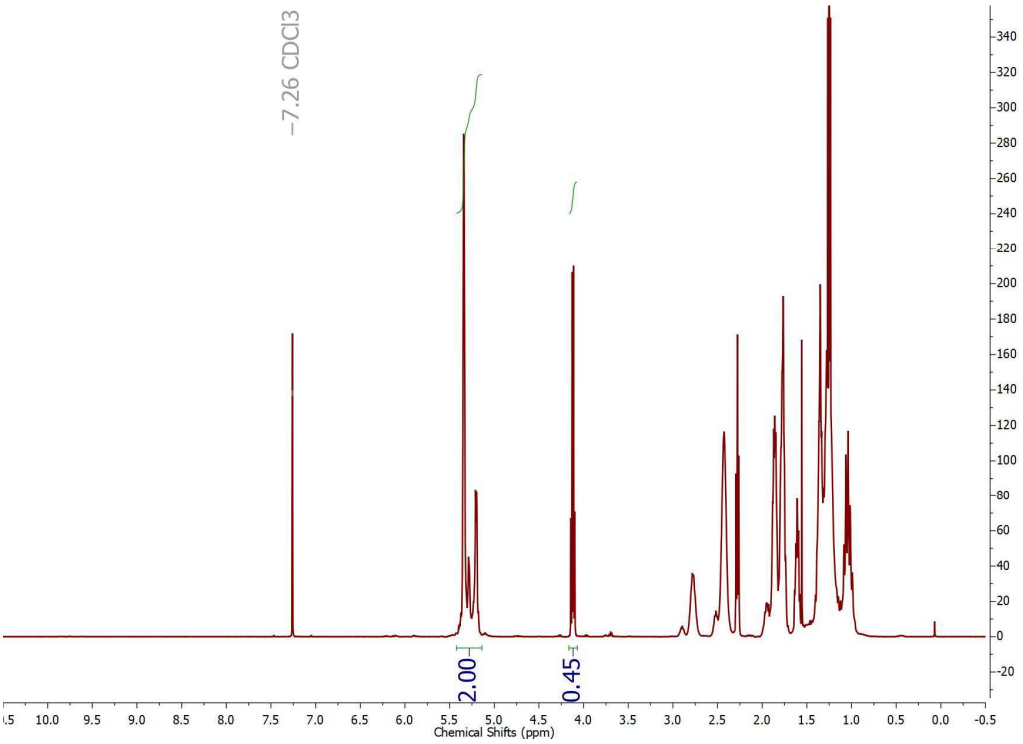

Figure 4.10 [1]H-NMR spectrum of copolymer from entry 1 in Table 4.6

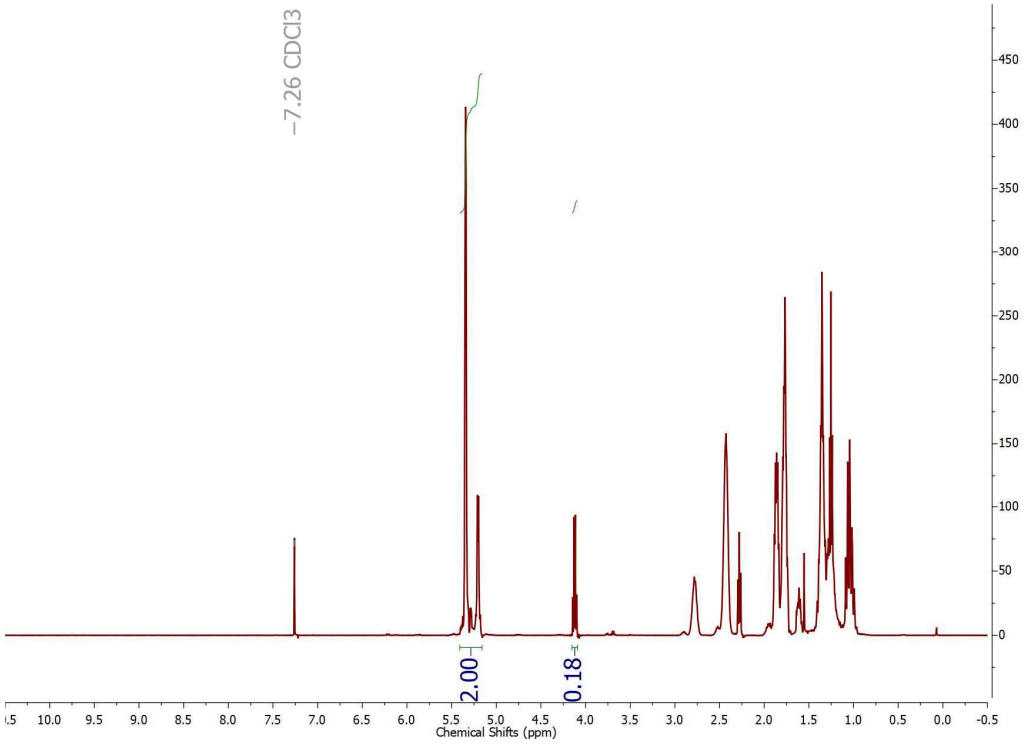

Figure 4.11 [1]H-NMR spectrum of copolymer from entry 2 in Table 4.6

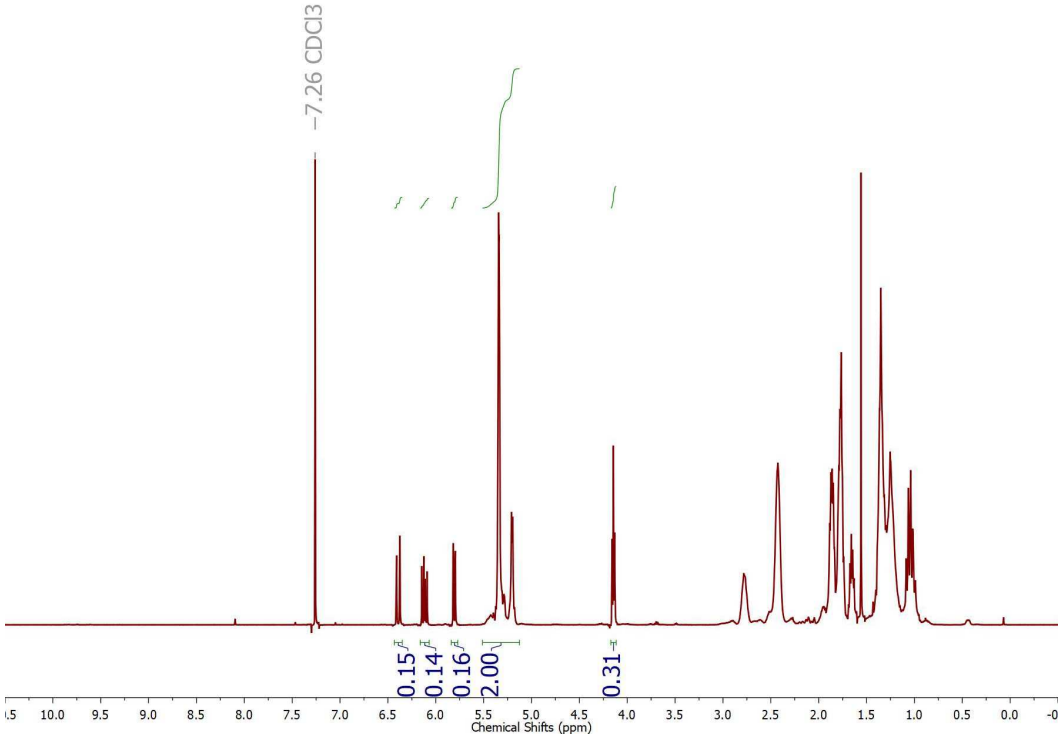

Figure 4.12 [1]H-NMR spectrum of copolymer from entry 3 in Table 4.6

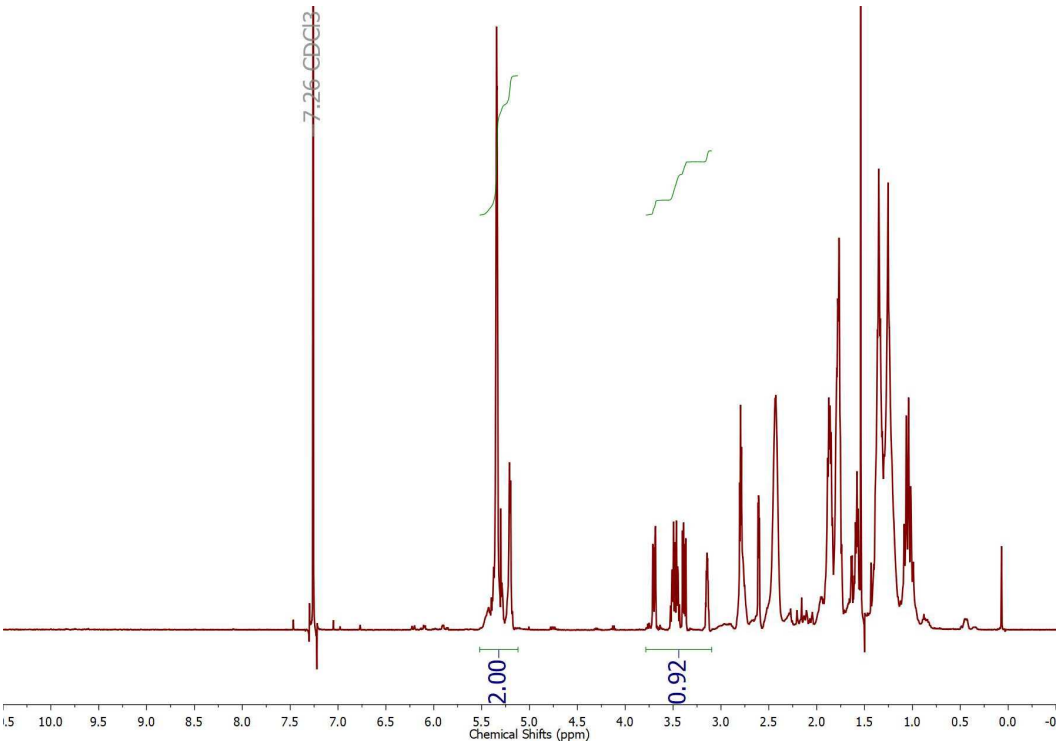

Figure 4.13 [1]H-NMR spectrum of copolymer from entry 4 in Table 4.6

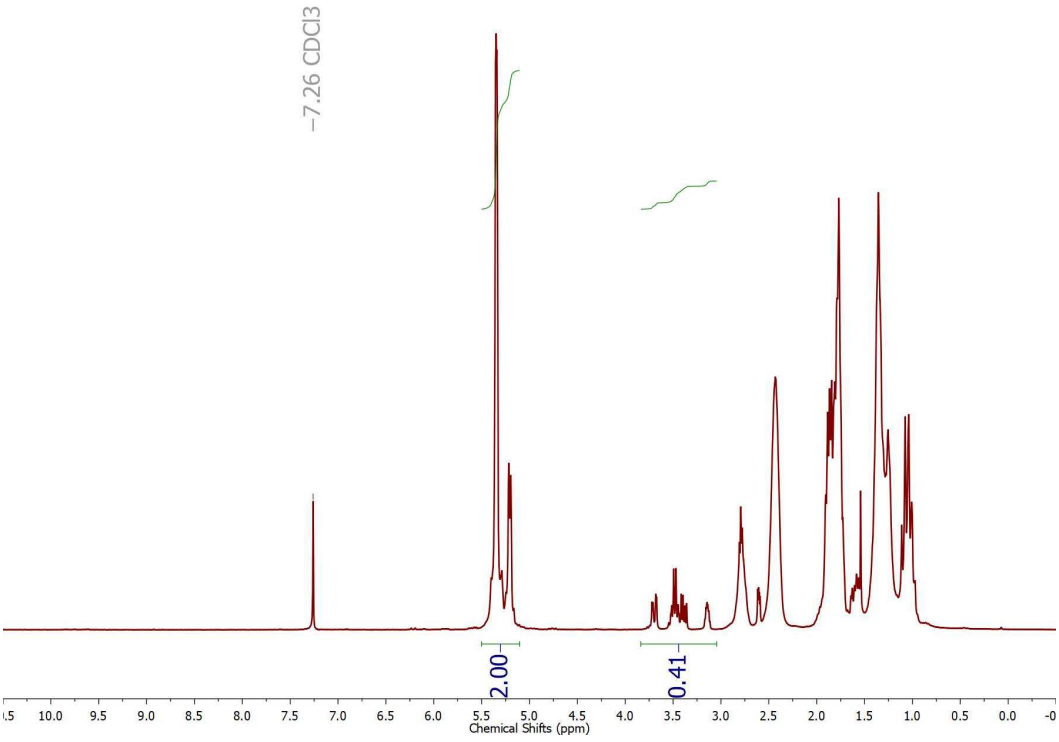

Figure 4.14 [1]H-NMR spectrum of copolymer from entry 5 in Table 4.6

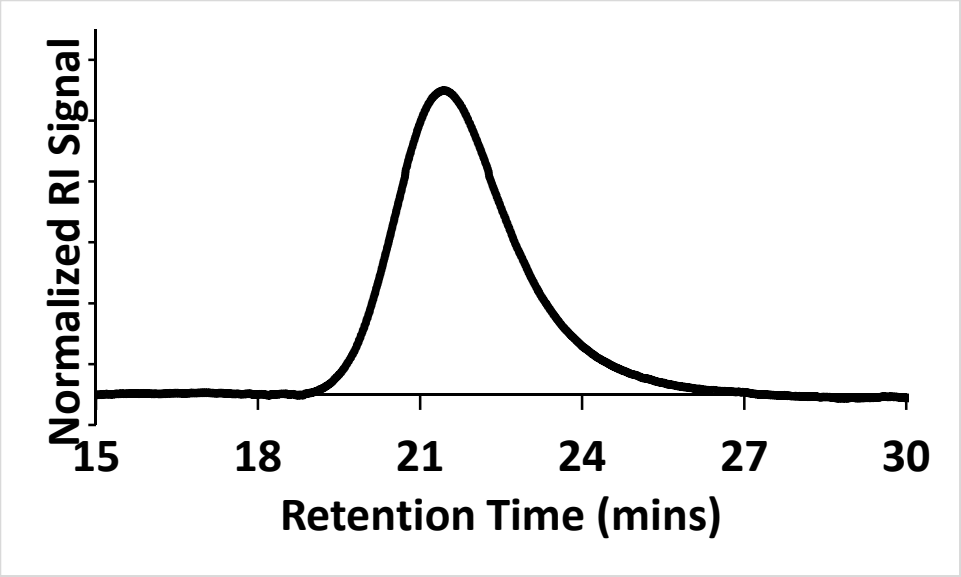

Figure 4.15 GPC spectrum of copolymer from entry 1 in Table 4.6

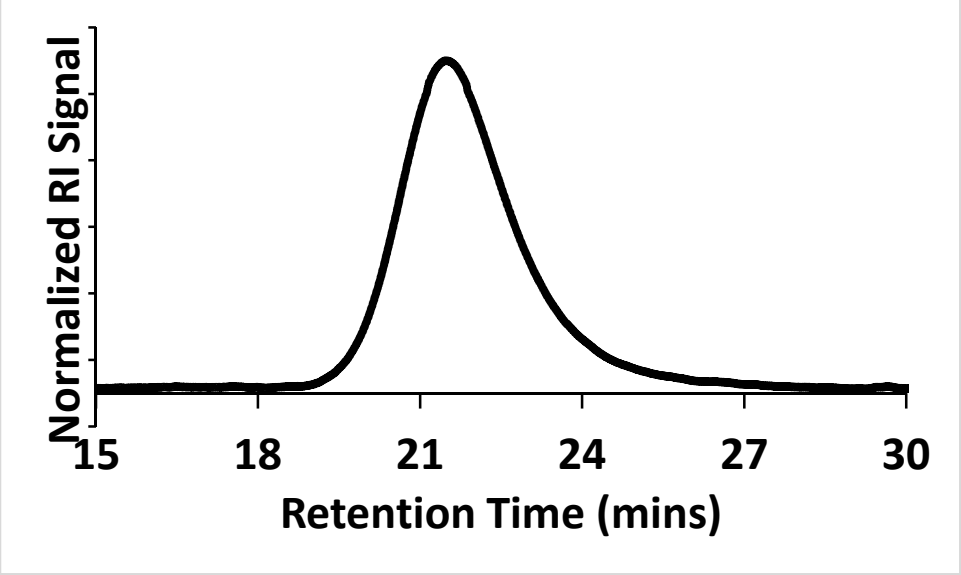

Figure 4.16 GPC spectrum of copolymer from entry 2 in Table 4.6

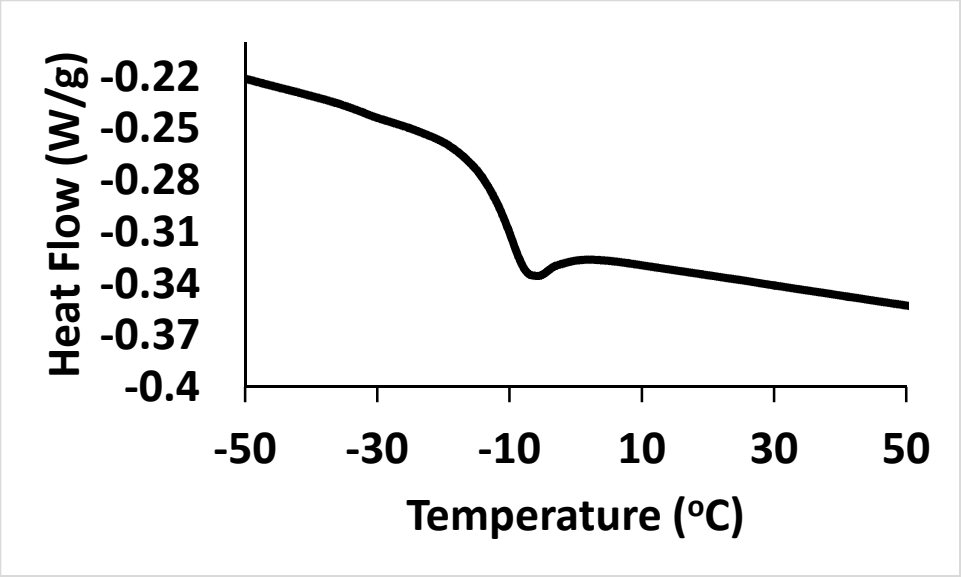

Figure 4.17 DSC (Exo up) of copolymer from entry 1 in Table 4.6

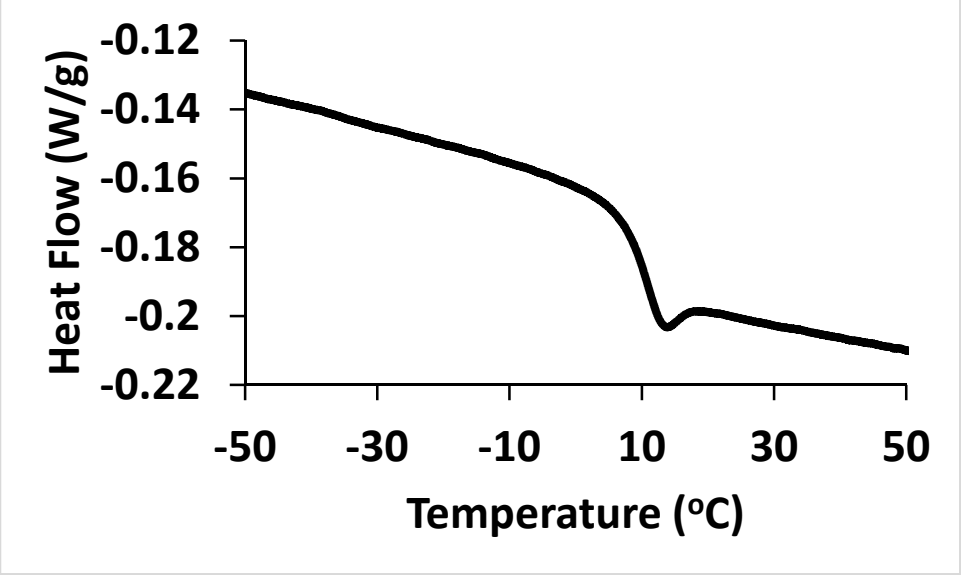

Figure 4.18 DSC (Exo up) of copolymer from entry 2 in Table 4.6

Notes and References for Chapter 4

[1] Bielawski, C. W.; Grubbs, R. H. *Prog. Polym. Sci.,* **2007**, *32*, 1.
[2] Ogawa, K. A.; Goetz, A. E.; Boydston, A. J. *J. Am. Chem. Soc.,* **2015**, *137*, 1400.
[3] Goetz, A. E.; Boydston, A. J. *J. Am. Chem. Soc.*, **2015**, *137*, 7572.
[4] Davidson, T. A.; Wagener, K. B.; Priddy, D. B. *Macromolecules*, **1996**, *29*, 786.
[5] Moeller, K. D. *Chem. Rev.*, **2018**, *118*, 4817.
[6] Goetz, A. E.; Pascual, L. M. M.; Dunford, D. G.; Ogawa, K. A.; Knorr, Jr. D. B.; Boydston, A. J. *ACS Macro Lett.*, **2016**, *5*, 579.
[7] Moeller, K. D. *Synlett*, **2009**, *8*, 1208.
[8] Blasco, E.; Sims, M. B.; Goldmann, A. S.; Sumerlin, B. S.; Barner-Kowollik, C. Macromolecules, **2017**, *50*, 5215.